Administration of Human Endothelial Colony Forming Cell-Derived Exosomes and miR-486-5p Protects Against Ischemia/Reperfusion Acute Kidney Injury

Matthew Spence

Department of Cellular and Molecular Medicine, Division of Nephrology, Department of Medicine, Kidney Research Centre, Ottawa Hospital Research Institute, University of Ottawa, Ottawa, Ontario, Canada

Dr. Kevin D Burns (Supervisor), Dr. Dylan Burger (Co-Supervisor)

This thesis is submitted as a partial fulfillment of the

M.Sc. program in Cellular and Molecular Medicine.

Department of Cellular and Molecular Medicine

Faculty of Medicine

University of Ottawa

Submitted on: June 24th, 2019

AUTHORIZATION

Viñas, J. L., Spence, M. et al. Receptor-Ligand Interaction Mediates Targeting of Endothelial Colony Forming Cell-derived Exosomes to the Kidney after Ischemic Injury. Sci. Rep. 8, 16320 (2018).

ABSTRACT

Background: Acute kidney injury (AKI) is a highly prevalent clinical disorder with significant mortality and no current treatment. The Burns Lab has previously shown that endothelial colony forming cells (ECFCs) release exosomes highly enriched in pro-survival micro-RNA-486-5p. In our mouse model of AKI, intravenous (i.v.) injection of ECFCs or their exosomes protects against kidney ischemic injury, associated with reduction in PTEN, a target of miR-486-5p. Mechanisms mediating recruitment and retention of exosomes are unclear. The interaction of CXC chemokine receptor type 4 (CXCR4) with stromal cell-derived factor (SDF)-1α promotes ECFC adhesion and migration in hypoxic endothelial cells. Whether exosomal miR-486-5p is critical to the prevention of ischemic injury is unclear. The current study aimed to investigate biodistribution and targeting mechanisms of ECFC-derived exosomes, to investigate the delivery and therapeutic potential of miR-486-5p alone, and to determine whether sex differences alter the treatment efficacy.

Methods: ECFC-derived exosomes were isolated from cultured media by differential centrifugation and characterized using nanoparticle tracking analysis and immunoblot. Kidney ischemic injury was induced in male and female FVB mice by bilateral renal vascular clamping (30 min). Exosomes (20 μg) or Invivofectamine-mimic complex containing miR-486-5p (1mg/kg) were injected at the start of kidney reperfusion via tail vein. Organs were removed and assays were performed to identify structure and function. *In vitro* cell studies were also used when necessary.

Results: ECFC-derived exosomes preferentially target the ischemic kidney, its endothelium and tubular epithelium, which correlates with increases in miR-486-5p. The transfer of exosomes may be mediated by macropinocytosis by target cells. The SDF-1α/CXCR4 axis plays a role in

targeting exosomes to the site of injury. miR-486-5p alone has a similar therapeutic efficacy in preventing ischemia/reperfusion injury as ECFC-exosomes in the mouse model of AKI. Both male and female mice respond to both therapies, however female mice are protected against ischemia reperfusion injury.

Conclusions: These results suggest that the protective effects of ECFCs or their exosomes in ischemic AKI may be largely mediated by pro-survival miR-486-5p. These data provide further support for the promising therapeutic potential of ECFC-derived exosomes and miR-486-5p in human AKI.

Keywords: acute kidney injury; ECFC; exosome; endothelium; miR-486-5p

TABLE OF CONTENTS

LIST OF FIGURES

SUPPLEMENTAL FIGURES

LIST OF ABBREVIATIONS

AFC	7-amino-4-trifluoromethyl coumarin
AKI	Acute Kidney Injury
ANOVA	Analysis of Variance
BUN	Blood Urea Nitrogen
CCD	Charged Coupled Device
CD34	Cluster Differentiation-34
CD81	Cluster Differentiation-81
CKD	Chronic Kidney Disease
CM	Cultured Media
CVD	Cardiovascular Disease
CXCR4	C-X-C Chemokine Receptor type 4
Cy3	Indocarbocyanine
DiR	1,1'-Dioctadecyl-3,3,3',3'-Tetramethylindotricarbocyanine Iodide
DTT	Dithiothreitol
ECFC	Endothelial Colony Forming Cell
EIPA	5-(*N*-Ethyl-*N*-isopropyl) amiloride
EPC	Endothelial Progenitor Cell
ESRD	End-Stage Renal Disease
EV	Extracellular Vesicle
EX	Exosome
FBS	Fetal Bovine Serum
FLK-1	Fetal Liver Kinase-1
FVB	Friend Leukemia Virus B-Sensitive Mice

GFR	Glomerular Filtration Rate
H+E	Hematoxylin and Eosin
HPF	High Powered Field
HUVEC	Human Umbilical Vein Endothelial Cell
I-CAM	Intercellular Adhesion Molecule
IR	Ischemia/Reperfusion
ISEV	International Society of Extracellular Vesicles
isRNA	Immunostimulatory Ribonucleic Acid
IVIS	In Vivo Imaging System
lcRNA	Long-coding Ribonucleic Acid
m/l EV	Medium/Large Extracellular Vesicles
MAPK	Mitogen Activated Protein Kinase
miRNA	Micro-Ribonucleic Acid
miRNA-486-5p	Micro-Ribonucleic Acid-486-5p
MNC	Mononuclear Cell
MP	Microparticle
mRNA	Messenger-Ribonucleic Acid
MSC	Mesenchymal Stem Cell
MVB	Multi-Vesicular Body
NIR	Near Infrared
nSMase2	Neutral Sphingomyelinase 2
NTA	Nanoparticle Tracking Analysis
OCT	Optimal Cutting Temperature
OI	Optical Imaging
PAS	Periodic acid-Schiff

PBS	Phosphate Buffered Saline
pre-miRNA	Precursor Micro- Ribonucleic Acid
pri-miRNA	Primary Micro- Ribonucleic Acid
PTEN	Phosphatase and Tensin Homolog
qPCR	Quantitative Polymerase Chain Reaction
RIPA	Radio Immunoprecipitation Assay
ROI	Region of Interest
SDF-1α	Stromal Cell Derived Factor-1α
SDS-PAGE	Sodium Dodecyl Sulfate Polyacrylamide Gel Electrophoresis
sEV	Small Extracellular Vesicles
TBS-T	Tris-Buffered Saline-polysorbate 20
TMB	3,3,5,5'-tetramethylbenzidine
TSG101	Tumor Suppressor Gene-101
TUNEL	Terminal deoxynucleotidyl transferase-mediated dUTP nick-end labeling
UTR	Untranslated Region
VEGF	Vascular Endothelial Growth Factor

ACKNOWLEDGEMENTS

I accomplished this work with the support of many individuals who kept me going throughout my time at the Kidney Research Centre.

I would like to thank Dr. Kevin Burns for giving me the opportunity to work in his lab. Your guidance and support have made this work the most fulfilling academic experience of my life. You have always been approachable and insightful, even during the ups and downs that invariably come with the task of completing a graduate degree. I would also like to thank my co-supervisor, Dr. Dylan Burger, for always assisting and providing important feedback. I appreciate the guidance and support provided by my thesis advisory committee members, Dr. Chris Kennedy and Dr. Richard Hébert.

A sincere thanks to my lab members, specifically Dr. Jose Viñas, Dr. Alexey Gutsol, and Joe Zimpelmann. While my supervisors and TAC were there to provide insight and assist with feedback, you were there every day in the lab helping me work through experimental failures, keep me motivated, and for support when I needed it. Other scientists at the KRC, including Dr. Jean-François Thibodeau, Dr. Chet Holterman, and Dr. Fengxia Xiao, thank you.

Finally, I'd like to thank my Mom and Dad, my sister Emily, girlfriend Siobhan, Adrianna, Marie-Ève, fellow Russell Firefighters, and other friends and family. You've all dealt with my rants about my project, have given valuable words of advice, and have kept me going. My greatest love and thanks to you.

These studies were supported by research grants from the Serata Italiana Committee, Department of Medicine (The Ottawa Hospital, University of Ottawa), The Kidney Foundation of Canada (KFOC), and The Canadian Institutes of Health Research (CIHR). There are no conflicting financial interests.

LIST OF PUBLICATIONS

The following papers were published/submitted during the completion of my masters (in chronological order). Not all pertain to the subject of this thesis.

Viñas, J. L., Spence, M. et al. Receptor-Ligand Interaction Mediates Targeting of Endothelial Colony Forming Cell-derived Exosomes to the Kidney after Ischemic Injury. Sci. Rep. 8, 16320 (2018).

Rodriguez, R. A, Hae, R, Spence, M. et al. A Systematic Review and Meta-analysis of Non-pharmacologic-based Interventions for Aortic Stiffness in ESRD. *Kidney Int. Reports* **0,** (2019).

AUTHOR CONTRIBUTIONS

All experiments in the current study were performed by the author, excluding the following:

Dr. Jose Viñas performed the Cy3-labeled pre-miR-486-5p in HUVECs experiment, the in vitro uptake experiment with plerixafor and SDF-1α neutralizing antibody and assembled the invivofectamine-mimic complex.

Dr. Alexey Gutsol performed labeling, staining, and microscopy for immunocyto- and immunohisto-chemistry experiments. He also served as our blinded pathologist.

Joe Zimpelmann performed the proximal tubule and glomerular microdissections.

Dr. David Allan and Lab performed ECFC isolations and phenotyping.

INTRODUCTION

Acute Kidney Injury: Definitions and Causes

Acute kidney injury (AKI) is a clinical syndrome defined as an abrupt reduction in kidney function, generally within 24-48 hours, and can be measured through increases in serum creatinine and/or a decline in urine output over a short period[1–3]. Factors such as sepsis and nephrotoxicity can result in AKI, although renal ischemia/reperfusion (IR) injury is the most common cause of AKI[1–3]. IR injury occurs when there is inadequate blood flow to the kidney, resulting in a rapid decline in glomerular filtration rate (GFR) and, consequently, reduced oxygen and nutrient delivery and the retention of nitrogenous wastes[4]. Reperfusion, or the restoration of circulation, is then accompanied by inflammation and oxidative stress, rather than normal function[5]. In humans, renal IR injury results in tubular cell necrosis and endothelial cell dysfunction through intrinsic cellular responses, as well as the innate and adaptive immune responses[6–8]. Despite few advancements, AKI continues to be correlated with high morbidity and mortality rates, which vary by institution and can be between 30 and 70%[2].

Acute Kidney Injury: Structural damage and functional loss

Although AKI is given an explicit definition, it encompasses both structural damage and functional impairment; rarely does it have a distinct pathophysiology case-to-case[3]. In the clinic, AKI will often have multiple etiologies which overlap and co-exist to impede diagnosis and treatment[3]. Proximal tubular cell damage is characteristic of AKI, however, renal endothelial impairment and decreased microvascular flow are also features of AKI[1,9]. During ischemic AKI, total renal blood flow is significantly reduced to the point where cellular ATP depletion leads to

cellular damage and dysfunction[4]. Immediately after reperfusion, continued hypoxia and the inflammatory response define the extension phase of AKI, where blood flow to the corticomedullary junction is even further decreased while inner medullary blood flow is recovered[10,11]. It is at this point where renal vascular endothelial cell damage significantly contributes to the continued ischemia of the renal epithelium and the inflammatory response[4]. Vessels which supply the renal endothelium undergo vasoconstriction in response to increased tissue levels of vasoconstrictive agents, such as endothelin-1 and angiotensin II, and is amplified in a positive feedback loop as more endothelial cells are damaged and reduce the release of nitric oxide[2].

Structurally, this causes swelling of endothelial cells, vacuolar degeneration, and coagulopathy **(Figure 1A)**. Endothelial cells lose cell-cell contacts leading to an increase in permeability and loss of fluid into the interstitium[12,13]. Endothelial cells increase their expression of the adhesion molecules “intercellular adhesion molecule” (I-CAM) and “P- and E-selectin” which allow enhanced endothelium-leukocyte interactions. Inflammatory cells migrate through the endothelium and into interstitium, causing edema, which exacerbates vasoconstriction[14]. Microvessels in the medulla decrease in density due to injury, which is facilitated by inhibitors of angiogenesis. Reduced vessels and lack of angiogenesis is linked with chronic hypoxia, and promotes further tubular injury and tubulointerstitial fibrosis[4,13]. Tubular epithelium undergoes dedifferentiation and death by apoptosis and/or necrosis.

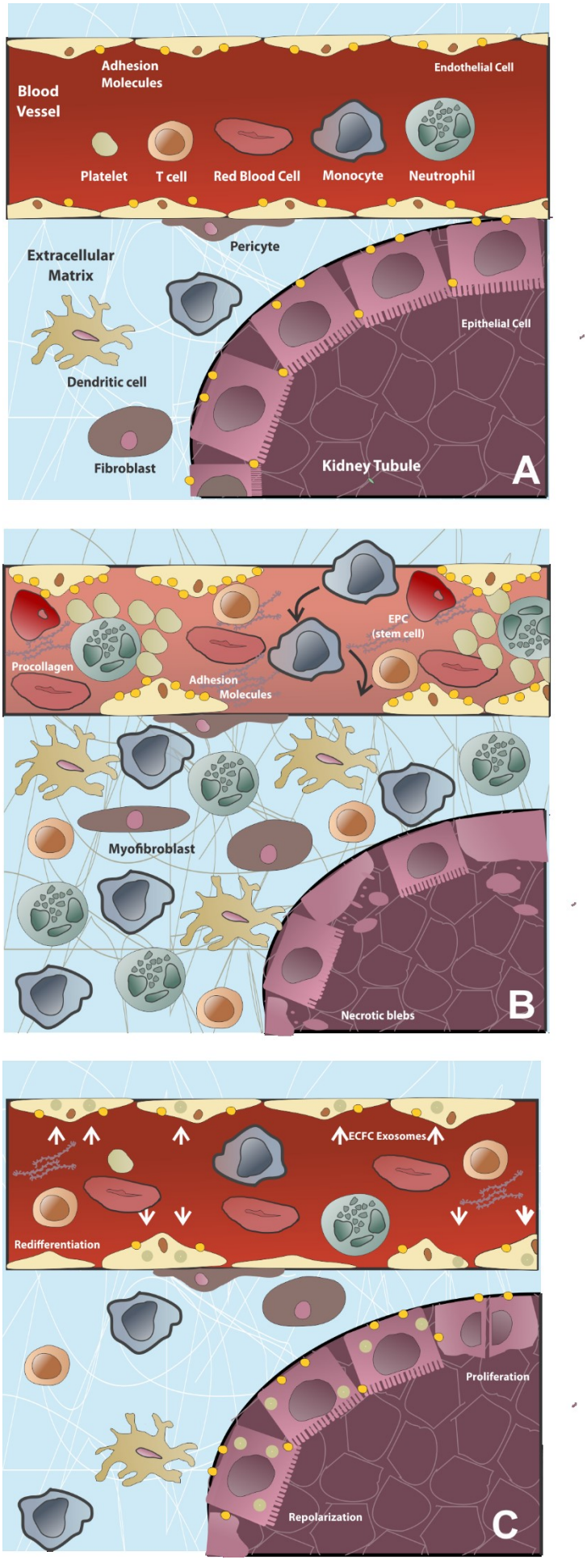

Figure 1 | Pathophysiology of ischemia/reperfusion in AKI and exosome behaviour. (A) Normal healthy tubular epithelium and endothelium separated by interstitium. (B) Ischemia/reperfusion injury causes swelling of endothelial cells, vacuolar degeneration, and coagulopathy. Endothelium lose cell-cell contacts leading to an increase in permeability. Endothelial cells increase their expression of adhesion molecules (I-CAM, P and E selectin) and cause enhanced leukocyte interactions. Inflammatory cells migrate through endothelium and into interstitium and cause edema. Tubular epithelium undergoes dedifferentiation. (C) ECFC exosomes may localize to endothelium (and possibly tubular epithelium) post-injection. Through inhibition of PTEN and activation of the Akt pathway, they inhibit apoptosis. Cells redifferentiate and repolarize.

Endogenous Renal Repair after AKI: Maladaptive and Abnormal

Proximal tubule epithelium proliferates at a low rate under normal circumstances, however, this changes quickly after ischemia, where the increase in cell death is balanced by cell proliferation[15]. These surviving epithelial cells dedifferentiate and migrate to the basement membrane where they proliferate and differentiate to restore cell number and the function of the nephron[2]. Renal blood flow can return to baseline levels within days, and histological structures recover within weeks[16]. Endogenous repair processes following AKI, however, are often maladaptive or incomplete, and may result in renal fibrosis[17]. There is often incomplete tubular repair, interstitial inflammation, and deposition of extracellular matrix, which all contribute to renal fibrosis[2] **(Figure 1B)**. In many cases, AKI patients never fully recover[17]. After AKI, patients have a 9-fold increase in risk for chronic kidney disease (CKD), a 3-fold increase in risk for developing end-stage renal disease (ESRD), cardiovascular disease (CVD), and all-cause mortality[2,17–19].

Despite medical advancements, AKI continues to affect up to 1 in 5 hospitalized patients and up to 40% of intensive care unit patients[20,21]. Further, epidemiology studies have shown that the percentage of hospitalized patients who are diagnosed with AKI is more than doubling every decade[9,22]. The most common cause of nephrology consultations in hospitalized patients remains to be AKI, and currently there is no treatment to accelerate repair[4,6]. New, effective therapeutics must be developed to assist in kidney repair and regeneration. There is evidence to suggest that the administration of endothelial progenitor cells (EPCs) may exert protective effects in AKI[23–25]. Analyses of endogenous renal repair after IR have also shown that hematopoietic stem cells exert paracrine effects on surviving cells that facilitate repair, an effect that may be mediated by extracellular vesicles which can transfer materials from cell to cell[26–28].

Cell Therapies in AKI

Ischemia/reperfusion injury causes significant vascular injury which leads to capillary loss. The administration of cells as therapies, specifically of endothelial lineage, have been studied as a possible approach. In a seminal study by Brodsky et al. in 2002, HUVECs were transplanted into mice post-IR which resulted in significant decrease in plasma creatinine and kidney injury scores, as well as significant return of peritubular capillary blood flow[29]. While this study does not use EPCs, it does show that endothelial dysfunction is a key trigger in the pathophysiological cascade resulting in AKI, and that targeting the repair of the endothelium post-IR is important to recovery.

Human EPCs are circulating cells which express similar markers as vascular endothelial cells, bind to the endothelium at sites of hypoxia or ischemia, and participate in vasculo- and angio-genesis[30]. Asahara et al. were the first to describe the isolation process and function of EPCs from human peripheral blood in 1997[31]. Briefly, cluster differentiation (CD) 34-positive and/or fetal liver kinase 1 (Flk-1; also known as vascular endothelial growth factor (VEGF) receptor 2) mononuclear blood cells were separated from whole human peripheral blood by magnetic microbeads and were plated on fibronectin plates with VEGF, bovine brain extract, and epidermal growth factor[31]. EPCs differentiate into two major populations, early out-growth – which express both stem cell and endothelial lineage markers – and late out-growth – which express only endothelial markers – and are more commonly known as endothelial colony forming cells (ECFCs)[32]. ECFCs are highly proliferative, are pro-angiogenic, anti-apoptotic, and have the potential to form vessels *in vivo*, qualities which remarkably characterize this cell type over other EPCs[23,24,30,32–34]. The homing of progenitor cells to the kidney after ischemia has been shown to play a vital role in mediating overall effects[35–39]. Further, the chemokine stromal cell-

derived factor (SDF) 1α, released post-ischemia, has a major role in the recruitment and retention of G protein-coupled protein receptor C-X-C chemokine receptor type 4 (CXCR4)-positive bone marrow-derived cells and endothelial progenitor cells[35,36,39].

Bone-marrow derived cells and endothelial progenitor cells such as ECFCs have been the focus of many AKI studies as they do not directly replace lost cells, but exert paracrine effects on the IR-injured vasculature to facilitate the reduction of the inflammation response, and do not require cell engraftment for repair and post-ischemic revascularization[2,27,28,32,40]. In previous studies, the Burns Lab has shown that isolated human cord blood ECFCs exerted protective effects against injury *in vivo*[25]. In 2015, ECFCs isolated from human umbilical cord blood and administered to male mice post-IR kidney injury were shown to significantly improve kidney function, defined by plasma blood urea nitrogen (BUN) and serum creatinine, as well as decreased inflammation, decreased apoptosis, and increased tubular and endothelial proliferation[25]. A subtype of extracellular vesicles (EV) isolated from ECFC conditioned media also demonstrated a similar protective effect in culture and in a IR murine model of AKI[6,25] **(Figure 1C)**. From this, in conjunction with hundred of other studies, EVs have emerged as important mediators of intercellular communication, which may mediate the protective effects of EPCs in animal models of IR injury.

Extracellular Vesicles: Background and Biogenesis

Extracellular vesicles (EVs) are a heterogeneous group of cell-derived, membrane-bound vesicles shed from healthy cells which play crucial roles in intercellular communication, physiologically and in disease pathogenesis[41,42]. EVs contain an assortment of biomolecules

including microRNA (miRNA), long coding RNA (lcRNA), messenger RNA (mRNA), proteins, lipids, and DNA which may be transferred from cell to cell. EVs are released by a cell into the extracellular space and can enter bodily fluids to reach downstream cells and tissues[42]. These EVs, separate from their stem or progenitor cells, have been shown to act as the mediators of the beneficial effects previously seen in cell therapies. EV therapies are advantageous over cell therapies as they reduce the risk of cell rejection defined by immune activation, the presence of differentiated cells, and neoplastic transformation. A major limitation of EV therapies is the ability be scaled-up as a therapeutic while maintaining their therapeutic potency. EVs are secreted at a relatively low rate in many cell types, which makes it difficult to separate enough to produce an effect[43].

Each type of EV follows a different pathway of production and may affect their target cell through different pathways **(Figure 2B)**. Exosomes (EX) are released into the extracellular space when multi-vesicular bodies (MVB) fuse to the cell membrane, and are classified by their diameter of 30-150 nm[44] **(Figure 2A)**. Microparticles (MP), or microvesicles, undergo membrane budding and have a diameter of 100-1000 nm[44]. With no scientific consensus for specific markers for each EV subtype, it is difficult to explicitly assign a particular biogenesis pathway for the EV sub-population being studied. EV populations in the literature, as described by the International Society of Extracellular Vesicles (ISEV), are therefore described using operational terminology, based on size, biochemical composition, or cell origin[45]. In the following studies, tumor suppressor gene (TSG)-101$^+$ and CD81$^+$ ECFC-derived small EVs are referred to as ECFC-derived exosomes, while TSG-101$^-$ and CD81$^-$ ECFC-derived medium/large EVs are referred to as ECFC-derived microparticles.

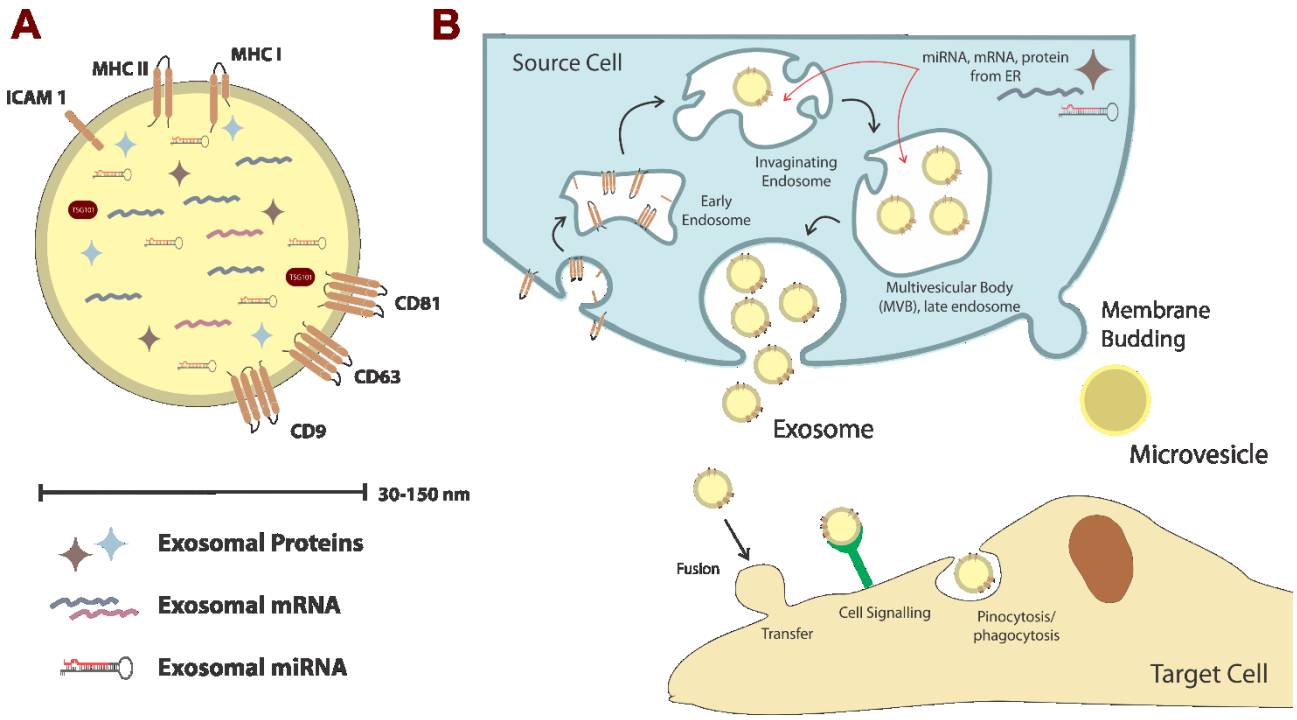

Figure 2 | Exosome Biogenesis. (a) Exosomes contain specific proteins, mRNA, and miRNA, as well as surface proteins inherited from their parent cell. (b) Exosomes originate from endosomes; endosomes are vesicles which originate from endocytosis of materials of the extracellular fluid. Endosomes are processed and packaged by the parent cell and are released into the extracellular fluid. From here, there are a variety of pathways through which they can interact with the target cell, including cell signalling, pino- or phago-cytosis, and fusion/transfer.

Extracellular Vesicles: Therapeutic Applications

Exosomes have received the most attention in the growing EV field as they can be released by a variety of cell types and have been implicated in immune responses and pathological conditions[32,46–50] **(Figure 2A)**. Exosomes may act upon a target cell through three different mechanisms: i) exosomes may activate a signalling pathway by binding a receptor on the surface of the target cell, ii) they may transfer proteins, nucleic acids, or other signalling molecules through membrane fusion, or iii) they may enter the cell through endo-, phago-, or macropinocytosis and have their content processed by the target cell[51–53].

Various populations of EVs, including those derived from endothelium and their progenitors, have been reported in the literature to attenuate IR injury. In 2012, Cantaluppi et al. intravenously delivered a mixture of large and small EVs derived from peripheral blood EPCs to Wistar rats after right nephrectomy and 45-minute left pedicle clamping. They were able to demonstrate that their EV population increased tubular proliferation, increased angiogenesis, decreased cell apoptosis, and less leukocyte infiltration[47]. Following the animals long-term, they were able to show reduced serum creatinine, tubulointerstitial fibrosis, and glomerulosclerosis in the EV-treated group compared to untreated, suggesting a slowed progression toward CKD[47]. In vitro, hypoxia significantly enhanced EV internalization, suggesting that internalization may be enhanced by injury[47]. The same group, led by G. Camussi, also demonstrated the same effects using mesenchymal stromal cell (MSC)-derived EVs in male severe combined immune deficiency spontaneous mutation (SCID) mice after cisplatin-induced AKI. They followed up this study in 2014, where they analyzed the biodistribution of intravenously injected MSC-derived EVs in male CD1 nude mice after glycerol-induced AKI. In this study, they show the ability of EVs to specifically accumulate in injured kidneys after 5 hours and were maintained up

to 24 hours after injection[54]. They speculate that MSC-derived EVs may exploit the same receptor-mediated interactions MSCs use to accumulate to the site of injury, although they present no hypothesis or data by which interactions.

Other studies have also shown similar beneficial effects using EVs from renal cells and their progenitors. After demonstrating success attenuating IR injury by infusing normal adult rat renal cells in female SD rats after bilateral renal clamping for 50 minutes, Dominguez et al. have also shown that EVs derived from adult rat renal tubular cells improved renal damage, 4-hydroxynanoneal adduct formation, neutrophil infiltration, fibrosis, and microvascular pruning. Further, a 2017 study from the Camussi group also showed that glomerular MSCs, along with their EVs, were able to improve kidney function and reduce damage post 35-minute renal clamping and right nephrectomy[55]. By contrast, $CD133^+$ progenitor cells isolated from cortical tubules and their EVs were unable to attenuate injury.

Upon comparative analysis of the contents of ECFC-derived exosomes and microparticles, it has been shown that microRNA-486-5p (miR-486-5p) is almost 300-fold more abundant in ECFC-derived exosomes than microparticles[6]. It has also been recently found that human bone marrow-derived mesenchymal stromal cell-derived exosomes also contain highly enriched miR-486-5p and protect against glycerol-induced AKI in mice[56,57]. As miR-486-5p has been linked to activate Akt and the cell-survival pathway, further studies have focused on the role of this specific miRNA in AKI[58,59].

Role of micro-RNA transfer by exosomes

miRNAs are small RNA molecules of approximately 18-22 nucleotides which are found to be abundant in extracellular vesicles, and are widely known for their role in the regulation of gene expression at the post-transcriptional level[60–62]. miRNAs are generated by the nucleus as primary pri-miRNAs, split by Drosha to form precursor pre-miRNA, then exported from the nucleus as mature miRNA[63]. Mature miRNA can then be processed by the target cell to lead to the degradation of one or more mRNA(s) and/or suppression of protein translation by interacting with the 3'-untranslated region (UTR) of mRNA[64]. Further, one gene can be regulated by several miRNAs, and one miRNA can regulate several genes[63,65]. In disease states, miRNA expression patterns can be altered, which can contribute to pathogenesis[64]. For example, miR-486-5p has been recently found to be downregulated in glomeruli and proximal tubules in kidney pathologies such as diabetic nephrophathy, focal segmental glomerulosclerosis, IgA nephropathy, and membranoproliferative glomerulonephritis, suggesting a protective role which is attenuated when not present[66]. miRNAs have also been implicated as possible therapeutics and potential biomarkers for disease[60,67].

EVs, whether circulating endogenous or administered exogenously can selectively transfer various miRNAs to specific target cells to regulate both protein expression and signalling cascades[6]. Circulating exosomes are shown as key mediators of intercellular transfer of uniquely packaged miRNA, a process which is regulated by ceramide, and its biosynthesis which is regulated by neutral sphingomyelinase 2 (nSMase2)[68,69]. Further, miRNAs may be selectively incorporated into EVs, as studies have shown many miRNAs to be enriched within miRNAs isolated from EVs relative to their parent cell[70]. Exosome-mediated transfer of miRNA has been

defined as a novel therapeutic technology in many disciplines such as immunotherapy, cardiovascular disease, ischaemic retinopathy, and cancer[52,62,70–72].

A study by Collino et al. shows that a global downregulation of miRNA by Drosha knockdown in MSCs can inhibit the efficacy of renal recovery by MSC-derived EVs after rhabdomyolysis-induced AKI[56]. In these animals, miR-483–5p, miR-191, miR-28–3p, miR-423–5p, miR-744, miR-129–3p, miR-24, and miR-148a families were found after MSC-EV treatment, and are associated with kidney repair and mitogen activated protein kinase (MAPK) signaling. In murine kidney IR, it has been shown that EPC-derived EVs decreased serum creatinine, BUN, renal cell apoptosis, and leukocyte infiltration, as well as increased tubular cell proliferation and angiogenesis[47]. Further, depletion of EPC-derived exosomal miR-126 and miR-296 by specific antagomiRs suppressed post-injury recovery[47]. miR-126-based therapies have been widely studied in the context of IR for its proliferative and pro-angiogenic properties[67]. miR-21 has also been implicated in mediating the effect of delayed ischaemic preconditioning against future IR events[73]. As a result of the success of EVs and their miRNA as therapeutics, studies with miRNA as therapeutic solutions are extending outside the EV realm to use nanotechnology to deliver endogenous miRNA in situ. The use of miRNA alone, or miRNA packaged in a synthetic vesicle, are becoming more popular as therapeutics in research.

The Burns Lab has demonstrated that post-IR protection and recovery by ECFC-derived exosomes was attenuated after the inhibition of exosomal miR-486-5p with antagomiR to miR-486-5p[6]. Therefore, the transfer of miRNA mediated by EVs may be responsible for much of the reparative activity seen by the administration of EVs post-injury. In recent studies, the Burns Lab has shown that ECFC exosomes, which are enriched with miR-486-5p, act by targeting the 3’

UTR and decreasing *phosphatase and tensin homolog* (PTEN) expression, stimulating the phosphorylation of proteins involved in the Akt pathway and subsequently blocking apoptosis[6].

Targeting of EVs to ischemic kidney

ECFC-derived exosomes play a vital role in the transfer of miR-486-5p to injured tissues, and therefore the *in vivo* localization of these exosomes is an important step in determining their therapeutic capacity. Little is known concerning EV biodistribution, and even less concerning the biodistribution of endothelial cell-derived exosomes specifically in the AKI model.

EVs, much the same as cell types, can accumulate in injured tissue due to increased permeability at the site of injury, as well as through receptor mediated interactions[54]. The transduction of a signal, however, is the responsibility of cell receptors and adhesion molecules[43,74]. EVs and their parent cell share many of the same membrane receptors, proteins, and ligands[42,75]. Targeting of specific EVs requires migration and adhesion, which is mediated by chemokines and receptors[35]. SDF-1α, a C-X-C type chemokine and a ligand for CXCR4, is a well known and widely expressed chemokine involved in vascular repair and retention of endothelial stem cells to the site of injury[35,76]. After vascular injury, such as limb ischemia, toxic liver damage, total body irradiation, and AKI, it has been found that SDF-1α is increasingly secreted from injured tissues[36,37,77–80]. CXCR4 is the most prevalent chemokine receptor found in endothelial cells[81]. SDF-1α has been shown to increase the adhesion and migration of EPCs to injured tissue[82]. E-selectin, another adhesion molecule found to regulate endothelial progenitor homing, is produced by endothelial cells post-injury to attract ECFCs[35,83]. Studies have found that E-selectin and the SDF-1α/CXCR4 axis exist co-operatively to assist in the adhesion and migration of ECFCs to

the site of injury[35]. A potential mechanism for homing of ECFC-derived exosomes could therefore include a variety of pathways, including SDF-1α/CXCR4.

The comparison between male and female differences in AKI studies are gaining interest in recent years. In 2014, Kang et al. showed that female mice were more resistant to bilateral renal clamping IR AKI compared to male mice[84]. It has been long studied and reviewed that male mice are more prone to AKI, but Kang et al. showed that estrogen was the mediator of this protective effect in female mice. Historically, the Burns Lab studied exclusively male mice for this reason: IR injury was easier to produce in male mice. Whether female mice respond to therapies against IR is unknown.

RESEARCH PROJECT

Studies have shown that ECFCs do not directly replace lost cells but exert paracrine effects on the IR-injured vasculature to facilitate the reduction of the inflammation response, and do not require cell engraftment for repair and post-ischemic revascularization. Paracrine factors, such as ECFC- derived exosomes and their enriched miR-486-5p, have been attributed to their therapeutic potential in ischemia/reperfusion injury. To evaluate whether ECFC-derived exosomes represent a therapeutic tool for AKI, the mechanism of action of ECFC-derived exosomes must be determined, and it is essential to investigate *in vivo* their biodistribution and recruitment mechanisms within the injured kidneys and other tissues. Further, stem cell therapies rely on targeting pathways involving chemokines and receptors to home to the site of injury, although EVs such as exosomes lack flexibility and motility as seen in their parental cells. Whether a chemokine axis is utilized by ECFC-derived exosomes, such as the SDF-1α/CXCR4 axis used in ECFC-cell targeting to the ischemic kidney, is unknown.

The ability of exosomes to be scaled-up as a therapeutic while maintaining their therapeutic potency is unknown. Therefore, investigation into other methods of administration to achieve similar effects, such as the administration of encapsulated miR-486-5p, must be performed before continuing to push forward towards a clinical setting.

Male mice have historically been the only sex of study for AKI therapies. Whether female mice respond to the delivery of miR-486-5p alone or via enriched exosomes remains unknown. A differential investigation into the therapeutic potency of ECFC-derived exosomes and encapsulated miR-486-5p was performed in order to determine variability between the two sexes. This study must be performed before either therapy can be pursued in a clinical setting.

The aim of the present study was to investigate the biodistribution and homing of ECFC-derived exosomes, determine the therapeutic potential of ECFC-derived exosomes and miR-486-5p, and determine sex differences in response to treatments, in immunocompetent FVB mice with AKI. With optical imaging, labelled exosomes were tracked during their systemic travel and eventual target. By in vitro assay, immunoblotting, and microscopy, study into the targeted site and mechanisms was performed. Investigation into the targeting and transfer mechanisms of ECFC-derived exosomes was done. The effect of protective miR-486-5p alone was determined, as well as any variability between the sexes. Results may help explain how ECFC-derived exosomes direct their proliferative and anti-apoptotic effects towards both local endothelium and tubular epithelium in the murine model of ischemic AKI.

Objectives

Aim 1 | Investigate the biodistribution and targeting of ECFC-derived exosomes and localization of miR-486-5p after delivery to mice with ischemia/reperfusion AKI.

Aim 2 | Study the targeting and transfer mechanisms of ECFC-derived exosomes and miR-486-5p to ischemic tissue and investigate the role of the CXCR4/SDF-1α axis.

Aim 4 | Investigate the effect of direct administration of encapsulated miR-486-5p to male and female mice with ischemia/reperfusion AKI and compare therapeutic efficacy to ECFC-derived exosomes. Determine sex differences in response to treatment.

Hypotheses

Hypothesis 1 | ECFC-derived, miR-486-5p-enriched exosomes will distribute preferentially to the kidney, and not to other organs after ischemia/reperfusion AKI. Without injury, exosomes will have a non-specific biodistribution. As ischemic injury mainly affects the proximal tubule S3 segment, in addition to the endothelium, ECFC-derived exosomes will localize to renal endothelial cells and tubular epithelium at the corticomedullary junction.

Hypothesis 2 | CXCR4, present on ECFC-derived exosomes, and SDF-1α, released from the ischemic kidney, will mediate the targeting of exosomes to the site of injury. The inhibition of CXCR4 or SDF-1α will attenuate the targeting of exosomes and the therapeutic potential.

Hypothesis 3 | Administration of miR-486-5p alone will be associated with the localization to the kidney, but not preferentially as no targeting or mediation is present. If miR-486-5p alone localizes to the kidney, its protective and reparative properties will be comparable to exosomes. Male and female mice will both respond to ECFC-derived exosomes and miR-486-5p alone equally, however, the level of injury in female mice will be less than as seen in male mice. Therefore, female mice will require less repair than male mice.

METHODS

Cell culture

Endothelial Colony Forming Cells (ECFCs) were isolated from human umbilical cord blood units obtained at The Ottawa Hospital following written informed consent in accordance with protocols approved by the Ottawa Hospital Research Ethics Board, as described[25,35]. Briefly, mononuclear cells (MNCs) from human umbilical cord blood were isolated by Ficoll density gradient centrifugation. 1.0 x 10^7 MNCs were plated on Costar Cell-BIND Surface plates (Corning, Corning, New York, USA) with Endothelial Basal Cell Growth Medium 2 with SingleQuots supplements (EGM-2) (Lonza, Basel, Switzerland) and 10% Fetal Bovine Serum (FBS). Non-adherent cells were discarded with every media change. Then, colonies with cobblestone morphology which appeared between days 9 and 16 were isolated and re-plated with the same conditions. Flow cytometry was used to phenotype ECFCs using the CyAn ADP9 analyser (Beckman Coulter Inc, Brea, CA, USA) and interpreted using Kaluza software (Beckman Coulter Inc)[35]. Human Umbilical Vein Endothelial Cells (HUVECs) were obtained from the American Type Culture Collection (Manassas, VA, USA). Isolated ECFCs (passages 3-5) and HUVECs (passages 3-7) were cultured in EGM-2 and 10% FBS. 2.1 x 10^6 cells were seeded onto T-75 BioLite Cell Culture Treated Flasks (Thermo Fisher Scientific, Waltham, Massachusetts, USA) at 37ºC and 5% CO_2 in a humidified incubator (Thermo Fisher Scientific). Media was changed the next day, and every other day following. In cell culture experiments, cells were used at confluence. In some experiments, cells were exposed to 24 hours of hypoxia (0.5% O_2) in the H35 Hypoxystation HypO2xygen humidified hypoxic chamber (Don Whitley Scientific, Shipley, West Yorkshire, UK).

Exosome and microparticle separation

Exosomes and microparticles were isolated from ECFC conditioned medium by serial centrifugations, as described with modification[6,85,86] after 24-48 hours of culture in vesicle-depleted FBS (Wisent, Saint-Jean-Baptiste, QC, Canada). After an initial centrifugation to discard cells and debris (2500 x *g* for 10 min), microparticles were isolated after two centrifugations (10,000 x *g* for 30 min and 20,000 x *g* for 20 minutes) at 4ºC using a type SS-34 rotor in a Sorvall RC6 Plus Centrifuge (Thermo Fisher Scientific). The supernatant was then used to pellet exosomes after two centrifugations at 100,000 x *g* for 90 min at 4ºC using type 45-Ti rotor in the Optima L-100 XP Ultracentrifuge (Beckman Coulter, Inc) and 100,000 x *g* for 90 min at 4ºC using type TLA-55 rotor in the Optima MAX Ultracentrifuge (Beckman Coulter, Inc). Exosome and microparticle fractions were then diluted in sterile PBS and protein was quantified using Bio-Rad DC Protein Assay (Bio-Rad Laboratories, Hercules, California, USA) and Biotek ELx808 Absorbance Reader & KC4 Data Analysis (BIO-TEK Instruments, inc. Winooski, Vermont, USA) and are expressed as μg/μL. Microparticles were used as controls in exosomal characterization.

Nanoparticle tracking analysis

Size and purity investigation of extracellular vesicle preparations was performed by nanoparticle tracking analysis (NTA) with the ZetaView instrument (Particle Metrix, Meerbusch, Germany). NTA determines the size of particles based on Brownian motion and was used in the analysis of vesicles[87]. Diluted extracellular vesicle preparations in ice-cold filtered and sterile PBS (1:100) were tracked. A frame rate of 30 frames per second and shutter speed of 70 ms was used with a brightness of 30 lumens.

Kidney Ischemia/Reperfusion Model

Isoflurane was used to anesthetize 7-10-week-old male and female FVB mice (Charles River, St Constant, QC, Canada). Baseline weight was established, and buprenorphine was given 1-hour pre-surgery. Ophthalmic ointment was given to protect the cornea from desiccation. 0.5-1 mL warmed saline was injected subcutaneously as fluid therapy. On a warm water blanket, the dorsal area was shaved using an electric clipper. The surgical site was prepared using a chlorhexidine scrub and ethyl alcohol. 1.5 cm bilateral incisions were made to expose the kidneys, followed by bilateral renal artery clamping for 30 min, and then release of the microclamps, as described[88,89]. Tail vein injection of either vehicle (200 μL PBS), exosomes (20 μg in 200 μL PBS) or mimic-invivofectamine complex (20 μg in 200 μL PBS) was then performed, at the time of reperfusion. The incisions were closed with sutures and/or silk stiches when required. Hot beads were used to sterilize the instruments between surgeries. Animal wellness was assessed, and buprenorphine was given every 12 hours post-surgery. For further experiments, mice were euthanized via CO_2 narcosis, followed by decapitation. In optical imaging experiments. Mice were euthanized by cervical dislocation while anesthetized, followed by the removal of all organs. Protocols were approved by the Animal Ethics Committee at the University of Ottawa and were performed according to the recommendations of the Canadian Council for Animal Care[90].

Immunoblots

Exosomes, microparticles, or kidney protein lysate were suspended and homogenized in radio immunoprecipitation assay (RIPA) buffer with a protease and phosphatase inhibitor cocktail (Aprotinin, Bestatin, E64, and Leupeptin against proteases, and sodium fluoride, sodium pyrophosphate, β-glycerophosphate, and sodium orthovanadate against phosphatases; Cell Signaling, Danvers, MA, USA). Homogenized tissue was then incubated at 4ºC on a shaker for 2

hours, followed by a 20-min centrifugation at 4ºC and 13,400 x g. Supernatant or exosomal and microparticle suspensions were combined with 6x Laemmli loading buffer (375mM Tris-HCl (pH 6.8), 9% SDS, 50% glycerol, 9% beta-mercaptoethanol, 0.03% bromophenol blue; Alfa Aesar, Haverhill, Massachusetts, USA). Samples were boiled at 100ºC for 5 min, cooled on ice, and loaded onto 10% sodium dodecyl sulfate polyacrylamide (SDS-PAGE) gels. Molecular weight marker (Precision Plus Protein Dual-Colour Standards, Bio-Rad Laboratories) was used in all gels. Gels ran at 150 V for 1 hour in running buffer. Proteins on the gel were transferred to nitro-cellulose membranes using the Bio-Rad Criterion system for 1 hour at 100 V. The membranes were blocked with a 5% milk solution in tris-buffered saline-polysorbate 20 (TBS-T) at room temperature for 1 hour with gentle shaking. Membranes were washed 3 times for 5 min each with TBS-T. Membranes were then incubated with antibodies against Tumor Susceptibility Gene (TSG) 101 (1:1000, Abcam Inc, Toronto, ON, Canada) and CD81 (1:1000, Abcam Inc) in TBS-T for 16 hours at 4ºC. Washed membranes were then incubated with horseradish peroxidase-conjugated secondary antibodies (1:2000, Cell Signaling) and incubated at room temperature for 1 hour. Membranes were then washed 3 times at 5 min with TBS-T. Membranes were incubated for 1 min in Amersham enhanced chemiluminescence reagents (GE Healthcare, Buckinghamshire, UK). Blots were developed using Konica Minolta SRX 101A Tabletop Medical Film Processor (Konica Minolta Medical Imaging USA, Inc., Wayne, NJ, USA) or Alpha Innotech FluorChem HD2 (Alpha Innotech, San Leandro, CA, USA) corrected for loading controls, and analyzed using ImageJ software (NIH, Bethesda, MD, USA).

miRNA isolation and real-time PCR

Total miRNA from extracellular vesicle preparations or homogenized tissue was extracted using the miRNeasy Micro Kit (Qiagen Inc., Toronto, ON, Canada), according to the manufacturer's

protocol. Isolated RNA was quantified using Spectronic Genesys 5 Spectrophotometer (Spectronic Instruments, Fitchburg, WI, USA). TaqMan MicroRNA Reverse Transcription Kit (Life Technologies, Inc., Carlsbad, CA, USA) was used to create cDNA. Real-time PCR reactions were performed in an Applied Biosystems 7000 sequence detection real-time PCR system (Applied Biosystems, Foster City, CA, USA) as described[6]. Both reverse transcription and real-time PCR experiments used primers specific to hsa-miR-486-5p (5' UCCUGUACUG AGCUGCCCCGAG 3') and mamm-U6 (5' GTGCTCGCTTCGGCAGCACATATACTAAAAT TGGAACGATACAGAGAAGATTAGCATGGCCCCTGCGCAAGGATGACACGCAAATTC GTGAAGCGTTCCATATTTT 3') (Thermo Fisher Scientific). The relative amount of miRNA to U6 RNA was expressed using the 2-ΔΔCt method[91].

Optical Imaging

Biodistribution of exosomes after tail vein injection was studied using the *In Vivo* Imaging System (IVIS; Perkin Elmer, Waltham, MA, USA) spectrum as described[44]. IVIS spectrum is an instrument that contains a high-sensitive charged coupled device (CCD) camera, which enables both fluorescence and luminescence measurements[44,92]. Exosomes were labeled with 1.7 µL 1,1'-Dioctadecyl-3,3,3',3'-Tetramethylindotricarbocyanine Iodide (DiR) dye and incubated at room temperature for 15 minutes, followed by a centrifugation at 100,000 x g for 90 minutes as per the manufacturer. Mice either received a vehicle (100 µL phosphate buffered saline; PBS), DiR dye alone (1.7 µL in 100 µL PBS), or 100 µL of DiR-dyed exosomes at the time of reperfusion by tail vein injection. Sham mice were subjected to surgery without renal vascular clamping. Fluorescence imaging used the excitation filter at 710 nm and the emission filter at 760 nm. The intensity of the region of interest (ROI) was drawn freehand and was plotted as photons/second/centimeter/ steridian (p/s/cm^2/sr). The mice were sacrificed, and organs were

harvested for further fluorescence analysis. Background fluorescence obtained from mice that had not been infused with DiR or exosomes was subtracted from experimental values. Images and data were obtained using IVIS Spectrum software (Living Image 4.3.1; Perkin Elmer).

Isolation of kidney cortices, medullae, proximal tubules, and glomeruli

24 hours post-reperfusion, kidneys were removed, decapsulated, and kept in ice-cold PBS until isolations. Cortices and medullae were surgically separated. Further dissection of cortices was performed to isolate proximal tubules and glomeruli. Cortices were minced in a glass dish kept on ice. Minced tissue was suspended in a solution containing: 105 mM NaCl, 24 mM $NaCO_3$, 5 mM KCl, 1.5 mM $CaCl_2$, 1.0 mM $MgSO_4$, 2.0 mM NaH_2PO_4, 5.0 mM glucose, 1.0 mM alanine, and 10.0 mM HEPES, pH 7.4, as well as 0.1% collagenase (type IV, Millipore Sigma). The tissue suspension was bubbled with 95% O_2-5% CO_2 for 30 min in a 37 °C water bath. After digestion, the kidney cortex suspension was strained through a 250-µm brass sieve (mesh no. 60, Newark Wire Cloth, ESBE Scientific, Markham, ON, Canada) and flow-through was centrifuged for 1 min at 1,000 x g. The pellet was then resuspended in the same digestion solution without collagenase and centrifuged for 1 min, repeated once. The tissue was then strained through a 106-µm brass sieve (mesh no. 150). Proximal tubules were microdissected from the tissue which did not pass through the sieve, and glomeruli were microdissected from the tissue which passed through. The purity of the tubular and glomerular preparations (>99%) was determined by light microscopy.

Isolation of kidney endothelial cells

24 hours post-reperfusion, kidneys were removed, decapsulated, and kept in ice-cold PBS until isolations. Kidneys were dissected into quarters and added to a GentleMACS C tube (Miltenyi

Biotech) along with the enzyme mixture in MACS Multi Tissue Dissociation Kit 2 (Miltenyi Biotech). C tubes with digestion mixture were then placed on the GentleMACS Dissociator (Miltenyi Biotech) which ran at 37ºC for 31 min. After the digestion, the single cell suspension was passed through a 100 μm strainer and incubated with $CD31^+$ microbeads for 20 min at 4ºC, to bind the endothelial cells. After incubation, the labeled suspension was applied to LS columns (Miltenyi Biotech) on a separator magnet, washed, and flushed out in 5 mL of buffer. To verify the contents of the $CD31^+$ rich fraction, some cells were subjected to primary culture and immunocytochemistry with CD31 antibodies (Abcam Inc).

Histology

Mice were sacrificed twenty-four hours post-reperfusion and kidneys were fixed in 4% formalin, dehydrated, embedded in paraffin, and stained. Tissues were cut into sections (5 μm thick) and stained with hematoxylin and eosin (H+E) and periodic acid-Schiff (PAS). All histological analyses were performed in a blinded manner by a renal pathologist (Dr. Alexey Gutsol). The extent of tubular injury was semi-quantified using a scoring system ranging from 0 to 4[25,93,94]. Briefly, scoring was performed by randomly scanning each section for the outer stripe of the outer medulla (at least 40 fields at x200 magnification). Signs of tubular injury were identified as tubular dilatation, loss of brush border, nuclear loss, sloughing of tubular cells, or cast formation. The scoring system was as follows: 0 indicates no tubular injury; 1,<25% of tubules injured; 2, 26% to 50% of tubules injured; 3, 51% to 75% of tubules injured; and 4, >75% of tubules injured. Neutrophil infiltration was assessed on kidney sections by quantitation of myeloperoxidase staining (polyclonal rabbit myeloperoxidase antibody, 1:200, Neomarker, Fremont, CA, USA)[6]. Tubular apoptosis was assessed using the terminal deoxynucleotidyl transferase-mediated dUTP nick-end labeling (TUNEL) Apoptosis Detection Kit (Genscript,

Piscataway, NJ. USA), according to manufacturer's instructions, and expressed as the number of TUNEL-positive nuclei per corticomedullary field, as described[29]. Images were acquired at room temperature on a Zeiss Imager A1 with a Zeiss AxioCam HRc using Axiovision version 1.6 (Carl Zeiss AG, Oberkochen, Germany).

Immunohistochemistry

Presence of megalin was evaluated in the corticomedullary regions of kidney sections. After deparaffinization, kidney sections were placed in sodium citrate (pH 6.0) and microwaved for 20 min for antigen retrieval. Sections were treated with 0.3% H2O2-H2O for 30 min, to inhibit endogenous peroxidase activity. Sections were blocked in 10% goat serum for 30 min and incubated with antibodies to megalin (1:500; Santa Cruz Biotechnology, Inc., Dallas, TX, USA) overnight at 4^{o}C. Sections were probed with Alexa 594 (Molecular Probes, Burlington, ON, Canada). For immunofluorescence microscopy, slides were mounted using Vectashield mounting medium (Vector Laboratories, Burlingame, CA, USA). 10 images were acquired at room temperature on a Zeiss Axioscop2 with a Zeiss AxioCam using Axiovision 3.1 (Carl Zeiss AG). Areas of red fluorescence were measured after background subtraction and counted as the sum of intensities per field area of view.

miRNA-invivofectamine complex preparation

Invivofectamine (Invitrogen) was used according to the manufacturer's protocol. Thus, miRNA stock solution containing miR-486-5p or scrambled miRNA (2.4 μg/μl) was combined with complexation buffer (25 μl) to create a 1.2 μg/μl solution. This was then added 1:1 to the invivofectamine 3.0 reagent (Thermo Fisher Scientific), vortexed, and incubated at 50^{o}C for 30 minutes. After complexation, the complex preparation was diluted 6-fold in sterile PBS.

Localization of PKH26-labeled exosomes

ECFC-exosomes were labeled with PKH26, a red lipophilic membrane dye (Millipore Sigma), according to the manufacturer's instructions. Briefly, the exosomal pellet was resuspended in 500 uL of Diluent C (from the manufacturer), and 500 uL prepared dye (0.4% dye v/v in Diluent C) was added. The sample was incubated for 10 min. To stop the reaction, 8 mL of 10% vesicle depleted FBS in EBM-2 media was added. Labeled exosomes were pelleted, resuspended in PBS, and stored at -80ºC. 20 μg PKH26-labeled exosomes were delivered via tail vein to mice with or without ischemia reperfusion injury. Within 30 min post-injection, mice were euthanized, and the lungs, heart, liver, spleen, and kidneys were extracted. Tissue was embedded in optimal cutting temperature (OCT) compound and frozen in liquid nitrogen. 20 μm sections were cut using the Leica CM3050 S freezing microtome (Leica Biosystems, Wetzlar, Germany). Sections were then fixed in in 3% paraformaldehyde for 10 min, and mounted in VectaShield (Vector Labs, Burlingame, CA, USA). Sections were analyzed in a blinded manner by a renal pathologist (Dr. Alexey Gutsol) using a Zeiss AxioObserver Z1 fluorescent microscope (Carl Zeiss AG).

Internalization of exosomes by HUVECS

PKH26-labeled ECFC-exosomes were administered to normoxic or hypoxic HUVECs in culture and cytoplasmic fluorescence was measured after 6 hours. In some groups, HUVECs were treated with 100 μM plerixafor (AMD3100, Millipore Sigma), a CXCR4 bicyclic reversible inhibitor, 10 μg/mL neutralizing antibody against SDF-1α (R&D Systems, Minneapolis, MN, USA), or 10 μg/mL of a control IgG isotype antibody (R&D Systems).

Exosomes and the transfer of miR-486-5p

In some experiments, Label IT siRNA Tracker Cy3 (Mirus Bio, Madison, WI, USA) was used to label pre-miR-486-5p before being transfected into ECFC cells using Lipofectamine RNAiMAX Reagent (Invitrogen). After 24 hours incubation at 37°C, conditioned medium containing ECFC-exosomes with Cy3-labeled miR-486-5p was applied to cultured HUVECs for 16 hours. GW4869 (10 μM, Cayman Chemical, Ann Arbor, MI, USA) was used in the ECFC culture to inhibit exosome release[69,71], while 5-(*N*-Ethyl-*N*-isopropyl) amiloride (EIPA; 10 μM, Sigma) was used in the HUVEC culture to inhibit micropinocytosis[72,95,96].

SDF-1 Alpha Assay

Secreted SDF-1α in conditioned media from cultured HUVECs was quantified using an ELISA kit (RayBiotech, Norcross, GA, USA) following the manufacturer's guidelines. Briefly, 100 μL of sample was added to microplate wells coated with anti-human SDF-1α, followed by a 2.5-hour incubation at room temperature. Following incubations with a biotinylated anti-human SDF-1α antibody and HRP-conjugated streptavidin, a 3,3,5,5'-tetramethylbenzidine (TMB) buffer solution was applied, incubated for 30 min, followed by 0.2 M sulfuric acid to stop the reaction. The concentration of SDF-1α was then calculated by reading the absorbance of the microplate at 450 nm.

Plasma Biochemistry

Plasma creatinine and BUN levels were analyzed by IDEXX Laboratories (Markham, ON, Canada).

Caspase-3 Activity Assay

Caspase-3 activity was measured using the Caspase-3 Assay Kit (Fluorometric) (Abcam Inc). Briefly, 5 mg of kidney tissue was homogenized in 300 µL of Cell Lysis Buffer. Using BioRad DC Protein Assay, protein concentration was standardized at 5 µg/µL. 100 µg of sample was added to a 96-well plate, and 50 µL of Reaction Buffer-Dithiothreitol (DTT) was added to each sample. 5 µL of an 1mM DEVD-7-amino-4-trifluoromethyl coumarin (AFC) substrate was added to the sample and the plate was incubated at 37ºC for 4 hours. Free-AFC was read at 400-nm excitation and 505-nm emission. Activity was recorded as relative fluorescence units.

Statistical analysis

Results are expressed as means ± standard error of the mean and were analyzed using a one- or two-way analysis of variance with a Bonferonni post-test as appropriate, or students t-test. Statistical analyses were performed using GraphPad Prism 5.0 (GraphPad Software, Inc., San Diego, CA, USA). $p < 0.05$ was considered significant.

RESULTS

Characterization of ECFC-derived exosomes

ECFCs were isolated from human umbilical cord blood, grown in culture, and characterized by flow cytometry[35]. ECFC exosomes were isolated from ECFC cultured media through a differential centrifugation technique after 24-48 hours of incubation.

To determine the purity of the exosome separation, immunoblotting was used to classify exosomes from larger extracellular vesicles, such as microparticles. Two exosomal markers, TSG101 and CD81 were used. TSG101 is an exosomal protein which has a role in the secretion of exosomes, and CD81 is a membrane-bound tetraspanin known to play a role in protein trafficking and sorting to exosomes[97]. By immunoblot, both TSG101 and CD81 were present in the exosome samples, but not in the microparticle fraction ($p<0.001$ vs MP, $n=3$) **(Figure 3).**

In some studies, both DiR and PKH26 dyes were used to visualize exosomes. To verify that the labeling of exosomes with either DiR or PKH26 did not impact exosome size, NTA was used. Fresh exosomes had a mean diameter of 88 nm, and the size distribution of exosomes after either dyeing procedure remained unchanged **(Figure 4)**. All size distributions measured using NTA were consistent with the accepted literature definition of exosomes in which exosomes are vesicles with a diameter of 30-150 nm. All preparations showed that more than 80% of the vesicles were within the accepted size range.

To verify that the contents of the isolated ECFC exosomes were similar to those previously reported, a PCR experiment was performed on isolated miRNA from both ECFC and HUVEC exosomes to determine whether the relative levels of miR-486-5p were consistent and much

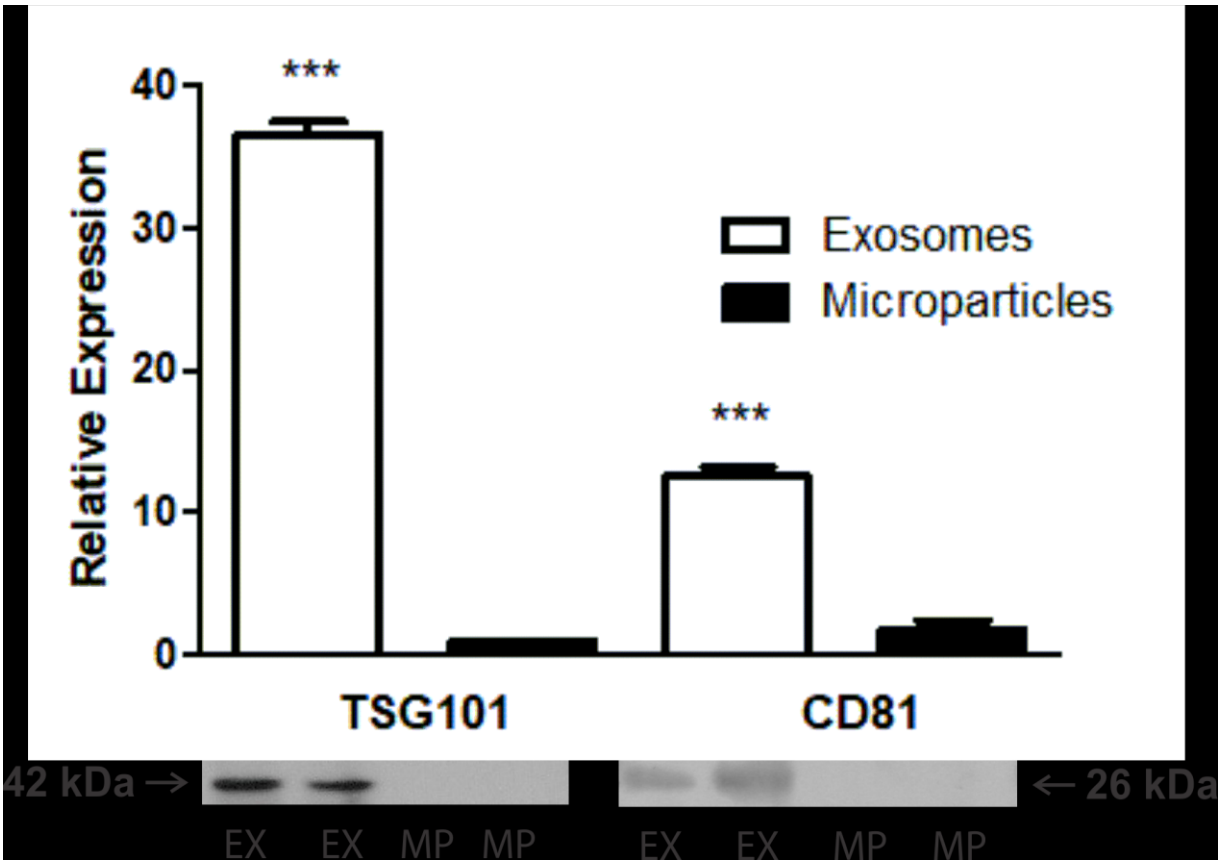

Figure 3 | ECFC-derived exosomes, but not microparticles, express both TSG101 and CD81. Graph depicts immunoblot analysis for exosomal markers Tumor Susceptibility Gene 101 (TSG101, left) and Cluster Differentiation 81 (CD81, right) present in ECFC-derived exosomes (EX), but not in ECFC-derived microparticles (MP). Representative immunoblots are shown below. Data are mean ± SEM; n = 3. ***P<0.001 vs MP.

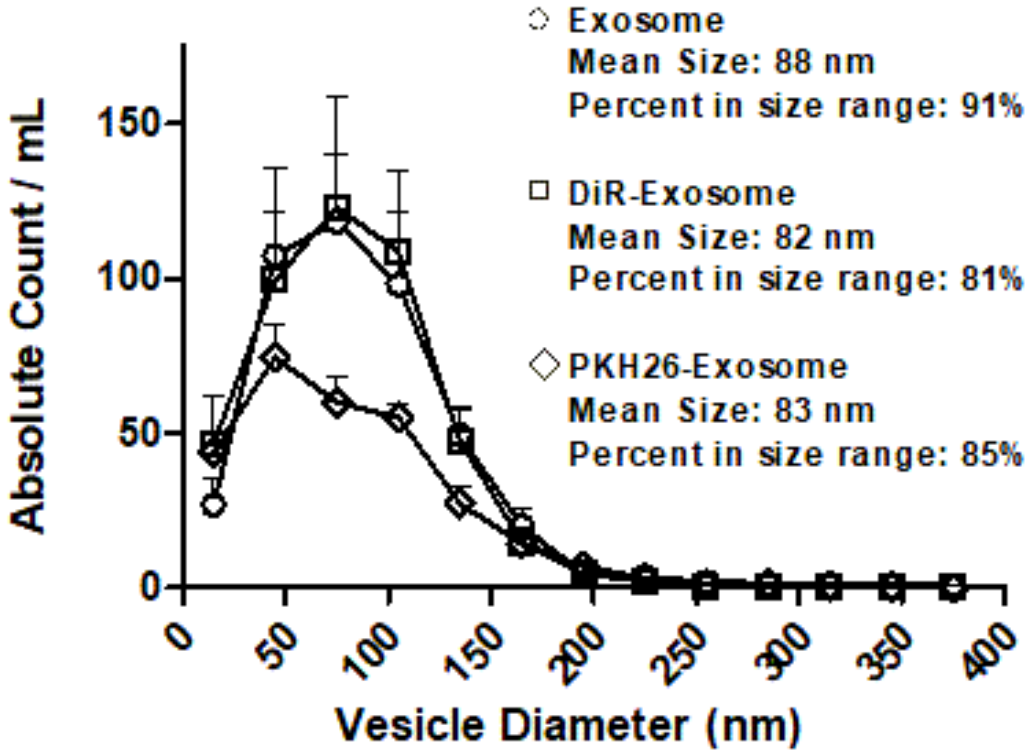

Figure 4 | DiR- and PKH-labeled exosomes, as well as unlabeled exosomes, have similar size distributions by nanoparticle tracking analysis. Nanoparticle analysis shows the absolute count and size distribution of vesicles within the exosomal fraction isolated by differential centrifugation. Exosomes are loosely categorized by their size interval of 30-150 nm. Data are mean ± SEM; n=3.

more abundant in ECFC exosomes **(Figure 5)**. HUVECs have been used as a model for the function and pathology of mature endothelial cells[59]. Exosomes from HUVECs had significantly less miR-486-5p present when compared with ECFC exosomes ($p<0.01$, $n=3$).

Biodistribution of ECFC-derived exosomes in vivo

Optical images taken using IVIS showed both a ventral and dorsal view of the biodistribution of ECFC-derived exosomes in live mice. An increase in fluorescence was observed in the ventral and dorsal views of the animal treated with 10 µL containing 15-20 µg DiR-labeled exosomes post-IR injury in the region of the kidneys after 30 min, and little change was found 4- or 24-hours post-reperfusion **(Figure 6)**. This increase of fluorescence was not present in sham mice, nor was it found when DiR alone was injected post-reperfusion. This shows that the exosomes may selectively target the kidney after IR compared to sham. To better conclude from which organ fluorescent signal was originating, mice were sacrificed and the lungs, heart, liver, spleen, vena cava (in IR group only) and kidneys were harvested, and *ex vivo* optical imaging was performed. When comparing dye alone vs DiR-exosomes administered to sham animals in *ex vivo* studies, little difference was noted **(Figure 7A)**. The sham experiments also showed low to moderate distribution to the lungs and kidney, and no distribution to the heart. While the biodistribution of DiR alone post-IR injury lacked significant change compared to sham, the biodistribution of DiR-exosomes after 30 min and 4 hours showed significant fluorescent levels in injured kidney, but not after 24 hours **(Figure 7A)**. The DiR-only treated mice post-reperfusion showed very similar distributions as sham animals, in which there was significant fluorescence in the liver and low to moderate fluorescence in the lung and kidneys. DiR-exosomes, however, demonstrated a decrease in the fluorescent signal to the lung or spleen,

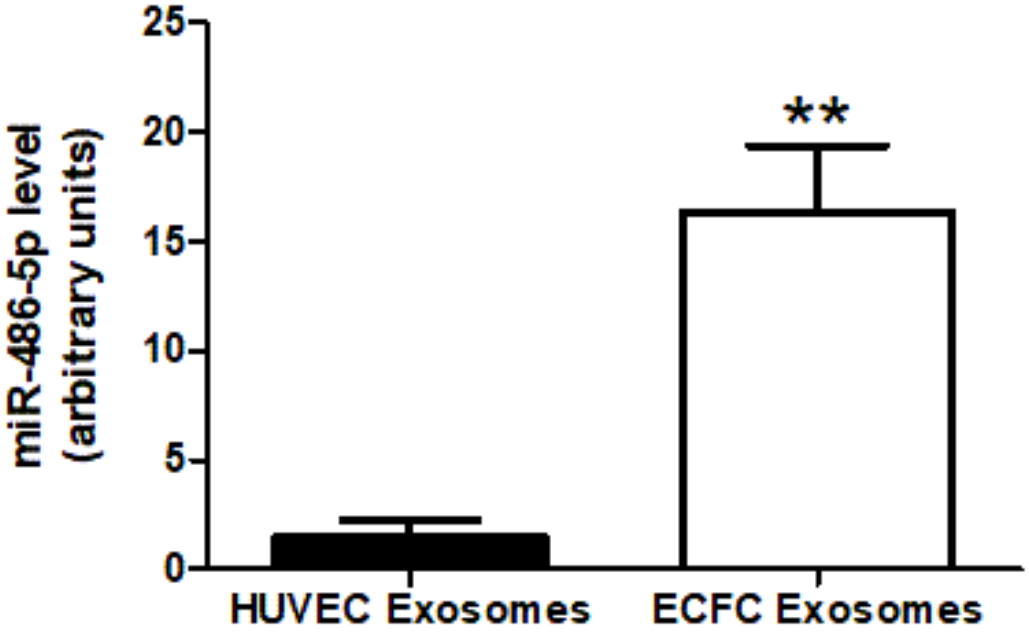

Figure 5 | ECFC-derived exosomes have significantly elevated miR-486-5p levels compared to other human endothelial cells. qPCR of miR-486-5p in HUVEC and ECFC exosomes using specific primers. miRNA isolation from fresh exosomes followed by miRNA quantification, reverse transcription, and qPCR. Data are mean ± SEM; n = 3. ** P<0.01 vs HUVEC exosomes.

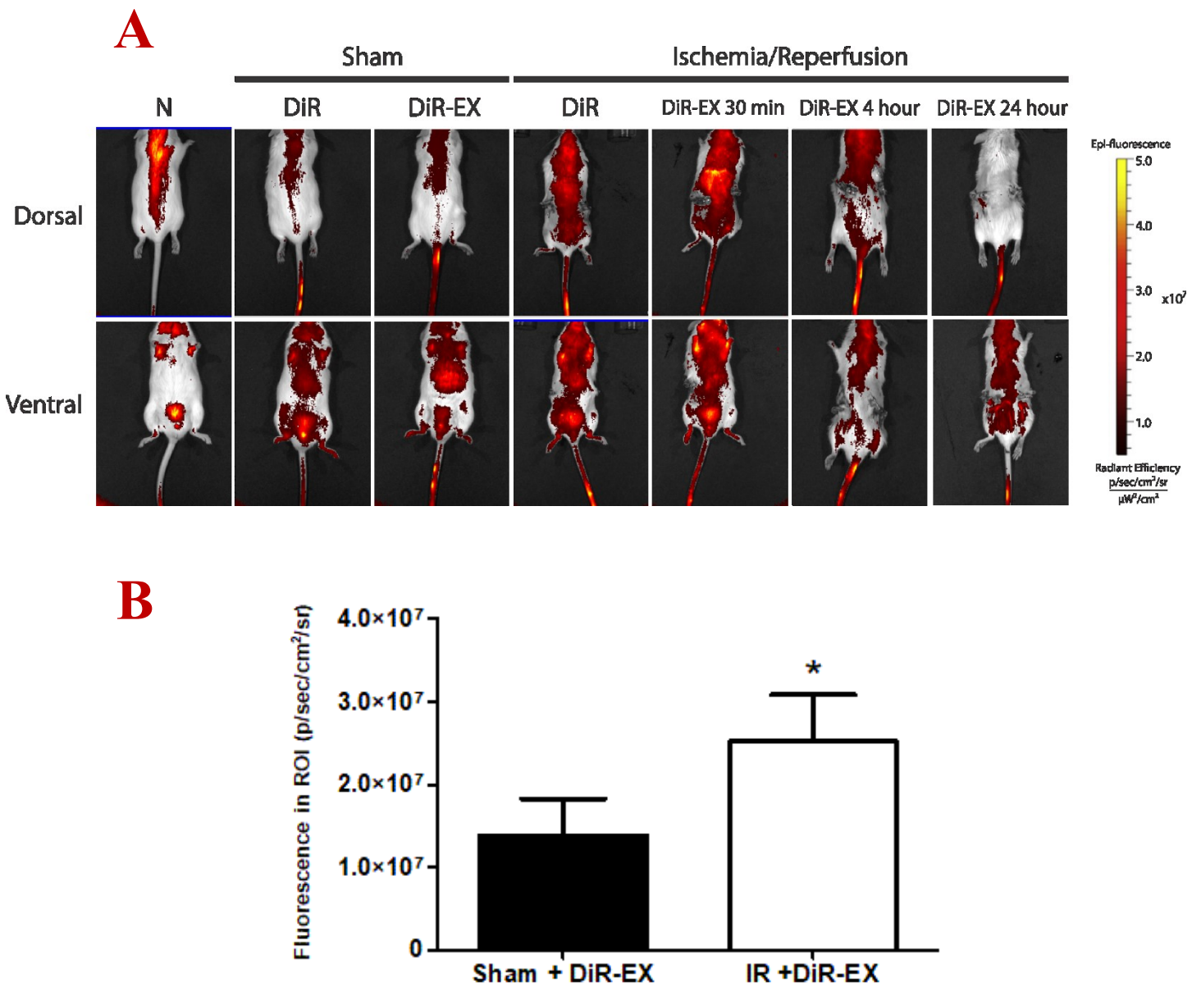

Figure 6 | | ECFC-exosome delivery after IR injury significantly increases biodistribution to the kidney by *in vivo* optical imaging. (a) Representative IVIS image of a live mouse injected i.v. with 10 µL DiR-exosomes or equal volume DiR alone. N, no surgery no injection negative control. Sham, 30-minute sham surgery without bilateral renal clamping. Ischemia/Reperfusion, surgery with bilateral renal clamping. DiR, DiR alone 30 minutes post-injection. DiR-EX, DiR-exosomes. (b) Quantification of fluorescence intensity in regions of interest (ROI) drawn free hand in the region of each organ, normalized to sham. Data are mean ± SEM; N=4. *P<0.05 vs Sham + DiR-EX.

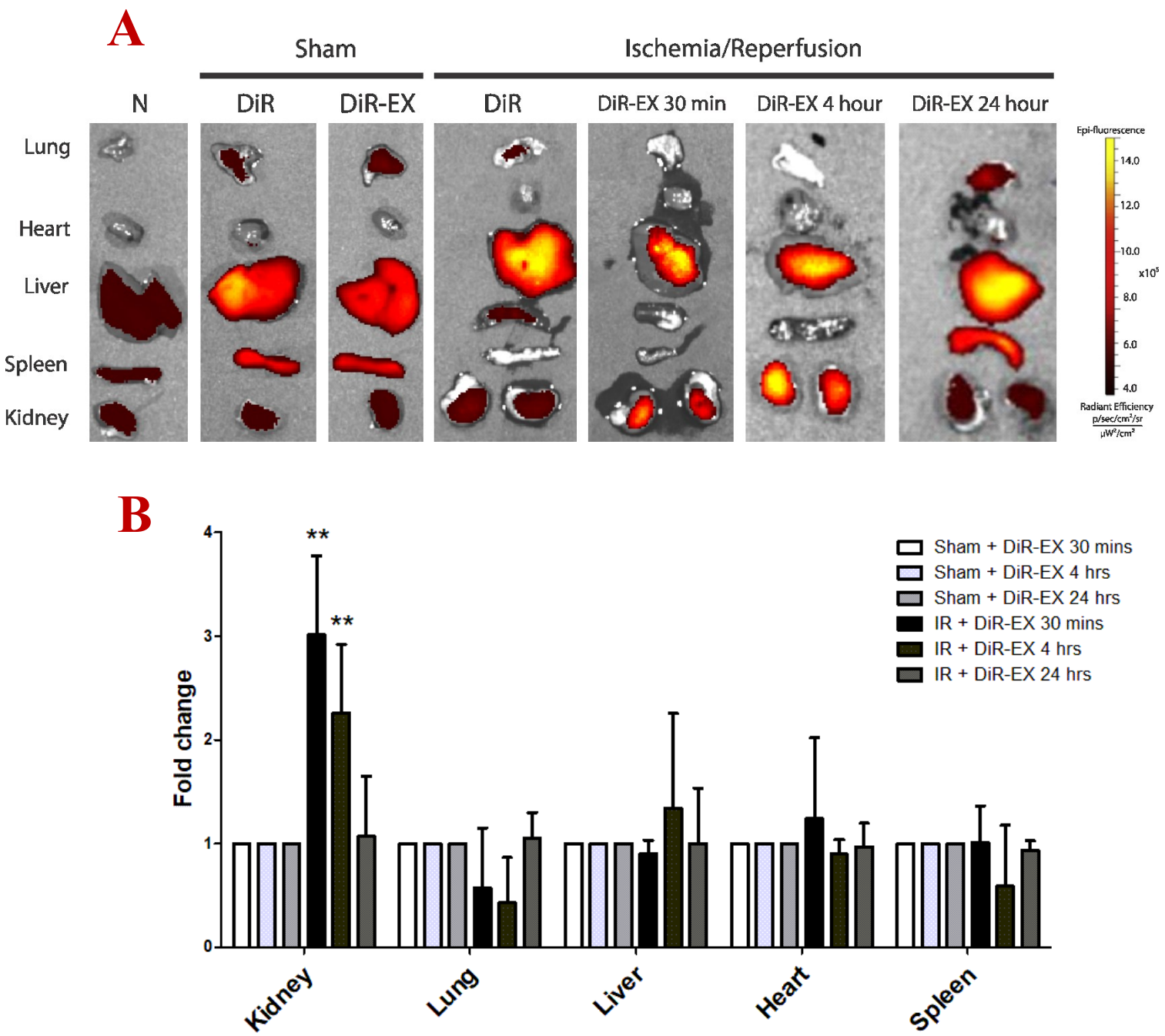

Figure 7 | ECFC-exosome delivery after IR injury significantly increases biodistribution to the kidney by *ex vivo* optical imaging. (a) Representative IVIS image of dissected organs 30 minutes, 4 hours, or 24 hours post injection of a mouse injected i.v. with 10 µL DiR-exosomes or equal volume DiR alone. N, no surgery no injection negative control. Sham, 30-minute sham surgery without bilateral renal clamping. Ischemia/Reperfusion, surgery with bilateral renal clamping. DiR, DiR alone 30 minutes post-injection. DiR-EX, DiR-exosomes. N=4. (b) Quantification of fluorescence intensity in regions of interest (ROI) drawn free hand in the region of each organ, normalized to sham. Sham + DiR-EX, sham animal treated with exosomes. IR + DiR-EX, surgery with bilateral renal clamping treated with exosomes. Data are mean ± SEM; N=4. **P<0.01 vs Sham + DiR-EX.

decreased liver fluorescence, and significantly increased fluorescence in both kidneys after 30 min and 4 hours ($p<0.01$, $n=4$). At 24 hours post-reperfusion, however, the DiR-exosomes distribution returned to that of a sham animal. **(Figure 7B)**.

miR-486-5p distribution mimics exosome distribution

qPCR was used to determine the effect of exosomes on tissue levels of miR-486-5p, and to identify whether the tissue levels of miR-486-5p follow a similar distribution as exosomes post-IR injury **(Figure 8)**. After IR alone, all tissues showed a non-significant increase of miR-486-5p, although a significant increase was seen in lung tissue after 24 hours ($p<0.05$, $n=4$). After 30 min, 4 hours, or 24 hours, only kidneys showed a significant increase in miR-486-5p after exosome infusion ($p<0.01$, $n=4$). Comparing the data from the IR alone group and with the increase seen after ECFC-exosome delivery showed that the significant difference was dependent on exosomes and was not simply the innate response caused from the injury itself.

ECFC-exosomes are visualized in the kidney and liver

PKH26-labeled exosomes were injected at the time of reperfusion and the lung, heart, liver, and kidney were sectioned to investigate the cellular localization of the injected exosomes. After 30 min of reperfusion, exosomes were found in the tubulointerstitium of the kidney and the Kupffer cells in the liver, but not in the heart or lungs **(Figure 9)**. In the images, produced with the help of Dr. Alex Gutsol, high background fluorescence was found in the heart and lung (red) and in the liver and kidney (green and yellow).

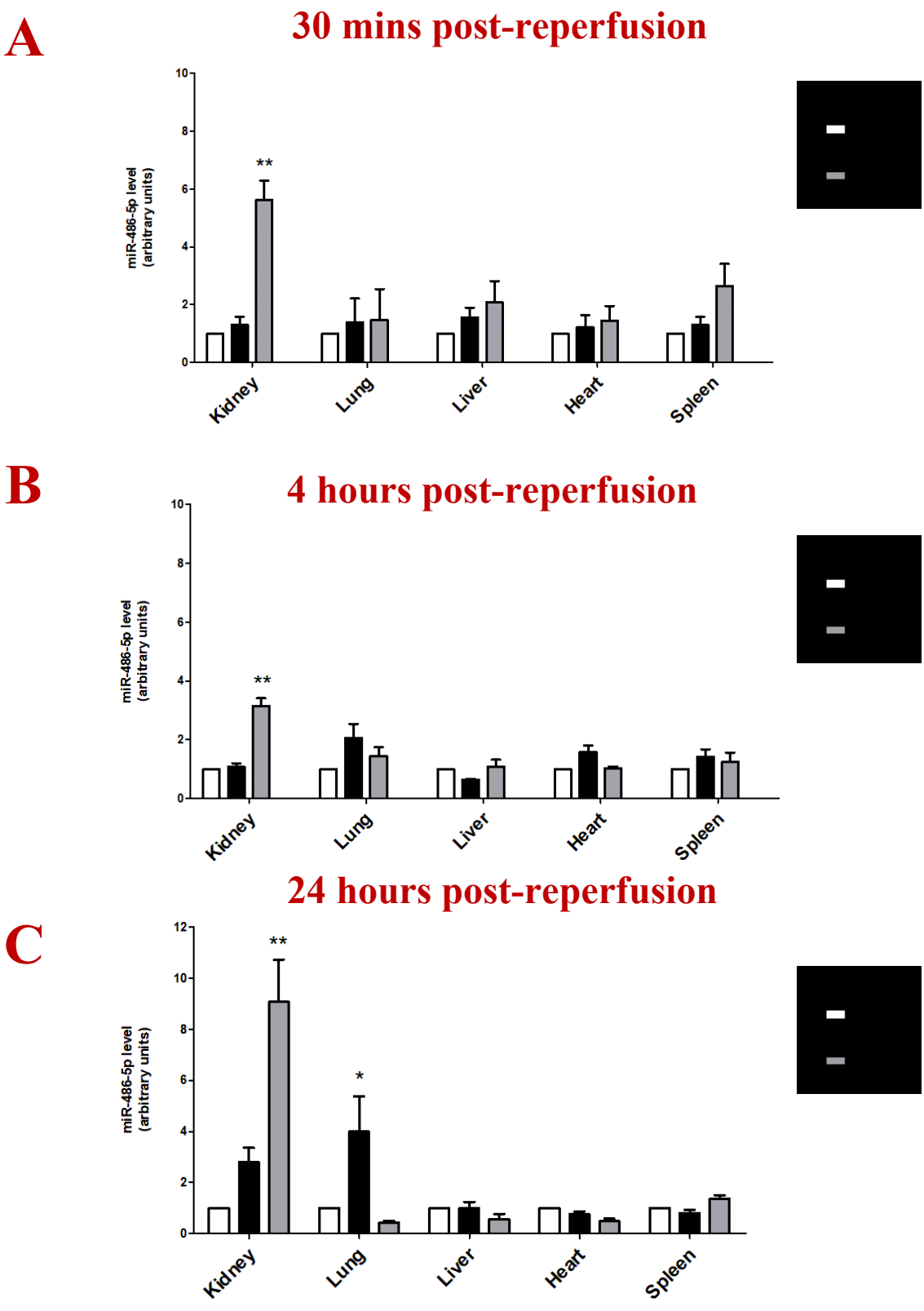

Figure 8 | Exosome delivery significantly increases miR-486-5p levels only in the kidney. Semi-quantitative analysis of miR-486-5p levels in the organs of interest (a) 30 minutes, (b) 4 hours, or (c) 24 hours post-reperfusion, normalized to sham. Sham; sham surgery, no exosomes. IR; ischemia reperfusion, no exosomes. IR+EX; ischemia reperfusion with exosome administration. Data are mean ± SEM; N=4. **P<0.01 vs sham, *P<0.05 vs sham.

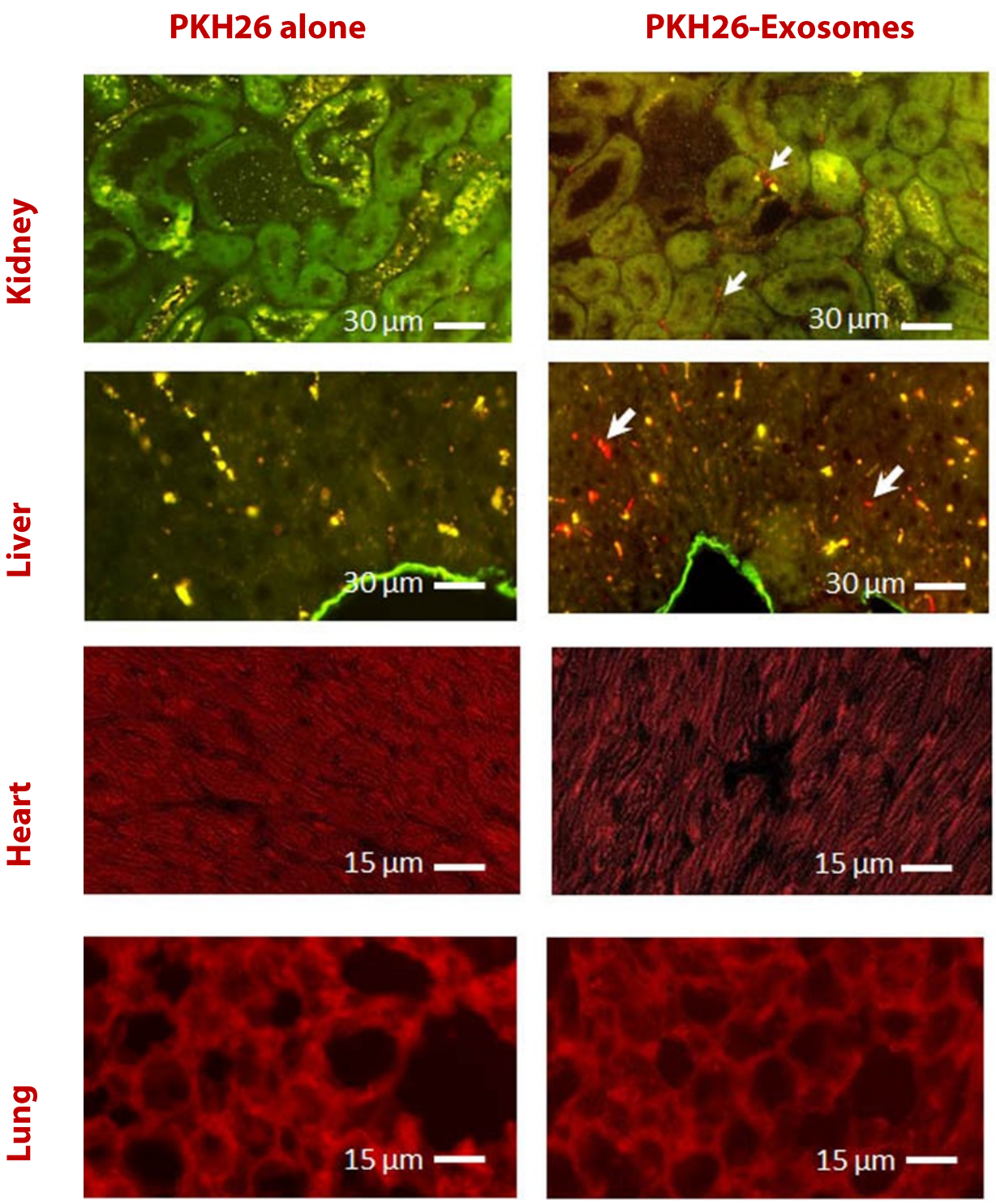

Figure 9 | PKH26-labeled ECFC-exosomes localize to the kidney interstitium within 30 minutes after injection. All micrographs show organs after ischemia reperfusion, while only the images on the right show the injection of PKH26-exosomes. Exosomes found in the kidney are found primarily in the tubulointerstitial space (arrows). Exosomes found in the liver are found within Kupffer cells (arrows). Exosomes are not found in the heart or lung. Images are representative of data from 6 mice.

ECFC-exosomes are delivered to cortical structures

The renal cortex, medulla, proximal tubules, glomeruli, and endothelial cells were isolated, and the tissue was subjected to miRNA isolation and qPCR **(Figure 10)**. When comparing whole kidney **(Figure 10A)**, cortex **(Figure 10B)**, and medulla **(Figure 10C)**, levels of miR-486-5p were elevated in the whole kidney ($p<0.05$ vs IR, n=4), while only the kidney cortex-rich tissue showed a significant increase in miR-486-5p 30 min after reperfusion ($p<0.05$ vs IR, n=4). The medulla-rich tissue did not have a significant increase in miR-486-5p.

The kidney cortex was then subjected to collagenase digestion and microdissection of both proximal tubule segments **(Figure 10D)** and glomeruli **(Figure 10E)**. Proximal tubule segments or glomeruli subjected to IR showed a non-significant increase of miR-486-5p compared to sham surgery after 30 minutes, however, the injection of exosomes led to a significant increase in proximal tubules (2-fold, $p<0.05$ vs IR alone, n=4) and glomeruli (3-fold, $p<0.05$ vs IR alone, n=4).

Kidneys were also subjected to an endothelial cell sorting technique using enzymatic digestion and magnetic bead sorting using CD31-labeled beads. miR-486-5p levels from isolated renal endothelial cells were only increased 30 min post-reperfusion with the injection of exosomes (2-fold, $p<0.01$ vs IR, n=4) **(Figure 10F)**. This is consistent with the other segment data, as the cortex (including the glomeruli and proximal tubule) is home to much of the renal vasculature. This, together with data suggesting that miR-486-5p levels in the cell correlates with protective effects against IR and suggests that miR-486-5p is being transferred via exosomes to specific cells in the kidney.

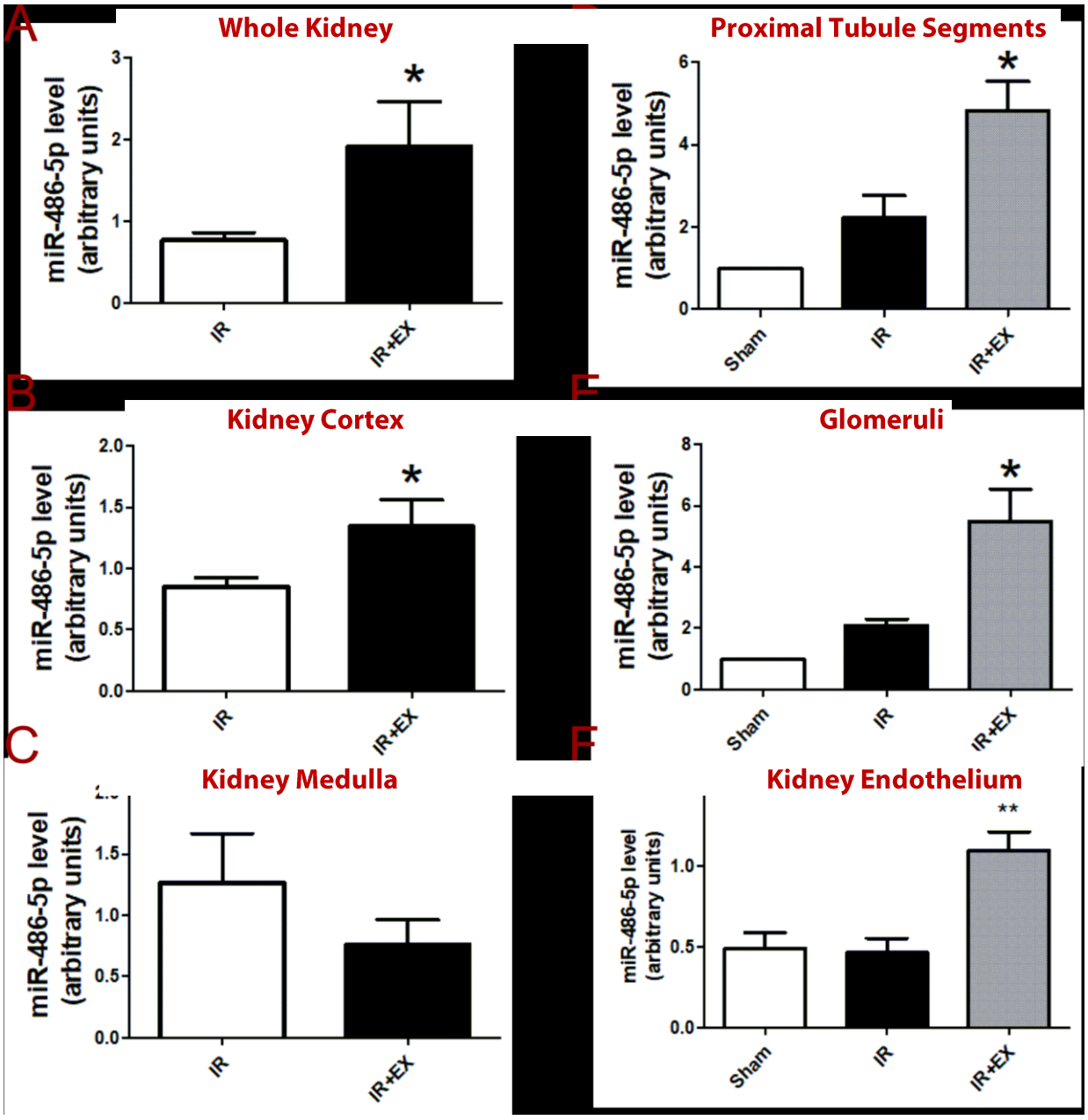

Figure 10 | ECFC-exosome injection after IR injury increases miR-486-5p levels in the kidney cortex, proximal tubule segments, glomeruli, and endothelium 30 minutes post-reperfusion. Depicted are results for real-time PCR of miR-486-5p in whole kidney (A), renal cortex (B), and medulla (C), dissected proximal tubules (D) and glomeruli (E), and isolated kidney endothelial cells (F). Sham (untreated mice), IR (mice with 30 min of bilateral kidney ischemia) and IR+EX (mice with 30 min of bilateral kidney ischemia followed by infusion of 20 µg of exosomes). *P<0.05 vs IR, **P<0.01 vs IR by one-way ANOVA, N=4 for each panel.

Exosomal transfer of miR-486-5p to target cells in vitro

ECFCs were transfected with previously labeled Cy3-pre-miR-486-5p and were cultured to produce exosomes containing Cy3-pre-miR-486-5p. Then, these exosomes (present in the cultured media) were delivered to a HUVEC culture to observe the transfer of miR-486-5p from ECFC-derived exosomes to their target cell **(Figure 11A, B)**. When cultured media was given alone (CM), we observed the presence of miR-486-5p in the cytosol surrounding the nucleus ($p<0.001$ vs control, n=4). When the ECFC culture was previously incubated along with GW4869, an exosome release inhibitor, no miR-486-5p was present ($p<0.001$ vs CM, n=4). Therefore, when exosomes were not present to mediate a transfer, no miR-486-5p localized to the HUVECs. Additionally, when the culture of HUVECs and ECFC cultured media was accompanied by EIPA, an exosome uptake inhibitor, miR-486-5p was also not present ($p<0.001$ vs CM, n=4). By inhibiting both release and uptake mechanisms, we can verify that the exosome is responsible for the transfer of miR-486-5p to the target cells.

CXCR4/SDF-1α axis plays a role in exosomal targeting

To test the hypothesis that CXCR4 and SDF-1α play a role in mediating the uptake of exosomes in vitro, an SDF-1α neutralizing antibody and plerixafor, a CXCR4 bicyclic reversible inhibitor, were used in culture with HUVECs treated with exosomes. By immunoblot, it was first confirmed that CXCR4 is present on the membrane of both ECFCs and their exosomes **(Figure 12C)**. The exosome uptake experiment confirmed the hypothesis that exosomes administered to cells cultured under hypoxia had a significantly higher uptake than exosomes administered to normoxic cells ($p<0.001$ vs normoxic control, n=4) **(Figure 12A, B)**. Further, when exosomes were treated with the CXCR4 antagonist, or when the cultured cells were treated with a neutralizing antibody to SDF-1α under hypoxia, exosome uptake was completely blocked

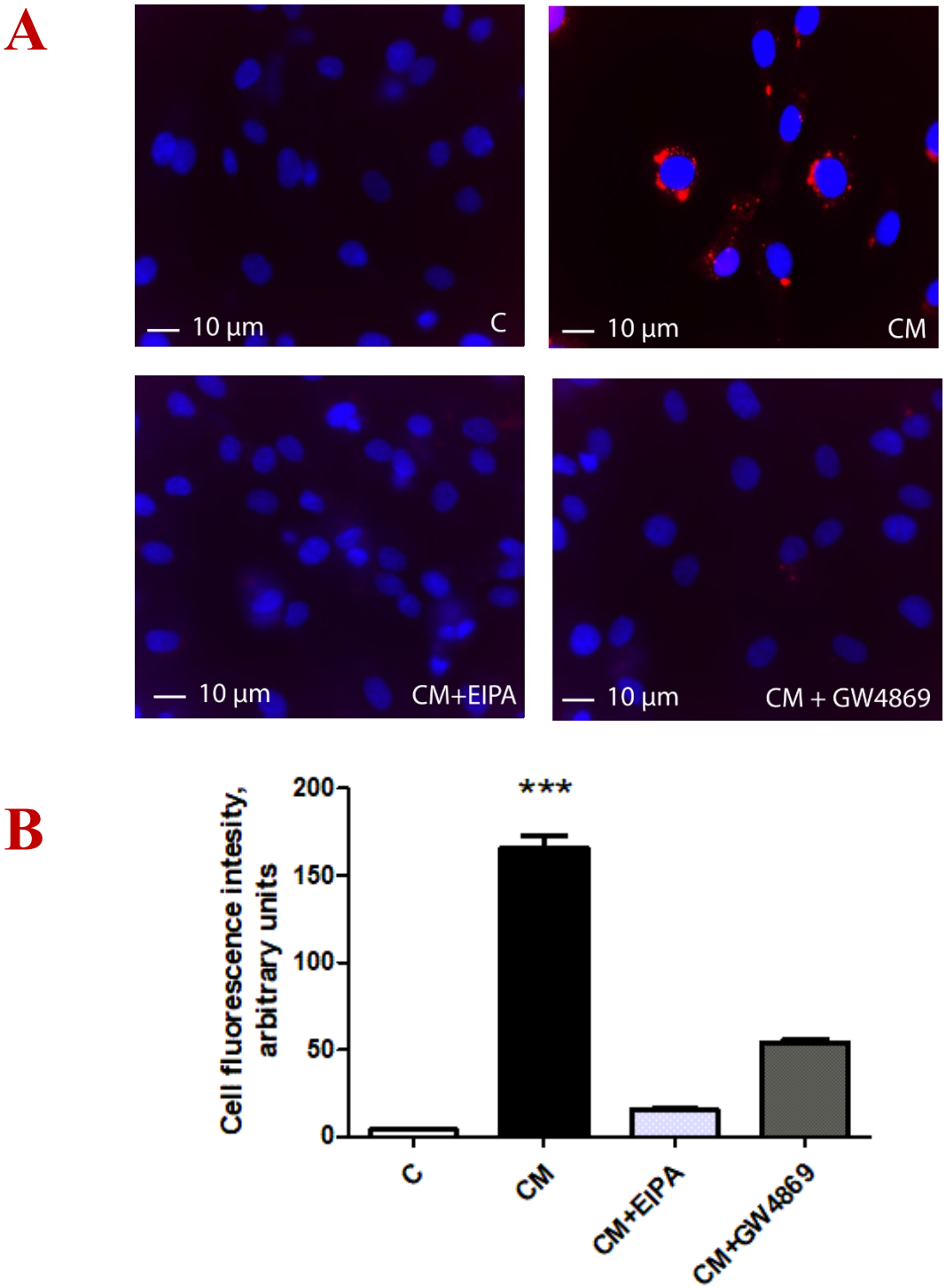

Figure 11 | Exosomes are required for the transfer of miR-486-5p to target human umbilical vein endothelial cells (HUVECs) *in vitro*. (a) Representative micrographs and (b) graph showing the uptake of Cy3-labeled pre-miR-486-5p (red) in HUVECs after16 hour incubation with cultured media (CM) from ECFCs. C; control. CM; cultured media from ECFCs previously transfected with Cy3-labeled pre-miR-486-5p. CM+EIPA; cultured media with 5-(*N*-Ethyl-*N*-isopropyl)amiloride (EIPA, 10 µM), an inhibitor of macropinocytosis. CM+GW4869; cultured media with exosome release inhibitor GW4869 (10 µM). HUVEC nuclear counterstaining was performed using Hoescht stain (blue). Data are mean ± SEM; N=4. ***P<0.001 vs all other groups, by one-way ANOVA.

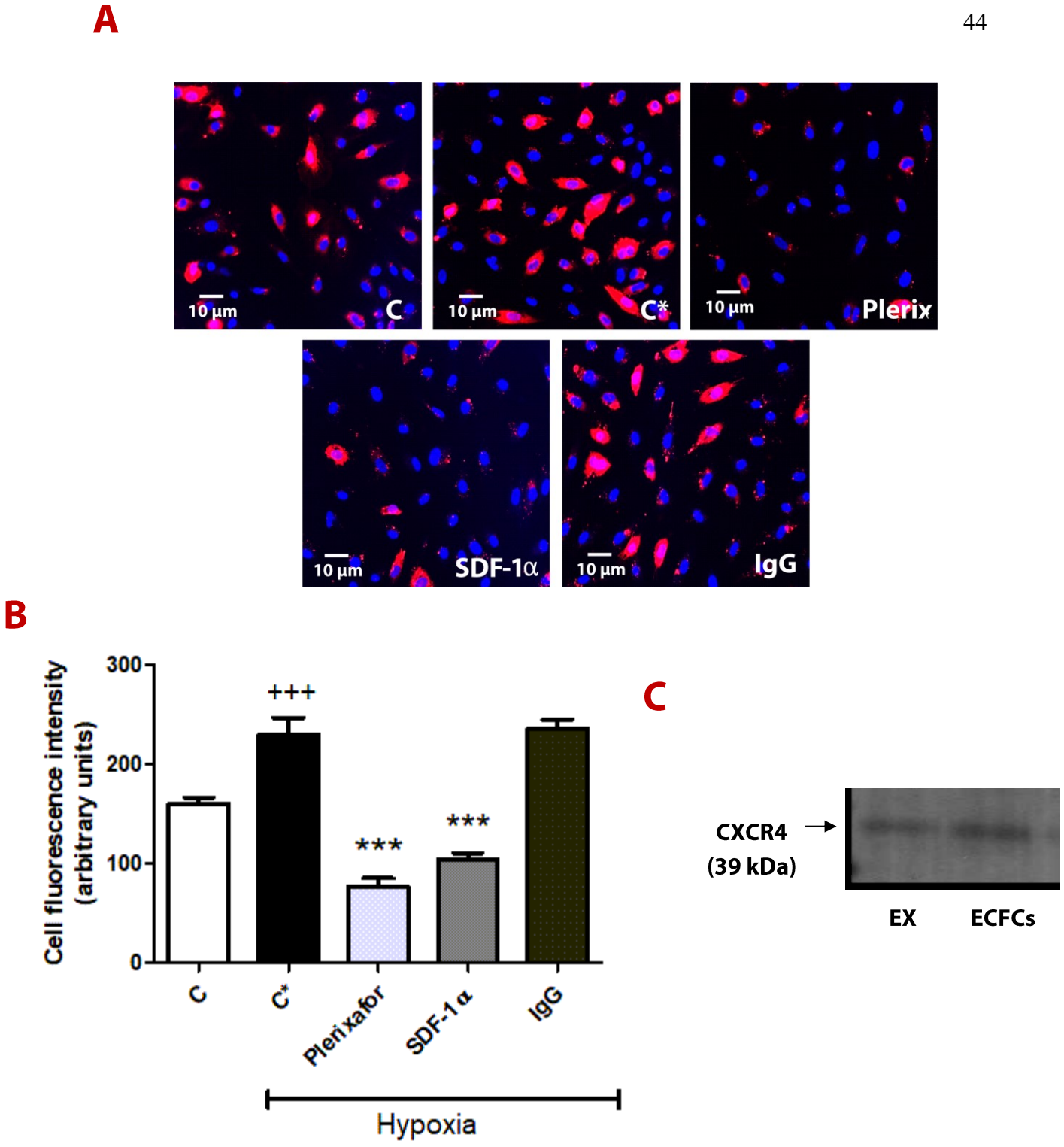

Figure 12 | Internalization of ECFC-derived exosomes by hypoxic HUVECs is blocked by plerixafor and neutralizing antibody to SDF-1α. (A) Representative images and graphs (B) of HUVECs incubated for 6 hrs with 20 µg/ml of PKH26-labeled exosomes (red) in normoxia (C), hypoxia (C*), hypoxia with 100 µM plerixafor (Plerix), hypoxia with 10 µg/ml of neutralizing antibody to SDF-1α (SDF-1α) and Isotype control (IgG). HUVEC nuclear counterstaining was performed using Hoescht stain (blue). +++P < 0.001 vs C, ***P < 0.001 vs C*, by one-way ANOVA, n = 4. (C) Immunoblot shows expression of CXCR4 in ECFCs and their derived exosomes (EX).

($p<0.001$ vs ischemic control, n=4). These data reinforced the impact of the CXCR4/SDF-1α axis as a key mediator in the uptake of exosomes, at least in endothelial cells.

Plerixafor attenuates the protective effect of ECFC exosomes in vivo

To test the hypothesis that CXCR4 and SDF-1α play a role in mediating the protective effect of exosomes *in vivo*, ECFC-derived exosomes were preincubated with plerixafor and administered to IR mice to determine whether the inhibition of CXCR4 at the exosomal level impacts the function of the exosome. To compare the function of ECFC-derived exosomes in our *in vivo* model, either saline, 20 μg exosomes, or 20μg exosomes preincubated with plerixafor were injected into mice with IR. Their organs and serum were then isolated 24 hours after reperfusion. When comparing the protective effects using either serum creatinine or blood urea nitrogen (BUN), administration of exosomes consistently lowered creatinine and BUN levels, but this protective effect was attenuated if the same exosomes were preincubated with plerixafor ($p<0.05$ vs IR + EX, n=5) **(Figure 13A, B)**. These data give compelling evidence towards the CXCR4/SDF-1α axis and its importance in the targeting of exosomes and the mechanism of action.

Histological analyses were performed with the help of Dr. Alex Gutsol to determine the injury scores and neutrophil counts 24 hours after injury. IR was associated with significant histologic injury, as shown, as well as significant neutrophil infiltration due to acute inflammation. When treated with exosomes, these negative effects were reduced, however, exosomes preincubated with plerixafor had no protective effect ($p<0.001$ vs IR + EX, n=4) **(Figure 14A, B)**.

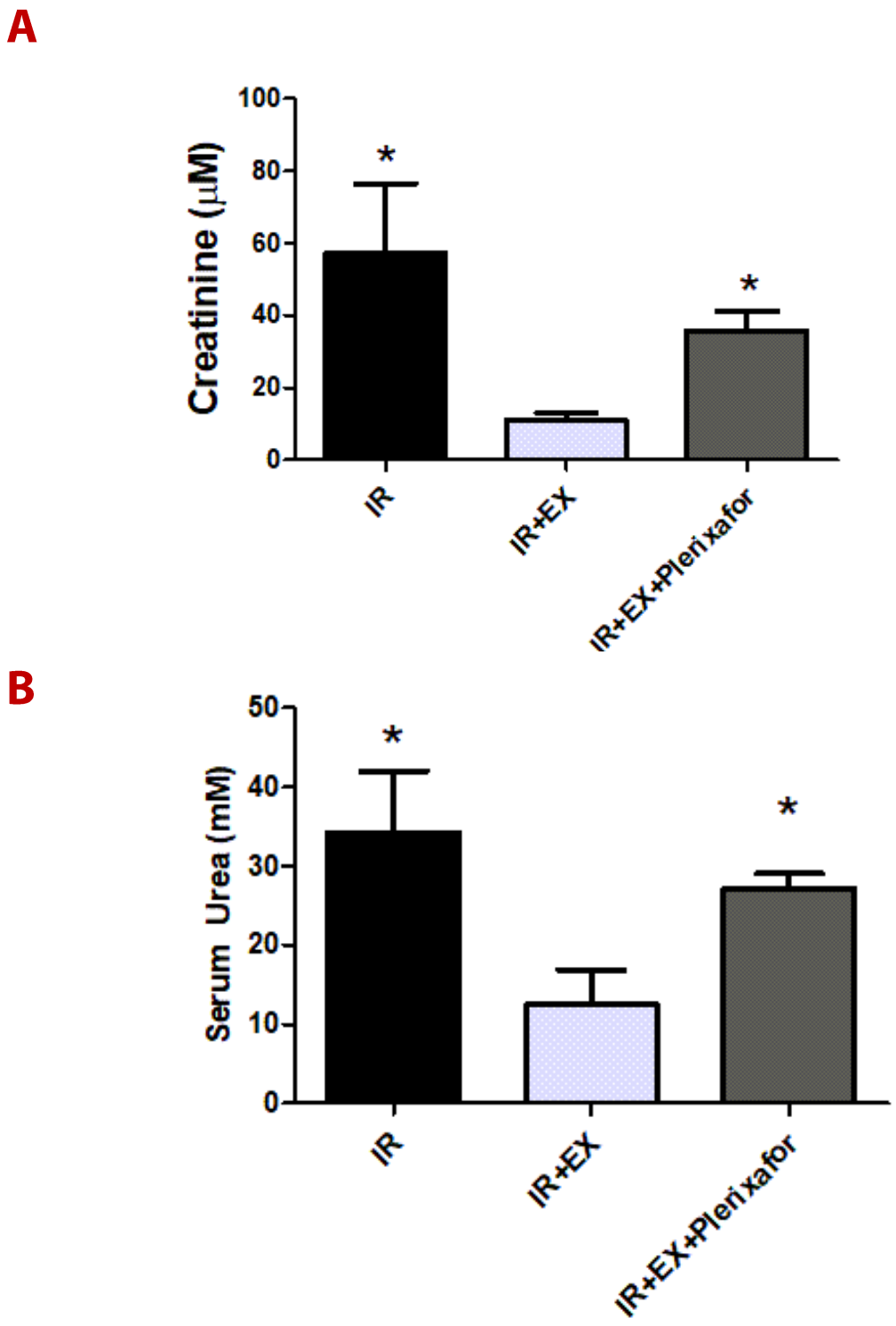

Figure 13 | Effect of exosomal CXCR4 on serum creatinine and blood urea nitrogen after ischemic injury. Graphs depict data obtained 24 hrs after reperfusion in mice subjected to ischemic kidney injury (IR), with or without i.v. administration of endothelial colony forming cell exosomes (IR+EX), or exosomes pre-incubated with the CXCR4 antagonist plerixafor (IR+EX+Plerixafor). (A) Serum Cr and (B) Blood Urea Nitrogen (BUN) levels 24 hrs after reperfusion. *P < 0.05 vs IR+EX.

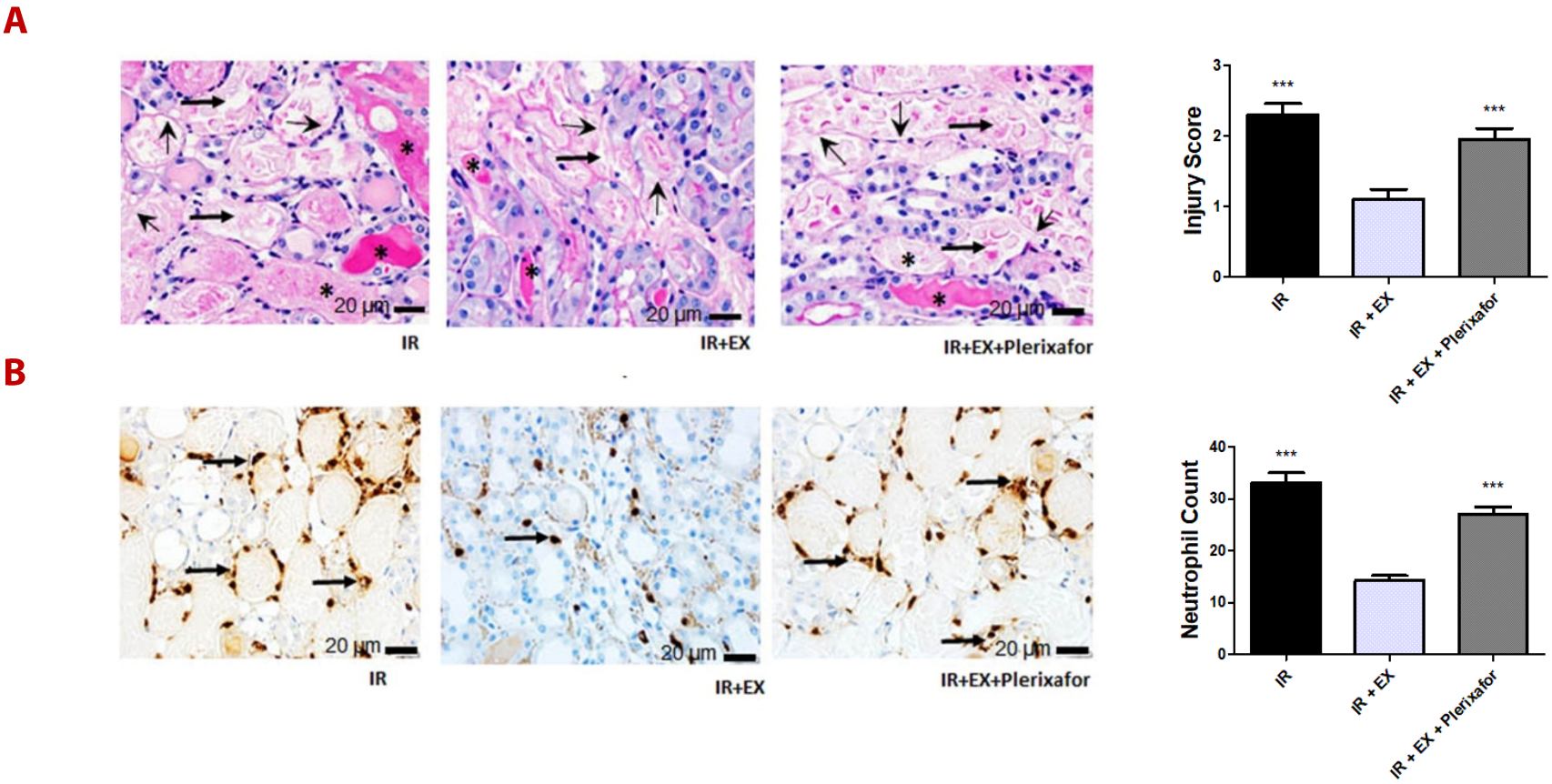

Figure 14 | Effect of exosomal CXCR4 on kidney ischemic injury histological scores and neutrophil infiltration. Graphs depict data obtained 24 hrs after reperfusion in mice subjected to ischemic kidney injury (IR), with or without i.v. administration of endothelial colony forming cell exosomes (IR+EX), or exosomes pre-incubated with the CXCR4 antagonist plerixafor (IR+EX+Plerixafor). (A) Kidney histologic injury scores for mice with kidney ischemia, 24 hrs after reperfusion, with or without exosomes. *P < 0.001 vs IR+EX; Representative photomicrographs are shown beside graph. Astericks (*) depict tubular cast formation, arrows depict hallmark tubular dilatation, and arrowheads depict nuclear loss. (B) Quantitative assessment of neutrophil infiltration in kidneys (number of neutrophils per field), for mice with kidney ischemia, 24 hrs after reperfusion, with or without exosomes. ***P < 0.001 vs IR+EX. Representative photomicrographs are shown beside graph. Arrows depict peritubular neutrophil infiltrate. N=4 in each group exceptIR alone N=6.

miR-486-5p is increased in liver, spleen, and kidney post-mimic injection

Following previous data suggesting that miR-486-5p is the mediator of the therapeutic efficacy of ECFC-exosomes, coupled with the difficult scalability of exosomes, we began to investigate the effects of the administration of encapsulated miR-486-5p. qPCR was used to comparatively quantify miR-486-5p levels in each *ex vivo* organ to determine whether the amount of miR-486-5p in the organs follows a similar distribution to that after exosome treatment. It was hypothesized that since there is no CXCR4 to guide the mimic-invivofectamine complex to the kidney specifically, there might be increases in other organs as well, such as the liver and spleen. The data show that there was an increase in miR-486-5p levels in both male and female kidney ($p<0.01$ vs IR, n=3-5) **(Figure 15F, 16F)**, even more than after exosome treatment, but there is also non-specific distribution to the liver and spleen ($p<0.001$ vs IR, n=3-5) **(Figure 15D, E, 16D, E)**.

miR-486-5p mimic increases miR-486-5p levels in endothelium

The kidney cortex was again subjected to enzymatic digestion and magnetic bead sorting of endothelial cells **(Figure 17 A, B)** and collagenase digestion and microdissection of proximal tubule segments **(Figure 17 C, D)** 24 hours post-IR. After 24 hours, we observe no significant increase in miR-486-5p after exosome injection in endothelium nor proximal tubule segments. Interestingly, after IR and miR-486-5p-invivofectamine injection alone, we observed a statistically significant increase in miR-486-5p in isolated endothelial cells ($p<0.001$ vs IR, n=3) and in proximal tubule segments ($p<0.01$ vs IR in male, $p<0.05$ vs IR in female, n=3).

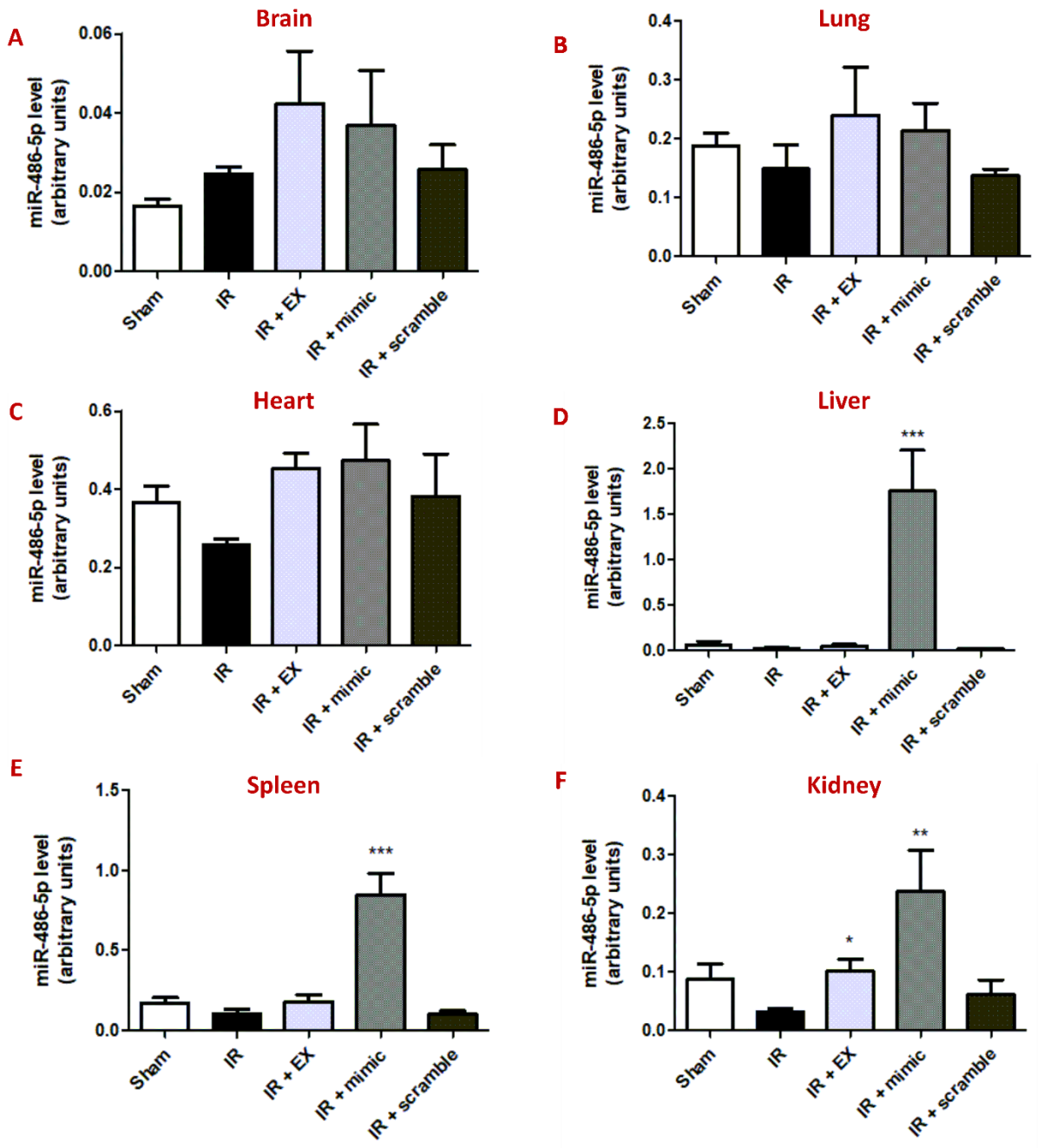

Figure 15 | miR-486-5p levels increase in male mouse liver, spleen, and kidney post- miR-486-5p injection. Depicted are q-PCR results for miR-486-5p in brain (A), lungs (B), heart (C), liver (D), spleen (E) and kidney (F) from IR kidneys, 24 hours after either ECFC-exosome injection (20 µg, IR + EX) or Invivofectamine-mimic complex containing miR-486-5p (1 mg/kg, IR + mimic) at the time of reperfusion**.** Sham (untreated mice), IR (30 minutes of ischemia) and IR + scramble (AKI mice injected with 1 mg/kg of Invivofectamine-scrambled miRNA complex at the beginning of reperfusion). *P<0.05 vs IR, **P<0.01 vs IR, ***P<0.001 vs IR. N=5.

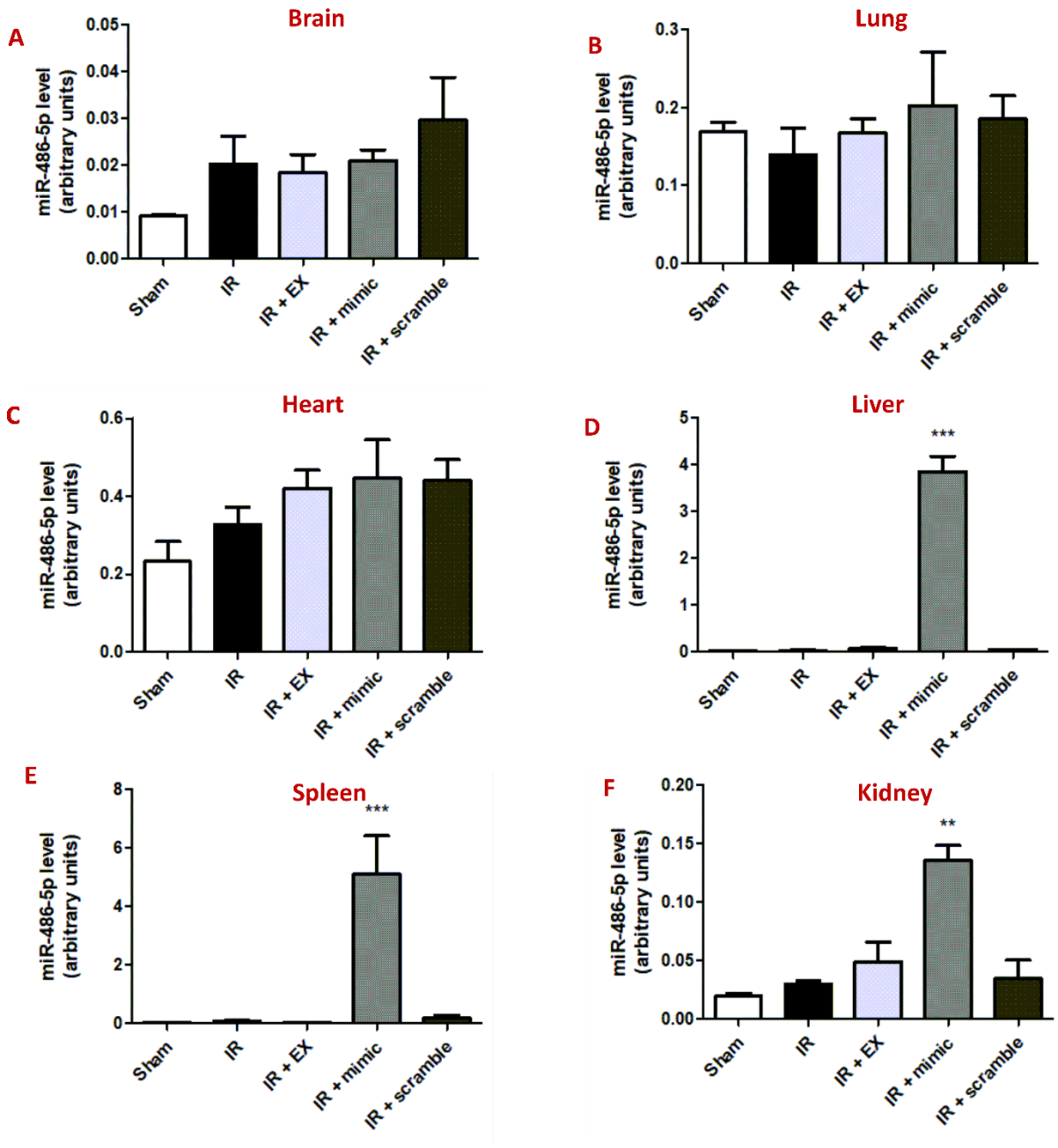

Figure 16 | miR-486-5p levels increase in female mouse liver, spleen, and kidney post- miR-486-5p injection. Depicted are q-PCR results for miR-486-5p in brain (A), lungs (B), heart (C), liver (D), spleen (E) and kidney (F) from IR kidneys, 24 hours after either ECFC-exosome injection (20 µg, IR + EX) or Invivofectamine-mimic complex containing miR-486-5p (1 mg/kg, IR + mimic) at the time of reperfusion**.** Sham (untreated mice), IR (30 minutes of ischemia) and IR + scramble (AKI mice injected with 1 mg/kg of Invivofectamine-scrambled miRNA complex at the beginning of reperfusion). **P<0.01 vs IR, ***P<0.001 vs IR. N=3.

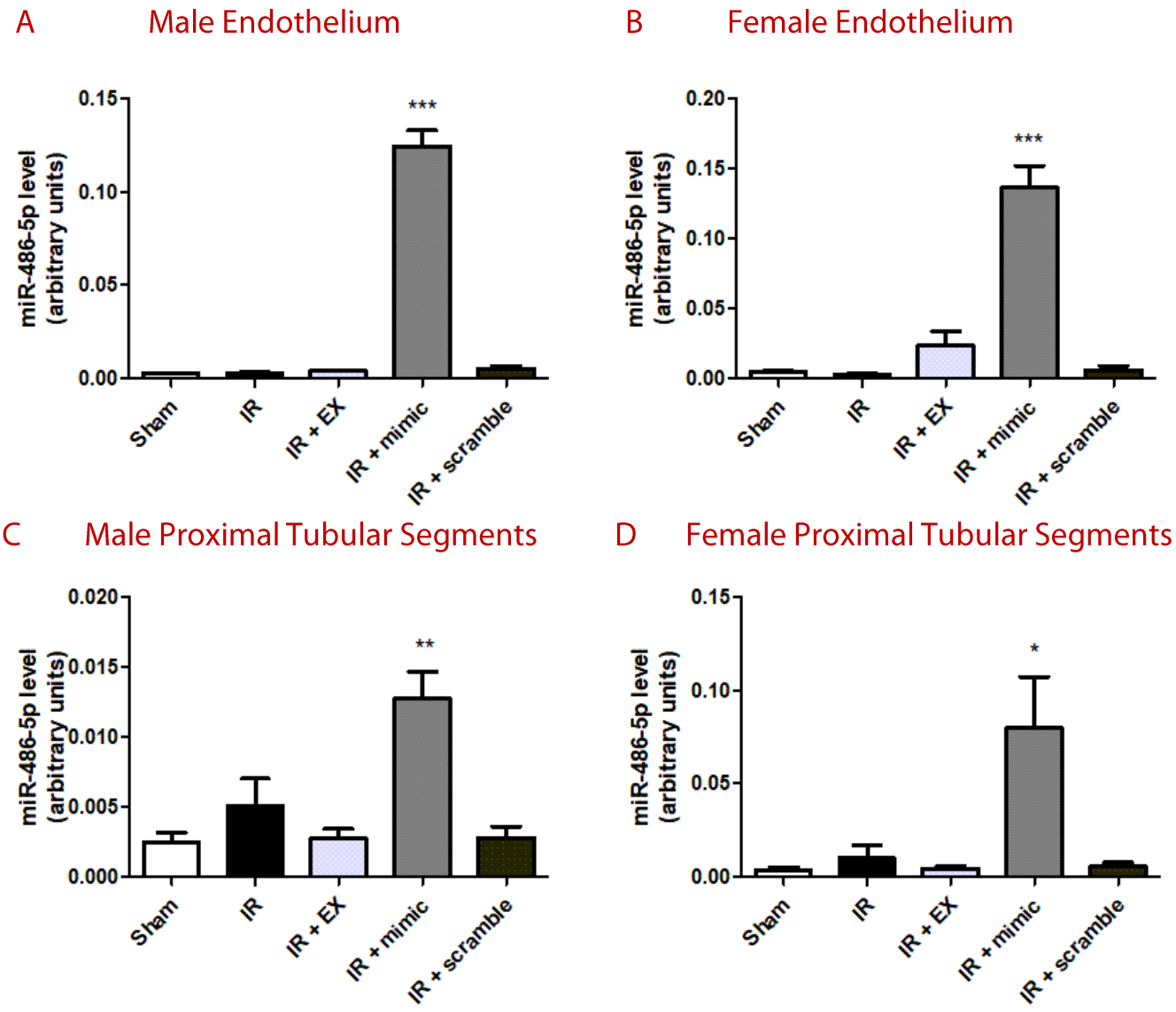

Figure 17 | Only miR-486-5p injection, and not exosome injection, after IR injury increases miR-486-5p levels in the endothelium and proximal tubule segments 24 hours post-reperfusion. Depicted are results for real-time PCR of miR-486-5p in isolated renal endothelial cells (A, B) or proximal tubule segments (C, D) from male (A, C) or female (B, D) in FVB mice 24 hours after either ECFC-exosome injection (20 µg, IR + EX) or Invivofectamine-mimic complex containing miR-486-5p (1 mg/kg, IR + mimic) at the time of reperfusion**.** Sham (untreated mice), IR (30 minutes of ischemia) and IR + scramble (AKI mice injected with 1 mg/kg of Invivofectamine-scrambled miRNA complex at the beginning of reperfusion). *P<0.05 vs IR, **P<0.01 vs IR, ***P<0.001 vs IR. N=3.

miR-486-5p mimic is as effective as exosomes in preventing injury post-IR

To determine whether miR-486-5p alone is as effective at preventing injury as exosomes are, serum was isolated from male and female mice 24 hours after IR injury and the injection of miR-486-5p-invivofectamine or exosomes to compare serum creatinine and serum BUN levels. miR-486-5p alone was just as effective as exosomes at preventing injury, measured by significantly lower BUN ($p<0.05$ vs IR and IR + scramble, n=3-5) and serum creatinine ($p<0.05$ vs IR and IR + scramble, n=3-5) levels compared to those after IR alone **(Figure 18)**. This effect of preventing injury, by contrast, was not present when mice were treated with the scramble-invivofectamine complex. The data were supported by histological injury scores **(Figure 19)**, where lower injury scores were attributed to exosome and miR-486-5p-invivofectamine groups compared to IR ($p<0.001$ vs IR and IR + scramble, n=3-5). Megalin staining also showed injury recovery post-IR in the exosome and miR-486-5p-invivofectamine groups ($p<0.001$ vs IR and IR + scramble, n=3-5), however it did not reach significance in the female group treated with miR-486-5p-invivofectamine **(Figure 20)**. Neutrophil infiltration was also decreased significantly in the exosome and miR-486-5p-invivofectamine groups ($p<0.05$ vs IR and IR + scramble, n=3-5) **(Figure 21)**. By contrast, histological evidence of apoptosis by TUNEL was decreased significantly only in mice treated with exosomes ($p<0.001$ vs IR and IR + scramble, n=3-5), and not miR-486-5p-invivofectamine alone **(Figure 22)**. Using Caspase-3 activity as a more sensitive method to measure apoptosis, caspase-3 activity significantly decreased in both the exosome ($p<0.01$ vs IR and IR + scramble male, $p<0.05$ vs IR and IR + scramble female, n=3-5) and miR-486-5p-invivofectamine ($p<0.05$ vs IR and IR + scramble male, $p<0.01$ vs IR and IR + scramble female, n=3-5) treated groups **(Figure 23)**. These data support the hypothesis that miR-486-5p is the key mediator of the protective effect of ECFC-exosomes, and that miR-486-5p alone can target the kidney and have the same effect.

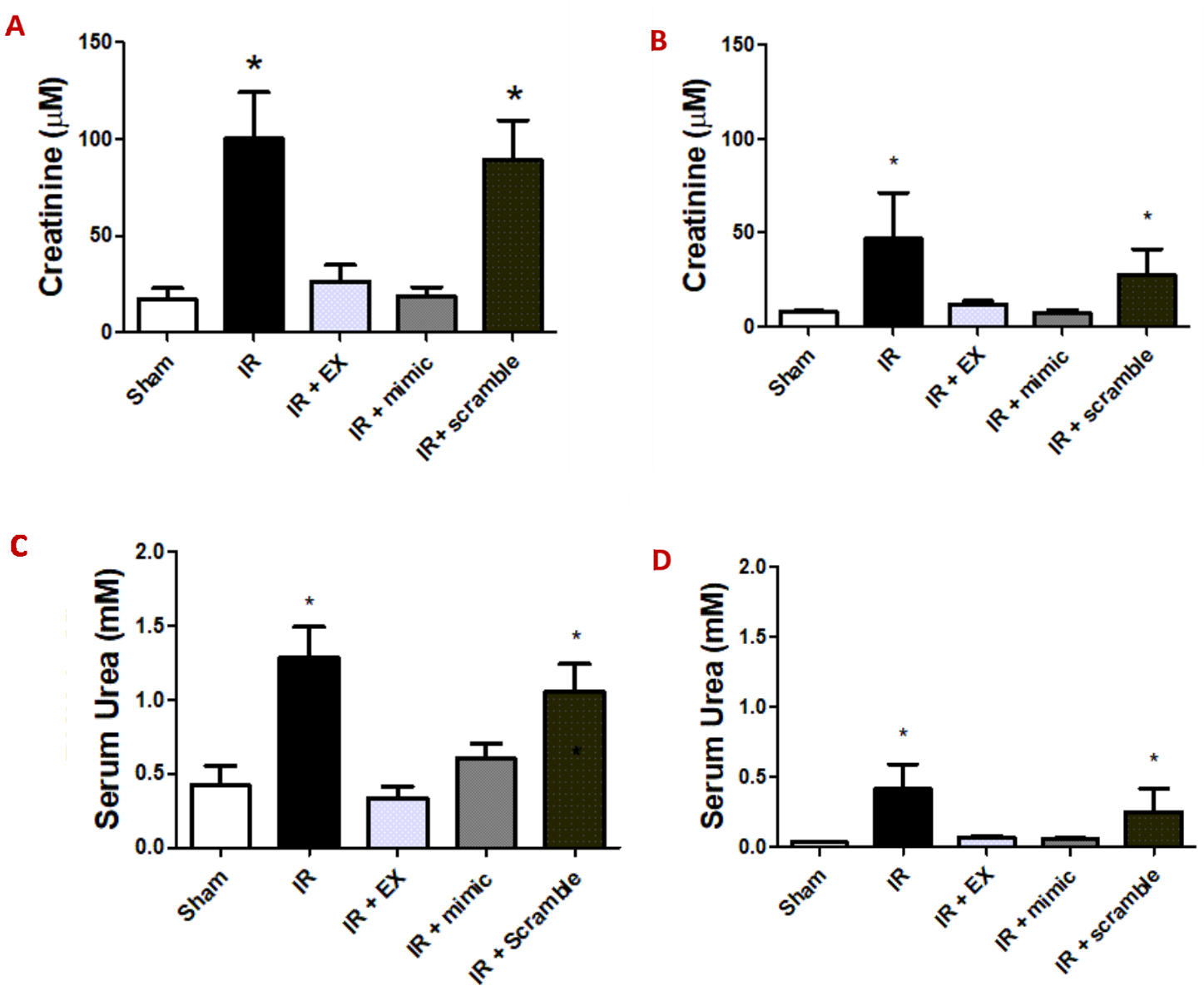

Figure 18 | miR-486-5p injection protects against IR injury by functional assessment in both male and female mice. Depicted are serum creatinine (A, B) or blood urea nitrogen (C, D) measurements from male (A, C) or female (B, D) in FVB mice 24 hours after either ECFC-exosome injection (20 μg, IR + EX) or Invivofectamine-mimic complex containing miR-486-5p (1 mg/kg, IR + mimic) at the time of reperfusion. Sham (untreated mice), IR (30 minutes of ischemia) and IR + scramble (AKI mice injected with 1 mg/kg of Invivofectamine-scrambled miRNA complex at the beginning of reperfusion). *P<0.05 vs IR + EX and IR + mimic. N=5 for male mice, n=3 for female mice.

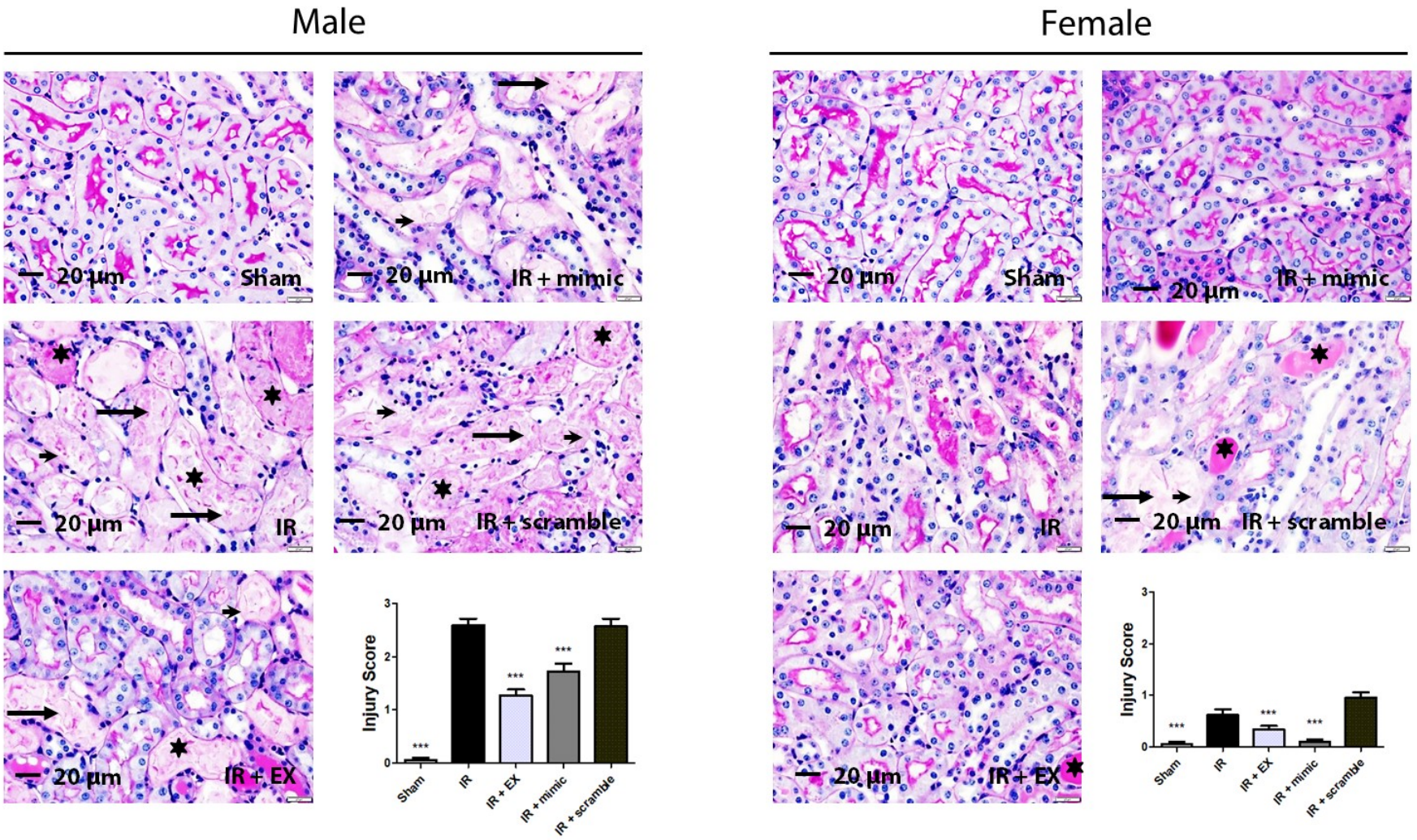

Figure 19 | miR-486-5p injection protects against IR injury by histological assessment in both male and female mice. Depicted are injury scores from male (A) or female (B) FVB mice 24 hours after either Invivofectamine-mimic complex containing miR-486-5p (1 mg/kg, IR + mimic) or ECFC-exosome injection (20 µg, IR + EX) at the time of reperfusion. Injury scores were calculated by a pathologist blinded to the slides. Sham (untreated mice), IR (30 minutes of ischemia) and IR + scramble (AKI mice injected with 1 mg/kg of Invivofectamine-scrambled miRNA complex at the beginning of reperfusion. Asterisks (*) depict tubular cast formation, arrows depict hallmark tubular dilatation, and arrowheads depict nuclear loss. *** P<0.001 vs IR, one-way ANOVA. n=5 for male mice, n=3 for female mice.

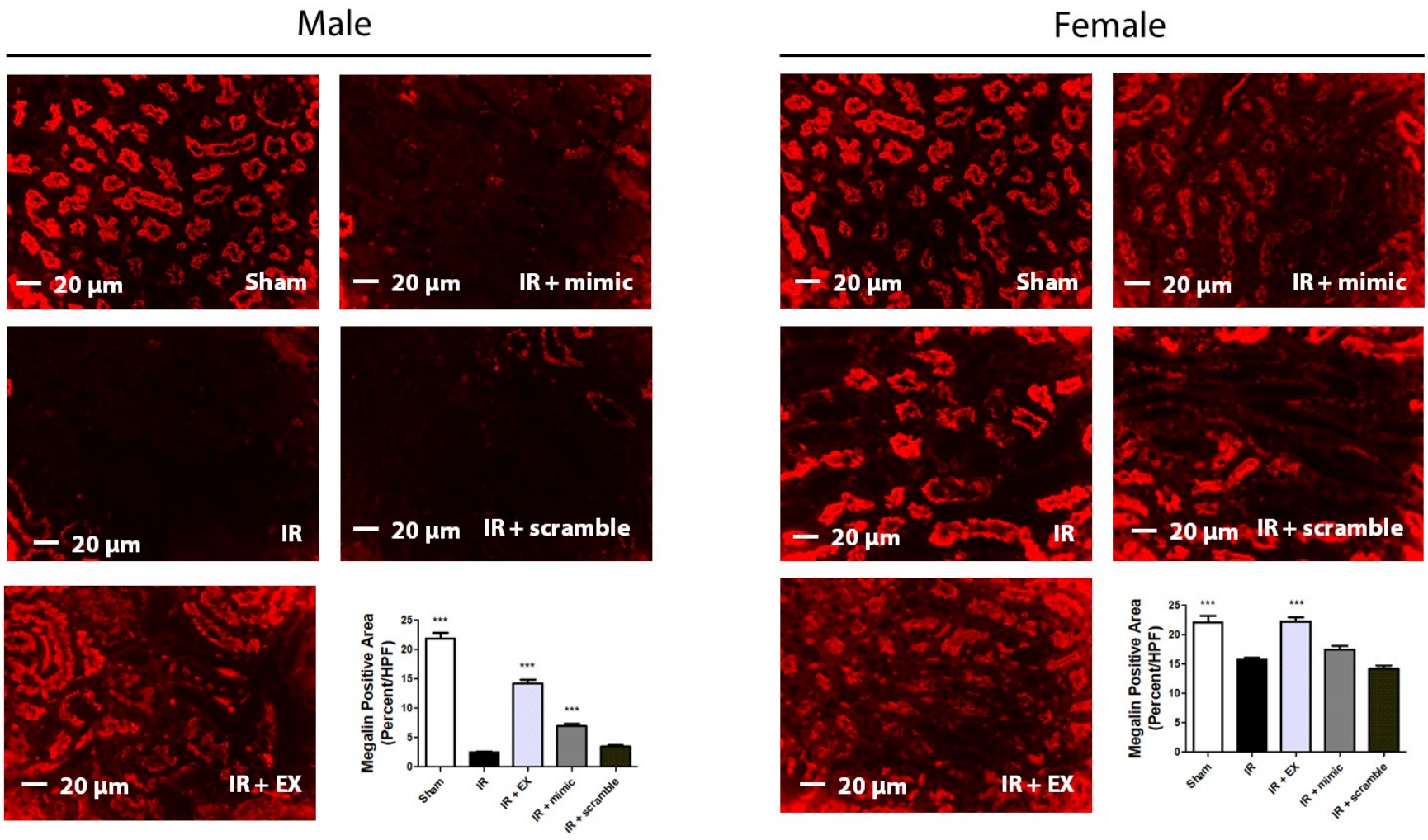

Figure 20 | miR-486-5p injection decreases megalin loss in male mice. Depicted is megalin staining from male and female FVB mice 24 hours after either Invivofectamine-mimic complex containing miR-486-5p (1 mg/kg, IR + mimic) or ECFC-exosome injection (20 µg, IR + EX) at the time of reperfusion. Megalin staining was performed by a pathologist blinded to the slides. Sham (untreated mice), IR (30 minutes of ischemia) and IR + scramble (AKI mice injected with 1 mg/kg of Invivofectamine-scrambled miRNA complex at the beginning of reperfusion. HPF; high-powered field. *** $P<0.001$ vs IR, one-way ANOVA. n=5 for male mice, n=3 for female mice.

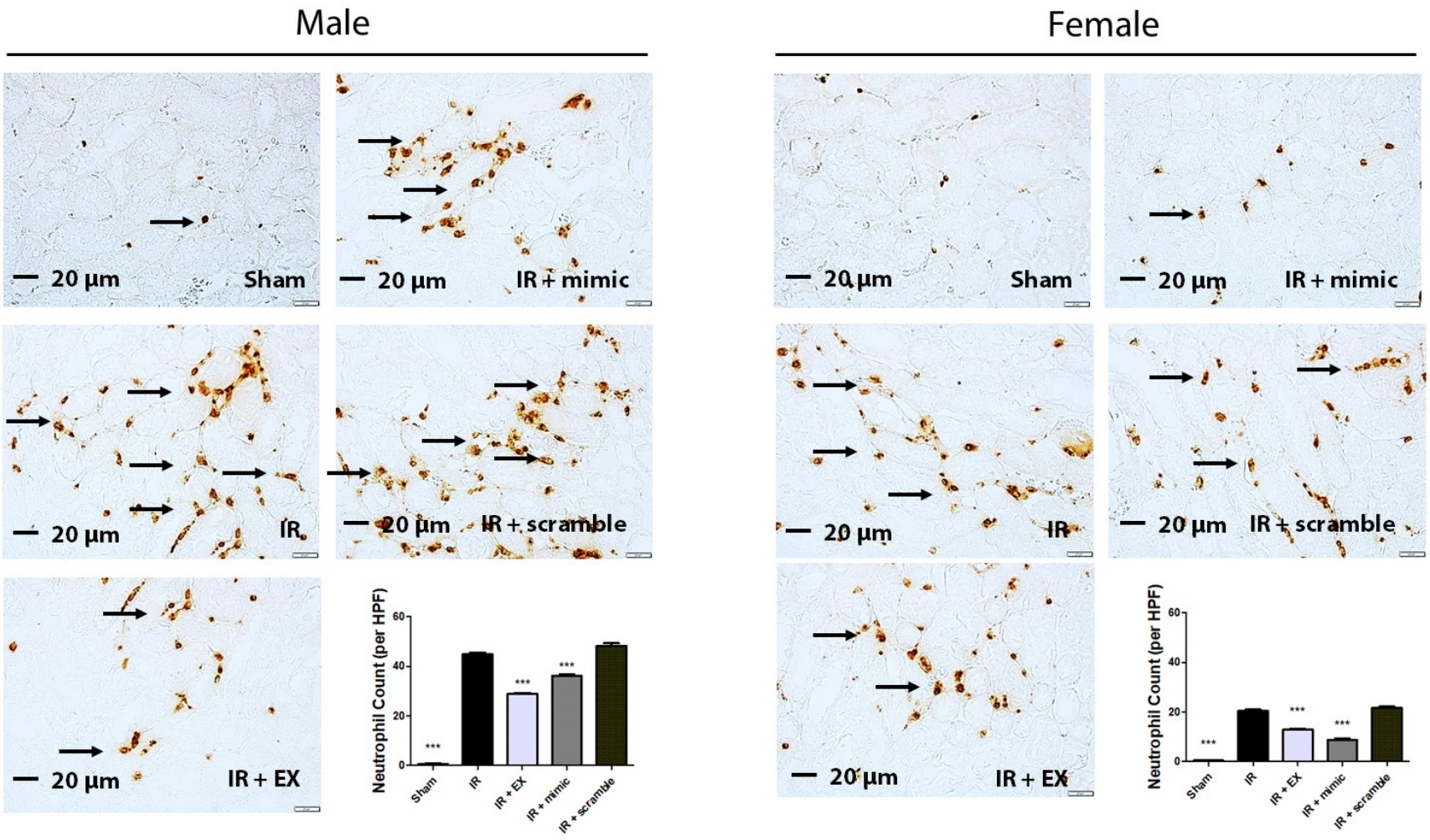

Figure 21 | miR-486-5p injection decreases neutrophil infiltration in male and female mice. Depicted are neutrophil counts from male or female FVB mice 24 hours after either Invivofectamine-mimic complex containing miR-486-5p (1 mg/kg, IR + mimic) or ECFC-exosome injection (20 µg, IR + EX) at the time of reperfusion. The quantitative assessment of neutrophil infiltration (number of neutrophils per field) was performed by a pathologist blinded to the slides. Sham (untreated mice), IR (30 minutes of ischemia) and IR + scramble (AKI mice injected with 1 mg/kg of Invivofectamine-scrambled miRNA complex at the beginning of reperfusion. *** P<0.0001 vs IR, one-way ANOVA. n=5 for male mice, n=3 for female mice.

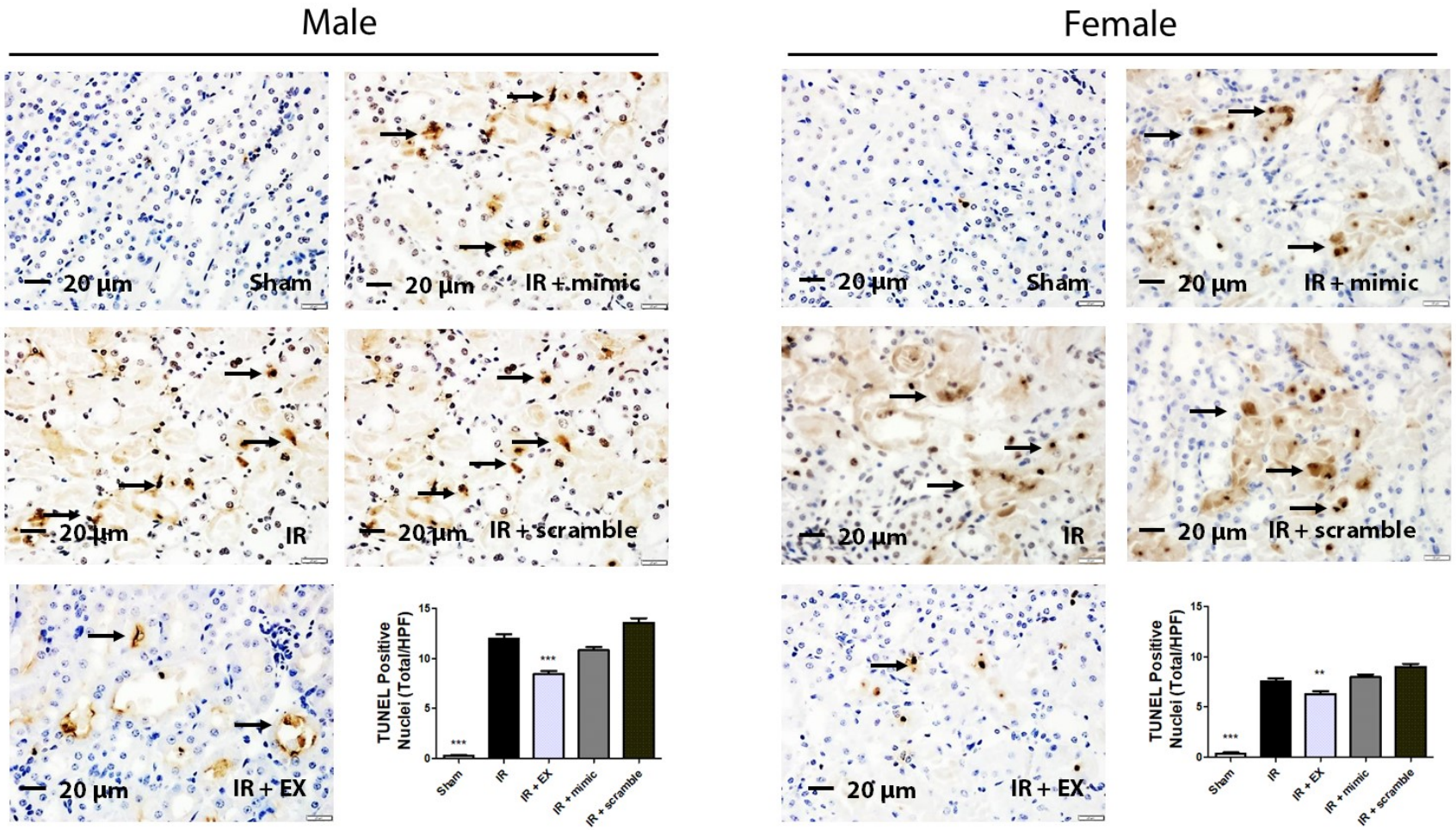

Figure 22 | Only ECFC-exosomes decrease histologic evidence of apoptosis after ischemic injury in male and female mice. Depicted is the semi-quantitative assessment of terminal deoxynucleotidyl transferase-mediated dUTP nick-ending labeling (TUNEL) staining in kidneys from male (A) or female (B) FVB mice 24 hours after either Invivofectamine-mimic complex containing miR-486-5p (1 mg/kg, IR + mimic) or ECFC-exosome injection (20 µg, IR + EX) at the time of reperfusion. TUNEL assessment (depicted as TUNEL-positive nuclei per high powered field) was performed by a pathologist blinded to the slides. Sham (untreated mice), IR (30 minutes of ischemia) and IR + scramble (AKI mice injected with 1 mg/kg of Invivofectamine-scrambled miRNA complex at the beginning of reperfusion. Arrows indicate TUNEL-positive nuclei, indicative of apoptosis. HPF; high-powered field. ** P<0.01 vs IR, *** P<0.0001 vs IR, one-way ANOVA. n=5 for male mice, n=3 for female mice.

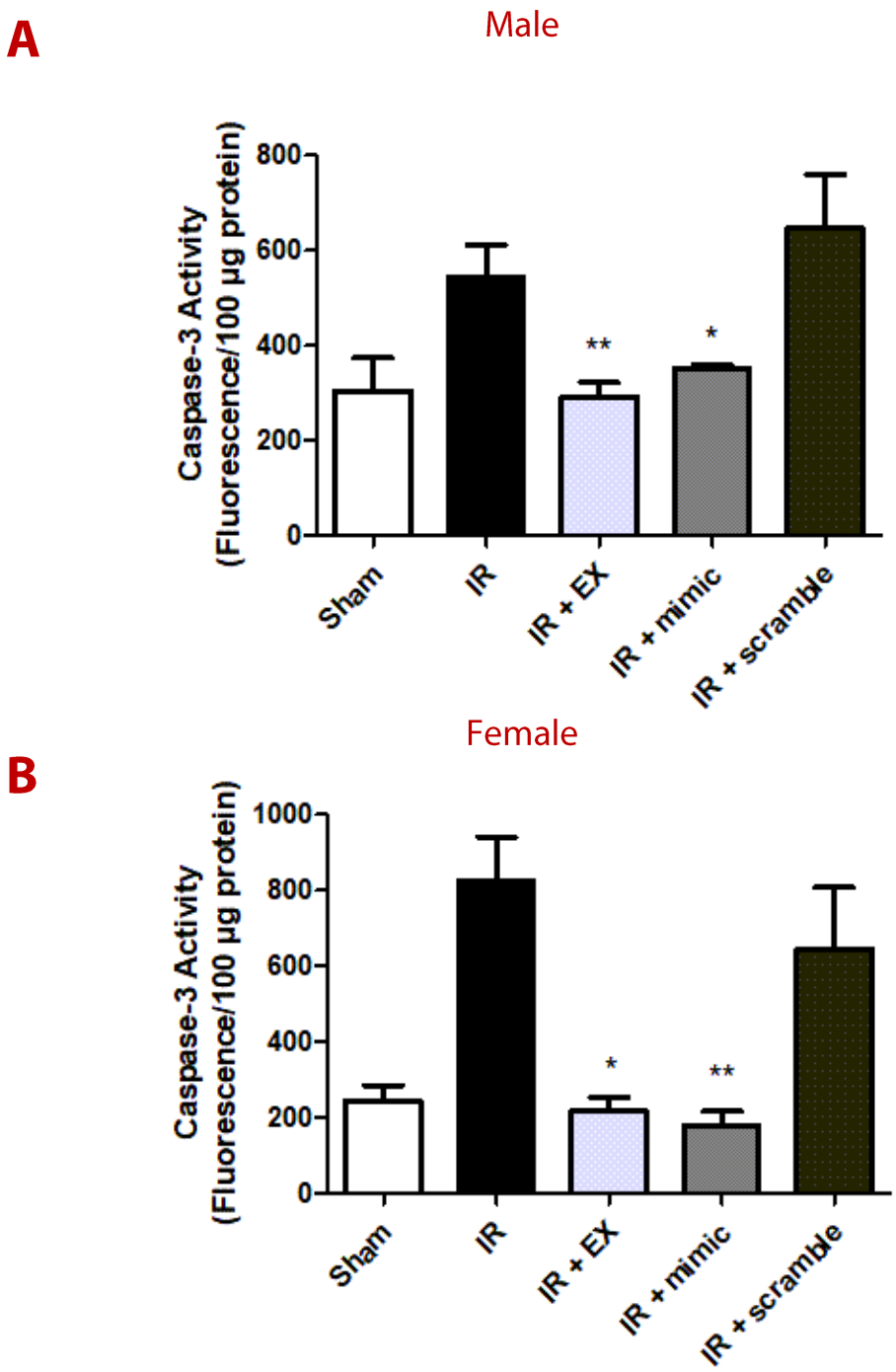

Figure 23 | miR-486-5p injection decreases kidney caspase-3 activity after ischemic injury in male and female mice. Depicted are caspase-3 activity assessments from male (A) or female (B) measurements in FVB mice 24 hours after either Invivofectamine-mimic complex containing miR-486-5p (1 mg/kg, IR + mimic) or ECFC-exosome injection (20 µg, IR + EX) at the time of reperfusion. Sham (untreated mice), IR (30 minutes of ischemia) and IR + scramble (AKI mice injected with 1 mg/kg of Invivofectamine-scrambled miRNA complex at the beginning of reperfusion). *P<0.05, **P<0.01 vs IR. n=5 for male mice, n=3 for female mice.

Female mice are less susceptible to IR injury

A key finding in these results is the sex differences between serum creatinine and BUN levels. When comparing each of the sexes explicitly for each experimental group by two-way ANOVA, we observed that females had a much lower serum creatinine ($p<0.01$ vs male) and BUN ($p<0.001$ vs male), even in sham mice **(Figure 18, S1)**. Female injury scores ($p<0.0001$ vs male) **(Figure 19, S2)**, neutrophil infiltration ($p<0.0001$ vs male) **(Figure 21, S4)**, and TUNEL-positive nuclei ($p<0.0001$ vs male) **(Figure 22, S5)**, are also much lower, except for sham. Megalin staining ($p<0.0001$ vs male) **(Figure 20, S3)** showed significantly lower loss in the female IR and IR-scramble groups.

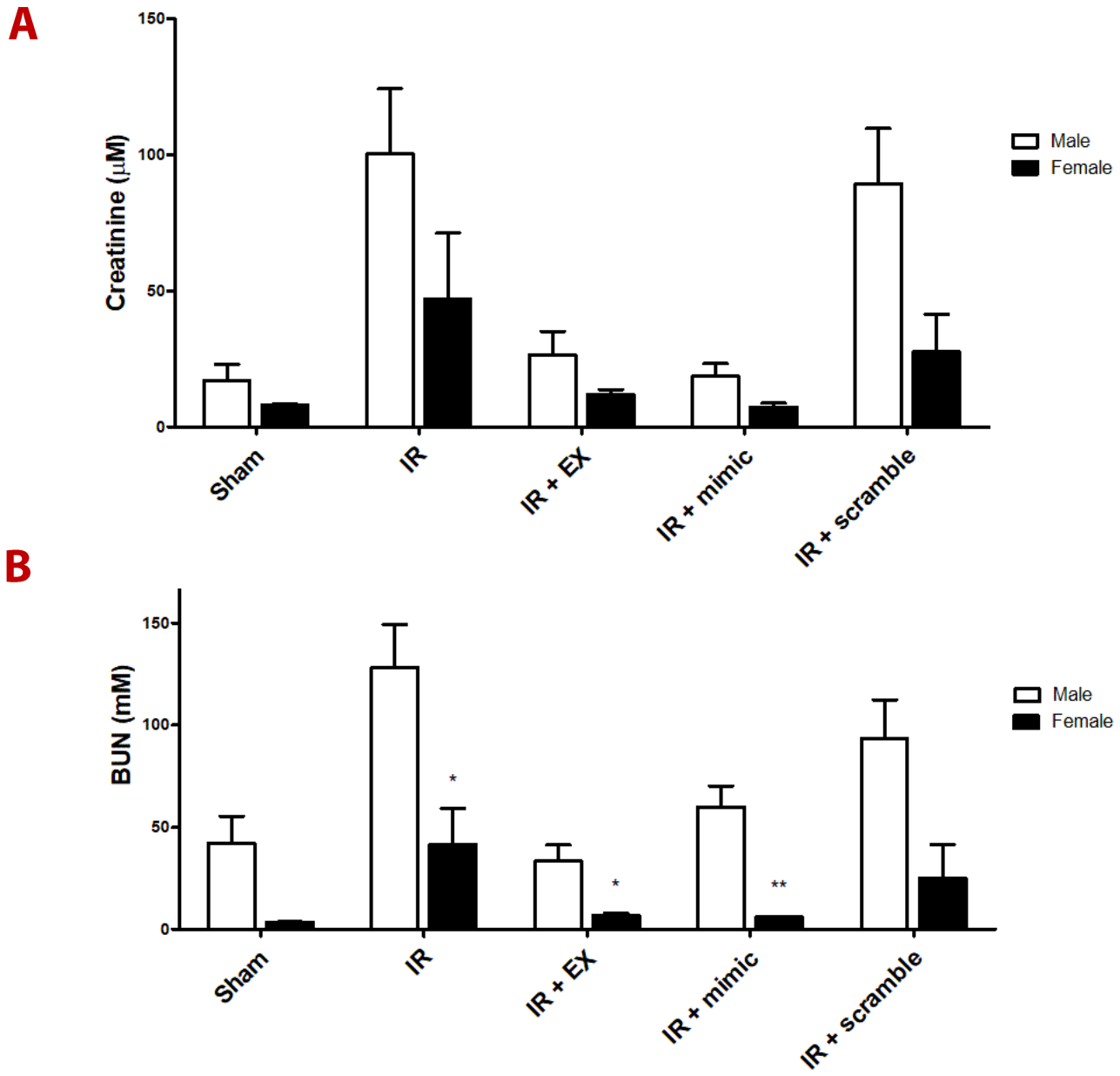

Supplemental Figure 1 | Female mice have significantly lower serum creatinine and BUN across experimental groups. Depicted are serum creatinine (A) or blood urea nitrogen (B) measurements from male and female FVB mice 24 hours after either Invivofectamine-mimic complex containing miR-486-5p (1 mg/kg, IR + mimic) or ECFC-exosome injection (20 μg, IR + EX) at the time of reperfusion. Sham (untreated mice), IR (30 minutes of ischemia) and IR + scramble (AKI mice injected with 1 mg/kg of Invivofectamine-scrambled miRNA complex at the beginning of reperfusion). Male is significantly different than female by two-way ANOVA, $P<0.01$ creatinine, $P<0.001$ BUN. *$P<0.05$ vs Male, **$P<0.01$ vs Male. n=5 for male mice, n=3 for female mice.

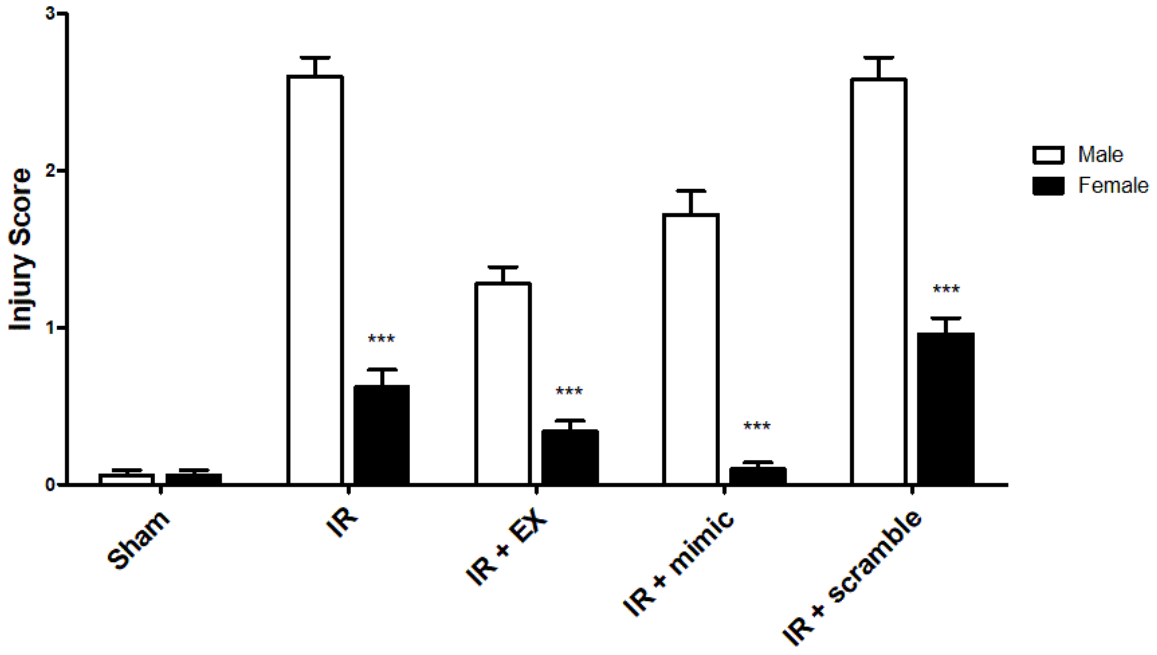

Supplemental Figure 2 | Female mice have significantly lower injury scores across experimental groups. Depicted are injury scores from male and female FVB mice 24 hours after either Invivofectamine-mimic complex containing miR-486-5p (1 mg/kg, IR + mimic) or ECFC-exosome injection (20 µg, IR + EX) at the time of reperfusion. Injury scores were calculated by a pathologist blinded to the slides. Sham (untreated mice), IR (30 minutes of ischemia) and IR + scramble (AKI mice injected with 1 mg/kg of Invivofectamine-scrambled miRNA complex at the beginning of reperfusion. Male is significantly different than female by two-way ANOVA, $P<0.0001$. *** $P<0.001$ vs Male, one-way ANOVA. n=5 for male mice, n=3 for female mice.

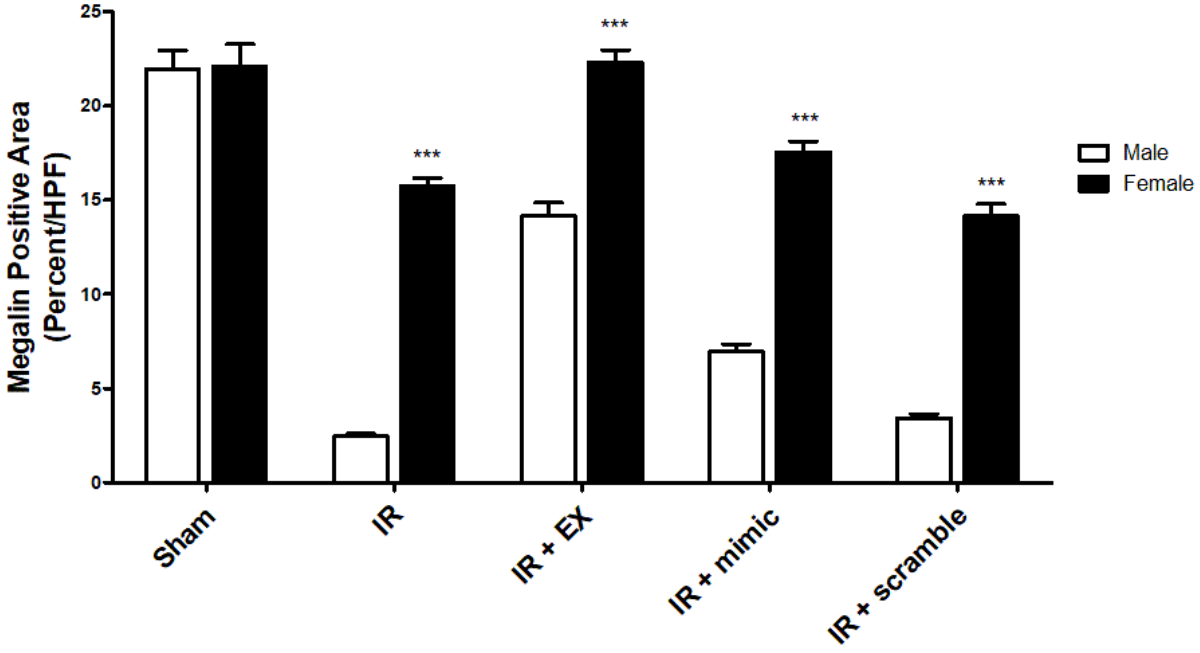

Supplemental Figure 3 | Female mice have significantly less megalin loss across experimental groups. Depicted is megalin staining from male and female FVB mice 24 hours after either Invivofectamine-mimic complex containing miR-486-5p (1 mg/kg, IR + mimic) or ECFC-exosome injection (20 µg, IR + EX) at the time of reperfusion. Megalin staining was performed by a pathologist blinded to the slides. Sham (untreated mice), IR (30 minutes of ischemia) and IR + scramble (AKI mice injected with 1 mg/kg of Invivofectamine-scrambled miRNA complex at the beginning of reperfusion. HPF; high-powered field. Male is significantly different than female by two-way ANOVA, $P<0.0001$.*** $P<0.001$ vs Male, one-way ANOVA. n=5 for male mice, n=3 for female mice.

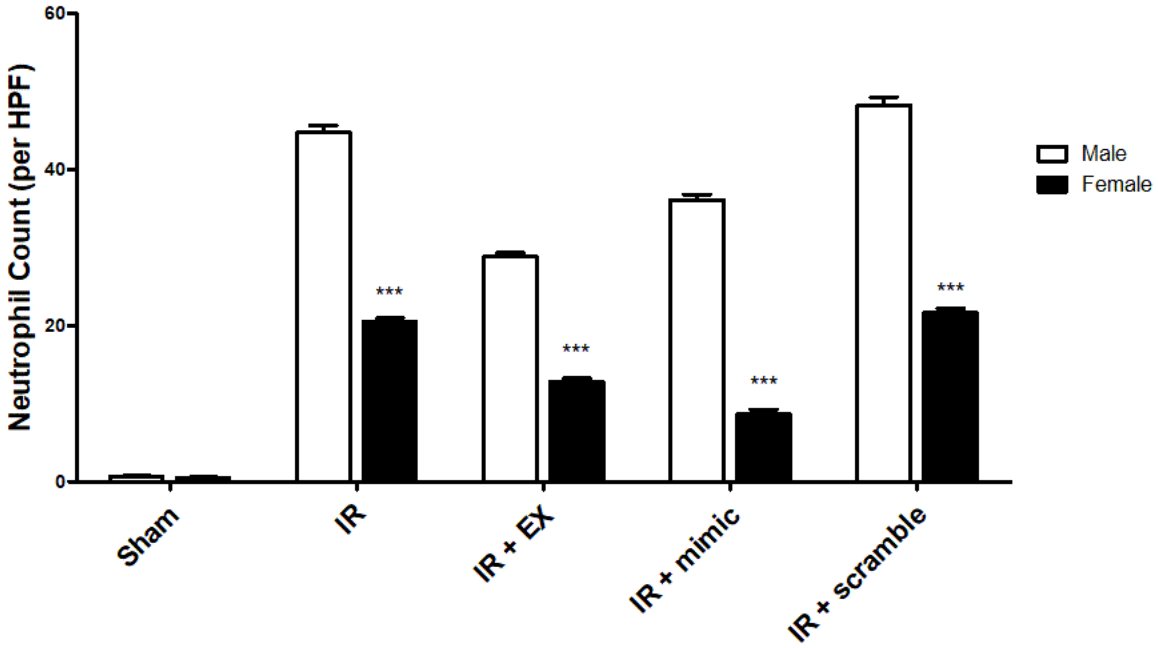

Supplemental Figure 4 | Female mice have significantly lower neutrophil infiltration counts across experimental groups. Depicted are neutrophil infiltration counts from male and female FVB mice 24 hours after either Invivofectamine-mimic complex containing miR-486-5p (1 mg/kg, IR + mimic) or ECFC-exosome injection (20 µg, IR + EX) at the time of reperfusion. Counts were performed by a pathologist blinded to the slides. Sham (untreated mice), IR (30 minutes of ischemia) and IR + scramble (AKI mice injected with 1 mg/kg of Invivofectamine-scrambled miRNA complex at the beginning of reperfusion. Male is significantly different than female by two-way ANOVA, $P<0.0001$. *** $P<0.001$ vs Male, one-way ANOVA. n=5 for male mice, n=3 for female mice.

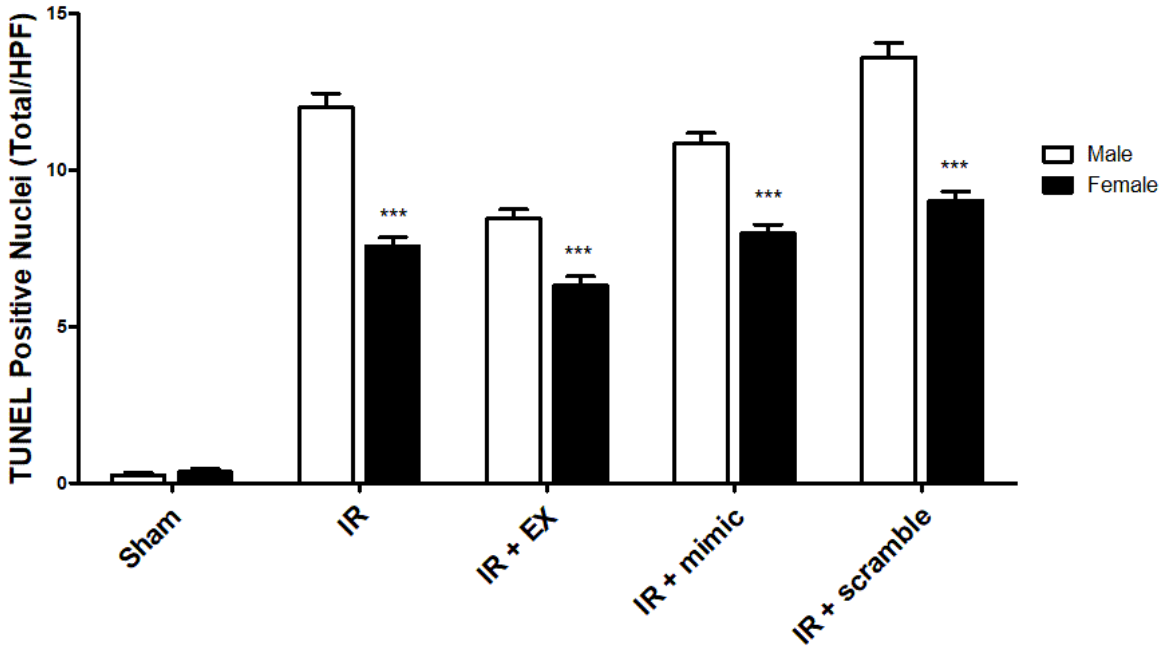

Supplemental Figure 5 | Female mice have significantly lower histologic evidence of apoptosis across experimental groups. Depicted are TUNEL-positive nuclei counts from male and female FVB mice 24 hours after either Invivofectamine-mimic complex containing miR-486-5p (1 mg/kg, IR + mimic) or ECFC-exosome injection (20 µg, IR + EX) at the time of reperfusion. Counts were performed by an independent pathologist. Sham (untreated mice), IR (30 minutes of ischemia followed by 30 minutes of reperfusion) and IR + scramble (AKI mice injected with 1 mg/kg of Invivofectamine-scrambled miRNA complex at the beginning of reperfusion. HPF; high-powered field. Male is significantly different than female by two-way ANOVA, $P<0.0001$. *** $P<0.001$ vs Male, one-way ANOVA. n=5 for male mice, n=3 for female mice.

DISCUSSION

The purpose of this study was to investigate the biodistribution, cellular localization, and targeting mechanisms of ECFC-derived exosomes and miR-486-5p after delivery to both male and female mice with ischemia/reperfusion AKI. The major finding of this study is that ECFC-derived exosomes selectively target the kidney post-IR, which leads to increased miR-486-5p in glomeruli, proximal tubule segments, and the endothelium of the injured kidney. The data also suggests that CXCR4, present on ECFC-derived exosomes, and SDF-1α, released from the ischemic kidney, mediates the targeting of the exosome to the site of injury. The interaction between CXCR4 and SDF-1α is also required for miR-486-5p transfer from the exosome to the injured tissue. Finally, encapsulated miR-486-5p can reach the injured kidney endothelium and proximal tubular segments and can attenuate injury just as efficacious as exosomes.

ECFC-derived Exosomes as a Biotherapeutic in AKI

Our current study uses exosomes, or $TSG101^+$ and $CD81^+$ ECFC-derived small EVs as a potential biotherapeutic in IR AKI. While absolute purification and isolation of this subset of EVs is not a feasible goal, the separation of EVs from other non-EV components from cultured cell medium and other cellular components is much more practical in EV research[45]. The choice of separation technique must be informed by the specific study. In this study, a differential centrifugation technique was chosen based on previous studies with this ECFC-EV population[6,25,89]. After the initial removal of contaminants (apoptotic bodies and medium/large EVs), the cultured media is subjected to a 90-minute 100,000 x g ultracentrifugation, where the pellet (containing sEV population) is resuspended and washed with EV-free buffer, and then subjected to a repeated 90-minute 100,000 x g ultracentrifugation. This allows better specificity

of sEV separation[45]. Even still, contamination by other non-small extracellular vesicles and/or macromolecular aggregate in the sEV fraction can occur[98].

Many experimental methods have been proposed to assess the purity of EVs, and ISEV has recommended multiple, complementary techniques to assess the results of separation techniques[45,99]. EVs must be defined by the source of EVs, characterized to determine the abundance of EVs, and tested for the presence of components associated with EV subtypes and for the presence of non-vesicular co-isolated contaminants. In this study, we define our EVs by the presence of exosome-specific markers TSG101 and CD81 **(Figure 3)**. Further, we quantify the EV abundance by both total protein and absolute particle number by nanoparticle tracking analysis **(Figure 4)**. In our sEV population, we found that 91% of the particles registered by light scatter NTA were within the exosomal size distribution (30 - 150 nm). Further, by total protein quantification, approximately 1.5 μg of protein was present after the sEV separation per 1 mL of ECFC conditioned media. This quantification was used to normalize the sEV dose per animal in the *in vivo* studies (the sEV population separated from approximately 14 mL of cultured ECFC media, or 20 μg of protein, was administered per animal). Both quantification techniques have limitations; nanoparticle tracking analysis may overestimate EV counts as the light scatter technique may also register other contaminant particles, such as lipoproteins and other types of EVs, while total protein quantification will overestimate due to protein aggregates and other co-isolated proteins. Unique to this study, we also characterized the separated ECFC-derived sEV population as enriched in miR-486-5p, in contrast to other endothelial cell line sEVs, such as HUVECs **(Figure 5)**. A limitation of this study is the absence of non-vesicular marker studies to determine the presence and/or absence of non-vesicular contaminants.

In this study, we demonstrated that ECFC-derived sEVs (as referred in this study as exosomes) may selectively target the injured kidney as of 30 minutes post-injection, remain at the site of injury past 4 hours, but are no longer found in the kidney at 24 hours **(Figure 6, 7)**. This may suggest that the exosomes are selectively homing to the injured kidney before 30 minutes post-reperfusion and are either degraded or excreted. It may also be possible that, after 24 hours, the dye itself is no longer able to produce a signal. The comparison between the labelled exosomes and DiR alone post-reperfusion is necessary to show that the fluorescent dye doesn't itself selectively home to the region of interest post-IR. Biodistribution of DiR alone is nonselective, whereas the labeled exosome distribution shows the increased targeting to the kidney.

Further, miR-486-5p levels were quantified relative to U6 in each organ, which shows a significant increase in miR-486-5p in the kidney at up to 24 hours after injection **(Figure 8)**. This data differs from the *ex vivo* OI data, which shows lack of exosomes in the kidney after 24 hours. It can be hypothesized that by 24 hours post-reperfusion, the exosomes have successfully delivered their cargo to the ischemic cells, and the exosomes themselves have been removed, degraded, or excreted. Both *in vivo* and *ex vivo* images were taken, as the level of detail from the whole mouse imaging did not present enough accuracy to definitively conclude the exact location from which the signal was originating. This experiment used a lipophilic near infrared (NIR) dye, DiR, which has a potential pitfall; the dyes have a much longer half-life compared to exosomes. This becomes a risk when imaging after 24-48 hours, as the fluorescence being analyzed may just be remaining dye and not the exosomes in question. After between 5 and 30 minutes, however, other studies have shown that injected exogenous extracellular vesicles reach their final destination[44]. A study by Grange et al. used OI to show that their EV population from

MSCs accumulate specifically in the glycerol-induced AKI-injured kidney after 5 and 24 hour post- intravenous injection, although an earlier timepoint was not investigated[54]. They also noted some uptake to the liver and spleen. Grange et al. was also able to show that direct labeling of EVs post-production and separation was more sensitive and intensity than using EVs which are obtained from previously labeled cells.

In the current study, fluorescence in the kidney returns to the level of the negative control after 24 hours, although the lung, liver, and spleen still show fluorescence past 24 hours. The fluorescence in the liver and spleen is likely due to non-specific accumulation of EVs in these organs, as seen in other studies[44,54]. When compared to the miR-486-5p levels in those organs, however, miR-486-5p is not increased in any other organ after exosome delivery at any time point. Therefore, this fluorescent signal may be attributed to degraded exosomes being processed and excreted in these organs.

Delivery routes other than intravenous were not analyzed in this study. It is hypothesized that despite the lack of delivery routes tested, the results of this study may not have been affected. A previous study by Wiklander et al. showed the change of distribution based on different injection routes of exosomes from a variety of cell-lines, inferring that the exosomes derived from different cell lines which wouldn't preferentially home in a specific organ[44]. The study presented that different injection routes change the distribution of exosomes to different organs - mostly in the liver, spleen, pancreas, and gastrointestinal tract. Notably, however, they reported little distribution to the kidney no matter the injection route and reported little to no change in distribution to the kidney when the injection route was changed. In the current study, very

similar data are seen in which there are high levels of distribution to the liver and spleen after injection of ECFC exosomes **(Figure 7)**. We specifically note differential targeting to the injured kidney. This does not negate the need for trials in the current study with the investigation into various injection routes and must be taken into consideration for future studies.

Exosomes were also labeled with PKH26 and injected immediately post-reperfusion, and the animals were sacrificed 30 minutes post-injection to determine histological localization. PKH26-labeled exosomes were found primarily in the tubulointerstitium of the kidney and were present in the Kupffer cells of the liver but were not localized in heart or lung tissue **(Figure 9)**. In other studies of IR injury, PKH26-labeled EVs were identified by confocal microscopy in large vessel and peritubular capillary endothelium, tubular epithelium, and glomeruli in as little as 2 hours post-injection[47,100]. While the current study was unable to colocalize the PKH26-labeled exosome with other endothelial structures, it was able to show that ECFC-derived exosomes are able to target the kidney and traverse the endothelial cell barrier into the tubulointerstitium in as little as 30 minutes post-injection, which may be due to increased vascular permeability in the IR injured kidney. With this data, it is possible to hypothesize that the exosomes may be targeted to the tissue, dumping their contents into the surrounding cells, and collecting in the tubulointerstitium. While this data was unable to specifically narrow in on the exosome to the sub-cellular level, we can conclude that ECFC-derived exosomes are able to travel through the vasculature and into the tissue.

As shown in this study, ECFC-derived exosomes have enriched miR-486-5p, and through the relative quantification after injection vs after IR alone, we are able to determine to which tissue

segments the injected ECFC-derived exosomes are delivering their cargo. Injection of miR-486-5p enriched ECFC-exosomes demonstrate selective increases in the kidney cortex after injury, but more specifically within proximal tubule segments, glomeruli, and endothelium **(Figure 10)**. Studies from the Camussi group using MSC-derived EVs in cisplatin-induced AKI have also showed the delivery of EVs to tubular epithelial cells and the renal vasculature[46,101]. This is also very consistent in other disease models. Wu et al. used EPC-derived exosomes in a model of acute lung injury, which was able to enhance proliferation, migration, and tube formation in vitro, while restoring pulmonary integrity *in vivo*[102]. They were also able to track miR-126, which was enriched in their EPC-derived exosomes, and show delivery of EPC-exosome cargo to the pulmonary endothelium. Dellett et al. also showed delivery of ECFC-derived EVs, also enriched in miR-486-5p, to retinal endothelium after ischemic retinopathy[70].

EVs contain an assortment of biomolecules including miRNA and have been shown to act as the mediators of the beneficial effects previously seen in cell therapies. Studies have shown that ECFCs do not directly replace lost cells but exert paracrine effects on the IR-injured vasculature to facilitate the reduction of the inflammation response, and do not require cell engraftment for repair and post-ischemic revascularization. The transfer of information from cell to cell may be dependent on EVs and their subsequent attachment or internalization into the target cell. Here, we show that the use of EIPA as an inhibitor of macropinocytosis attenuates the ability of ECFC-derived exosomal transfer of Cy3-labeled miR-486-5p, which suggests a major role for the macropinocytosis pathway **(Figure 11)**. In exosome biogenesis, nSMase2 and ceramide plays a key role in creating the invaginations in the MVB and in the packaging miRNA and other biomolecules into exosomes[103]. In this study, we show that inhibiting exosome formation and

packaging using GW4869, an inhibitor of nSMase2, also attenuates the ability of ECFC-derived exosomal transfer of Cy3-labeled miR-486-5p. Together, these data demonstrate the importance of exosomes and macropinocytosis in the transfer of miR-486-5p from ECFCs to target cells.

As mentioned, cells isolated from different tissues have been previously shown to target in various locations *in vivo*. Similarly, EVs are also shown to have different homing capacities based on the cell origin[44]. It is possible that, as EVs are shed from their parent cells, they acquire a subset of the same surface receptors and binding proteins. If this is in fact that case, it is obvious that EVs from a specific type of cell are more likely to home to a similar tissue as the cells which they were shed from. When applied to AKI, we can assume that exosomes shed from ECFCs possess surface receptors and binding proteins similar to those on ECFCs and other more mature endothelial cells, and that these may assist the ECFC-derived exosome to localize to the tissue. Previous studies have shown that EVs from EPCs are able to be effectively delivered to both tubular epithelial and endothelial cells[32,40]. This may help to localize the exosomes to their tissue of origin or a similar tissue, but this still doesn't explain how these exosomes are able to, in the current model, localize specifically to the point of injury over tissue elsewhere.

SDF-1α, a C-X-C type chemokine and a ligand for CXCR4, is a well known and widely expressed chemokine involved in vascular repair and retention of endothelial stem cells to the site of injury[35,76]. The interaction and signaling between SDF-1α, which is upregulated in ischemic tissue, and its receptor CXCR4 have been implicated as having a major role in the homing of EPCs and ECFCs to injured tissue post-ischemia. In EVs, the mechanisms

of targeting to specific tissues remain poorly understood. In animal models of IR AKI, renal expression of SDF-1α increases throughout ischemia, and the gradient produced allows homing and migration of CXCR4 expressing EPCs to the injured tissue [36,37]. *In vivo*, EVs are thought to interact with the plasma membrane of cells[104]. Through dynamic interactions, vesicles roll across the plasma membrane, which is followed by the binding of specific membrane proteins to their cell receptors, fusion, and release of EV cargo into the target cell's cytoplasm[104].

In the current study, PKH26-labeled ECFC-derived exosomes were delivered to normoxic and hypoxic HUVECs to demonstrate the importance of hypoxia to the retention and internalization of delivered exosomes **(Figure 12)**. CXCR4 was expressed in both ECFCs and exosomes. Importantly, exosome uptake into HUVECs exposed to hypoxia was increased compared to normoxic cells and was inhibited by incubation with the CXCR4 inhibitor plerixafor, or by a neutralizing antibody to SDF-1α. From this, the CXCR4/SDF-1α axis is shown to be necessary for the delivery of ECFC-derived exosomal cargo. This is also supported by functional experiments *in vivo*, where serum creatinine, BUN, renal injury scores, and neutrophil infiltration are all decreased post-exosome injection 24 hours post-reperfusion, while treating IR AKI mice with ECFC-derived exosomes previously incubated with plerixafor eliminated the protective effects of exosomes **(Figure 13, 14)**. It was chosen to preincubate the exosomes with plerixafor rather than administer in conjunction with exosomes at the time of reperfusion to avoid any confounders through the action of plerixafor on murine CXCR4[36]. Therefore, it can be interpreted that the effect seen is due to the inhibition of exosomal CXCR4, and not CXCR4 present in the mouse.

While many studies indicate a role for the CXCR4/SDF-1α axis in cell therapies using EPCs and MSCs, fewer studies indicate a role in EV therapies[105–108]. In 2015, Kang et al demonstrated that MSC-derived EVs expressing CXCR4 could reduce left ventricular remodeling after myocardial infarction in mice, and that overexpressing CXCR4 had increased protective effect[109]. In 2019, Milano et al. replicated the results in a similar study, while concluding that overexpressing CXCR4 in cardiac-resident progenitor cell-derived exosomes increased both their cardioprotective effects as well as targeting and bioavailability to the ischemic heart[110]. While the exact mechanism behind the increased exosome mobilization is unclear, these studies continue to point towards the CXCR4/SDF-1α axis as a key targeting axis for cells and their EVs to ischemic injury. Not to be forgotten, other mechanisms and pathways may also play a role in the selective targeting of ECFC-derived EVs to the ischemic kidney, such as exosomal integrins, tetraspanins, and target cell adhesion molecules, among others[41,65].

miR-486-5p as a Biotherapeutic in AKI

Previous data from the Burns Lab shows that ECFC cells transfected with antagomir to miR-486-5p create exosomes with lower exosomal miR-486-5p, and FVB mice after IR injury treated with antagomir-ECFC exosomes do not induce an increase in kidney miR-486-5p levels, nor does it prevent injury through the PTEN/Akt pathway[6]. The Burns Lab has also shown that a miR-486-5p mimic can be given to HUVEC cells and can enter the cell in small amounts even without lipofectamine (data not published). These data, combined with previous data showing the importance of miR-486-5p to the exosome's therapeutic effect, led us to the hypothesis that delivering miR-486-5p alone *in vivo* could potentially offer a similar protection to IR as the injection of ECFC-derived exosomes. Invivofectamine, a nanoparticle technology that can

encapsulate and protect nucleic acids for delivery, was complexed with miR-486-5p mimic in this experiment to test the hypothesis. Further, in the following studies, both male and female mice were used and separated for analysis.

In the current study, delivery of miR-486-5p using the invivofectamine-mimic complex led to significantly increased levels of miR-486-5p in the liver, spleen, and kidney over IR alone as well as with exosome treatment 24-hours post-injection in both male and female mice **(Figure 15, 16)**. 24 hours post-invivofectamine-mimic injection, miR-486-5p was significantly increased in male and female endothelium and tubular segments over IR alone or treatment with exosomes **(Figure 17)**. This may indicate that miR-486-5p alone is somewhat protected when complexed with invivofectamine in the cell and can withstand 24 hours. These data also compare miR-486-5p levels post-exosome delivery at 30 minutes and 24 hours post-reperfusion. While exosomes significantly raised endothelial and proximal tubule miR-486-5p levels after 30 minutes post-injection **(Figure 10)**, this increase returns to baseline after 24 hours. Further, we show that miR-486-5p levels remain elevated in the whole kidney 24 hours after exosome injection **(Figure 8)**. While exosome injection does not increase miR-486-5p levels in the endothelium nor proximal tubular segments as shown, it can be hypothesized that the miR-486-5p is elsewhere in the kidney, perhaps the interstitium, and have moved out of the endothelium and proximal tubular segments after 24 hours.

While we have no earlier comparison for miR-486-5p levels post-invivofectamine-mimic delivery, the highly elevated levels which remain after 24 hours lead to the hypothesis that the miR-486-5p level has increased over time. It cannot be determined, however, how long it took

the invivofectamine-mimic complex to be delivered to the kidney. Without CXCR4 acting to target the complex to the site of ischemic injury, we can hypothesize that it may have taken longer for the levels to increase in the kidney compared to ECFC-derived exosomes.

Previous studies with invivofectamine have shown its effectiveness in delivering immunostimulatory RNA (isRNA) and miRNA to targets within various organs. In 2012, Inaba et al. show that their isRNA-invivofectamine complex increases isRNA levels in the liver, spleen, kidney, lung, and heart, while atelocollagen as a vehicle did not[111]. Further, they were able to show that invivofectamine can deliver isRNA post-intravenous injection to the kidney to harbour an effect, second only to the liver. Another more recent study by Schlosser et al. in 2018 demonstrated that delivery of a synthetic miRNA mimic with no mammalian homologue could be delivered intravenously to the liver, spleen, kidney, heart, and lung in as little as 2 hours, and remain past 24 hours[112]. Interestingly, both subcutaneous and intraperitoneal injections also delivered equal amounts to the kidney as compared to intravenous. Intratracheal and intranasal were also studied, however, these methods of delivery were less effective for delivery to the kidney. In addition to the current study, these studies demonstrate the effectiveness of invivofectamine as a delivery method for RNA.

In the current study, analysis of the invivofectamine-mimic complex as a delivery method for miR-486-5p in comparison to exosomes was performed to demonstrate potential differences in therapeutic potential. The invivofectamine-mimic complex yielded similarly significant results compared to exosomes in many functional aspects. Invivofectamine-mimic was able to significantly reduce serum creatinine and BUN compared to IR alone, but were insignificant compared to ECFC-exosome treatment **(Figure 18)**. Invivofectamine-mimic was also able to

significantly decrease injury scores **(Figure 19)**, neutrophil infiltration **(Figure 21)**, and apoptosis by caspase-3 activity **(Figure 23)**. To our knowledge, this is the first study to comparatively analyse exosomes and mimic delivery as potential biotherapeutics in IR AKI.

Sex Differences in Response to ECFC-derived Exosomes and miR-486-5p

A surprise finding in these results is the sex differences between serum creatinine and BUN levels. When comparing each of the sexes explicitly for each experimental group by two-way ANOVA, we see that females have a much lower serum creatinine and BUN, even in sham mice **(Figure S1)**. It is widely known that male mice are more susceptible to IR injury than female mice, but these data show that even baseline functional tests are lower in females than in males. This could be due to an increased muscle mass, increased protein catabolism, and/or increased GFR, but can also be due to kidney and glomerular injury. Female injury scores are also much lower **(Figure S2)**, and female mice have significantly less megalin shedding **(Figure S3)**, lower neutrophil infiltration **(Figure S4)**, and less apoptosis **(Figure S5)**, except for sham. While female mice show significantly less injury across experimental groups, the ECFC-exosome and invivofectamine-mimic treatments still show significant protection against kidney ischemic injury in females. The high creatinine and BUN levels seen in the experimental groups must be due, in some part, to IR injury. Using the same IR model as the current study, Kang et al. showed that female mice were more resistant to bilateral renal clamping IR AKI compared to male mice[84]. They also demonstrated that castration of male mice reduced injury, while supplementation with testosterone to castrated male mice reversed the protective effect. Further, ovariectomized female mice were no longer resistant to injury, while estrogen supplementation to ovariectomized female mice attenuated injury. While the current study was only able to show

the protective effect of female mice against IR injury, in combination with the literature we can hypothesize that the effects seen in the current study may be due to hormone differences.

In order to continue towards the development of a therapeutic tool for AKI treatment, further studies must be performed. Route of administration studies, along with dosage, toxicity, and long-term effects of the use of both ECFC exosomes and invivofectamine-mimic must be investigated. Previous studies have shown the acute use of exosomes in the proliferation and repair of the kidney[6,33,89,101], but many studies lack data showing full renal recovery or the complete reversal of fibrosis. Dose, therapy regiment, and length of treatment are questions which still require answers before ECFC exosomes can be considered as a therapy for AKI. Further, ECFCs only secrete a very small number of exosomes. For use as a therapeutic tool, an immense volume of cultured media and improved isolation techniques would be needed. An alternate technique to improve yield of exosomes would be to engineer novel exosomes to mimic the properties of ECFC exosomes. This can be done through various methods: exosomes could be fully engineered from generic liposomes and vital membrane proteins as found on the ECFC exosome membrane could be added[113]; ECFCs could be used and the endosomal release pathway could be manipulated to secrete exosomes which can be then loaded with miR-486-5p[113]; or a hybrid technique in which ECFC exosomes are fused with liposomes to form bigger exosomes to increase the dosage[114]. In the current study, work with the invivofectamine complex began these studies to attempt to mimic the properties of exosomes, however, future studies will involve a synthetic nanoparticle enriched in miR-486-5p. Further, attempts will be made to adhere CXCR4 and other necessary integrins to increase targeting and cellular uptake. These techniques will assist in the production of a viable biotherapeutic for future human studies.

Taken together, the current study strongly suggests the protective and reparative pathway for ECFC-derived exosomes, but more importantly, their miR-486-5p. These data help explain how the beneficial effects of ECFC-derived exosomes influence the recovery of local endothelium and tubular epithelium in post-ischemic AKI.

REFERENCES

1. Mehta RL, Kellum JA, Shah S V *et al.* Acute Kidney Injury Network: report of an initiative to improve outcomes in acute kidney injury. *Crit. Care* 2007; **11**: R31.

2. Bonventre J V., Yang L. Cellular pathophysiology of ischemic acute kidney injury. *J. Clin. Invest.* 2011; **121**: 4210–4221.

3. Makris K, Spanou L. Acute Kidney Injury: Definition, Pathophysiology and Clinical Phenotypes. *Clin. Biochem. Rev.* 2016; **37**: 85–98.

4. Basile D, Anderson M, Sutton T. Pathophysiology of Acute Kidney Injury. *Compr. Physiol.* 2012; **2**: 1303–1353.

5. Carden DL, Granger DN. Pathophysiology of ischaemia-reperfusion injury. *J. Pathol.* 2000; **190**: 255–266.

6. Viñas JL, Burger D, Zimpelmann J *et al.* Transfer of microRNA-486-5p from human endothelial colony forming cell-derived exosomes reduces ischemic kidney injury. *Kidney Int.* 2016: 1–13.

7. Jang HR, Ko GJ, Wasowska BA *et al.* The interaction between ischemia-reperfusion and immune responses in the kidney. *J. Mol. Med.* 2009; **87**: 859–864.

8. Godwin JG, Ge X, Stephan K *et al.* Identification of a microRNA signature of renal ischemia reperfusion injury. *Proc. Natl. Acad. Sci. U. S. A.* 2010; **107**: 14339–14344.

9. Ishani A, Xue JL, Himmelfarb J *et al.* Acute Kidney Injury Increases Risk of ESRD among Elderly.

10. Karlberg L, Norlén BJ, Ojteg G *et al.* Impaired medullary circulation in postischemic acute

renal failure. *Acta Physiol. Scand.* 1983; **118**: 11–7.

11. Olof P, Hellberg A, Källskog O *et al.* Red cell trapping and postischemic renal blood flow. Differences between the cortex, outer and inner medulla. *Kidney Int.* 1991; **40**: 625–31.

12. Rabelink TJ, de Boer HC, van Zonneveld AJ. Endothelial activation and circulating markers of endothelial activation in kidney disease. *Nat. Rev. Nephrol.* 2010; **6**: 404–414.

13. Basile DP. The endothelial cell in ischemic acute kidney injury: implications for acute and chronic function. *Kidney Int.* 2007; **72**: 151–6.

14. Brezis M, Rosen S. Hypoxia of the Renal Medulla — Its Implications for Disease. Epstein FH, ed. *N. Engl. J. Med.* 1995; **332**: 647–655.

15. Li L, Jaiswal PK, Makhoul G *et al.* Hypoxia Modulates Cell Migration and Proliferation in Placenta-derived Mesenchymal Stem Cells. *J. Thorac. Cardiovasc. Surg.* 2017.

16. Basile DP, Collett JA, Yoder MC. Endothelial colony forming cells and proangiogenic cells: clarifying definitions and their potential role in mitigating acute kidney injury. *Acta Physiol.* 2017.

17. Basile DP, Bonventre J V, Mehta R *et al.* Progression after AKI: Understanding Maladaptive Repair Processes to Predict and Identify Therapeutic Treatments. *J. Am. Soc. Nephrol.* 2016; **27**: 687–697.

18. Chawla LS, Eggers PW, Star RA *et al.* Acute Kidney Injury and Chronic Kidney Disease as Interconnected Syndromes. *N. Engl. J. Med.* 2014; **371**: 58–66.

19. Coca SG, Singanamala S, Parikh CR. Chronic kidney disease after acute kidney injury: a systematic review and meta-analysis. *Kidney Int.* 2012; **81379**: 442–448.

20. Singbartl K, Kellum JA. AKI in the ICU: definition, epidemiology, risk stratification, and outcomes. *Kidney Int.* 2012; **81**: 819–825.

21. Humphreys BD, Cantaluppi V, Portilla D *et al.* Targeting Endogenous Repair Pathways after AKI. *J. Am. Soc. Nephrol.* 2015; **27**: 1–9.

22. Xue JL, Daniels F, Star RA *et al.* Incidence and Mortality of Acute Renal Failure in Medicare Beneficiaries, 1992 to 2001. *J Am Soc Nephrol* 2006; **17**: 1135–1142.

23. Patschan D, Krupincza K, Patschan S *et al.* Dynamics of mobilization and homing of endothelial progenitor cells after acute renal ischemia: modulation by ischemic preconditioning. *Am J Physiol Ren. Physiol* 2006; **291**: F176-85.

24. Collett JA, Mehrotra P, Crone A *et al.* Endothelial colony-forming cells ameliorate endothelial dysfunction via secreted factors following ischemia-reperfusion injury. *Am. J. Physiol. Renal Physiol.* 2017; **312**: F897–F907.

25. Burger D, Viñas JL, Akbari S *et al.* Human Endothelial Colony-Forming Cells Protect against Acute Kidney Injury: Role of Exosomes. *Am. J. Pathol.* 2015; **185**: 1–15.

26. Tögel FE, Westenfelder C. Kidney protection and regeneration following acute injury: Progress through stem cell therapy. *Am. J. Kidney Dis.* 2012; **60**: 1012–1022.

27. Lange C, Tögel F, Ittrich H *et al.* Administered mesenchymal stem cells enhance recovery from ischemia/reperfusion-induced acute renal failure in rats. *Kidney Int.* 2005; **68**: 1613–1617.

28. Camussi G, Deregibus MC, Bruno S *et al.* Exosomes/microvesicles as a mechanism of cell-to-cell communication. *Kidney Int.* 2010; **78**: 838–848.

29. Brodsky, S.V., Yamamoto, T., Tada, T., Kim, B., Chen, J., Kajiya, F. et al. Endothelial

dysfunction in ischemic acute renal failure: rescue by transplanted endothelial cells. *Am. J. Physiol.* 2002; **282**: F1140–F1149.

30. Yoder MC. Human endothelial progenitor cells. *Cold Spring Harb. Perspect. Med.* 2012.

31. Asahara T, Murohara T, Sullivan A *et al.* Isolation of putative progenitor endothelial cells for angiogenesis. *Science* 1997; **275**: 964–7.

32. Patschan D, Patschan S, Müller GA. Endothelial progenitor cells in acute ischemic kidney injury: strategies for increasing the cells' renoprotective competence. *Int. J. Nephrol.* 2011; **2011**: 828369.

33. Yoder MC, Mead LE, Prater D *et al.* Redefining endothelial progenitor cells via clonal analysis and hematopoietic stem/progenitor cell principals. *Blood* 2007; **109**: 1801–1809.

34. Moubarik C, Guillet B, Youssef B *et al.* Transplanted Late Outgrowth Endothelial Progenitor Cells as Cell Therapy Product for Stroke.

35. Sun J, Li Y, Graziani GM *et al.* E-Selectin Mediated Adhesion and Migration of Endothelial Colony Forming Cells Is Enhanced by SDF-1a/CXCR4. Bolego C, ed. *PLoS One* 2013; **8**: e60890.

36. Tögel F, Isaac J, Hu Z *et al.* Renal SDF-1 signals mobilization and homing of CXCR4-positive cells to the kidney after ischemic injury. *Kidney Int.* 2005; **67**: 1772–1784.

37. Togel FE, Westenfelder C. Role of SDF-1 as a regulatory chemokine in renal regeneration after acute kidney injury. *Kidney Int. Suppl.* 2011; **1**: 87–89.

38. Smadja DM, Dorfmüller P, Guerin CL *et al.* Cooperation between human fibrocytes and endothelial colony-forming cells increases angiogenesis via the CXCR4 pathway. *Thromb.*

Haemost. 2014; **112**: 1002–1013.

39. Petit I, Jin D, Rafii S. The SDF-1-CXCR4 signaling pathway: a molecular hub modulating neo-angiogenesis. *Trends Immunol.* 2007; **28**: 299–307.

40. Morigi M, Rota C, Remuzzi G. Mesenchymal Stem Cells in Kidney Repair. *Methods Mol. Biol.* 2016; **1416**: 89–107.

41. Raposo G, Stoorvogel W. Extracellular vesicles: Exosomes, microvesicles, and friends. *J. Cell Biol.* 2013.

42. Lv L-L, Wu W-J, Feng Y *et al.* Therapeutic application of extracellular vesicles in kidney disease: promises and challenges. *J. Cell. Mol. Med.* 2017.

43. Rovira J, Diekmann F, Campistol JM *et al.* Therapeutic application of extracellular vesicles in acute and chronic renal injury. 2017; **3**: 126–137.

44. Wiklander OPB, Nordin JZ, O'Loughlin A *et al.* Extracellular vesicle in vivo biodistribution is determined by cell source, route of administration and targeting. *J. Extracell. vesicles* 2015; **4**: 26316.

45. Théry C, Witwer KW, Aikawa E *et al.* Minimal information for studies of extracellular vesicles 2018 (MISEV2018): a position statement of the International Society for Extracellular Vesicles and update of the MISEV2014 guidelines. *J. Extracell. vesicles* 2018; **7**: 1535750.

46. Bruno S, Grange C, Collino F *et al.* Microvesicles derived from mesenchymal stem cells enhance survival in a lethal model of acute kidney injury. Câmara NOS, ed. *PLoS One* 2012; **7**: e33115.

47. Cantaluppi V, Gatti S, Medica D *et al.* Microvesicles derived from endothelial progenitor

cells protect the kidney from ischemia-reperfusion injury by microRNA-dependent reprogramming of resident renal cells. *Kidney Int.* 2012; **82**: 412–27.

48. El Andaloussi S, Mäger I, Breakefield XO *et al.* Extracellular vesicles: biology and emerging therapeutic opportunities. *Nat. Rev. Drug Discov.* 2013; **12**: 347–57.

49. Ratajczak J, Miekus K, Kucia M *et al.* Embryonic stem cell-derived microvesicles reprogram hematopoietic progenitors: evidence for horizontal transfer of mRNA and protein delivery. *Leukemia* 2006; **20**: 847–856.

50. Peinado H, Alečković M, Lavotshkin S *et al.* Melanoma exosomes educate bone marrow progenitor cells toward a pro-metastatic phenotype through MET. *Nat. Med.* 2012; **18**: 883–91.

51. Clayton A. Adhesion and signaling by B cell-derived exosomes: the role of integrins. *FASEB J.* 2004.

52. Mittelbrunn M, Gutiérrez-Vázquez C, Villarroya-Beltri C *et al.* Unidirectional transfer of microRNA-loaded exosomes from T cells to antigen-presenting cells. *Nat. Commun.* 2011; **2**: 282.

53. Février B, Raposo G. Exosomes: Endosomal-derived vesicles shipping extracellular messages. *Curr. Opin. Cell Biol.* 2004; **16**: 415–421.

54. Grange C, Tapparo M, Bruno S *et al.* Biodistribution of mesenchymal stem cell-derived extracellular vesicles in a model of acute kidney injury monitored by optical imaging. *Int. J. Mol. Med.* 2014; **33**: 1055–1063.

55. Ranghino A, Bruno S, Bussolati B *et al.* The effects of glomerular and tubular renal progenitors and derived extracellular vesicles on recovery from acute kidney injury. *Stem Cell*

Res. Ther. 2017; **8**: 24.

56. Collino F, Bruno S, Incarnato D *et al.* AKI Recovery Induced by Mesenchymal Stromal Cell-Derived Extracellular Vesicles Carrying MicroRNAs. *J Am Soc Nephrol* 2015; **26**: 2349–2360.

57. Bruno S, Tapparo M, Collino F *et al.* Renal regenerative potential of different extra-cellular vesicle populations derived from bone marrow mesenchymal stromal cells. *Tissue Eng. Part A* 2017: ten.TEA.2017.0069.

58. Small EM, O'Rourke JR, Moresi V *et al.* Regulation of PI3-kinase/Akt signaling by muscle-enriched microRNA-486. *Proc. Natl. Acad. Sci. U. S. A.* 2010; **107**: 4218–23.

59. Alexander MS, Casar JC, Motohashi N *et al.* MicroRNA-486-dependent modulation of DOCK3/PTEN/AKT signaling pathways improves muscular dystrophy-associated symptoms. *J. Clin. Invest.* 2014; **124**: 2651–2667.

60. Mendell JT, Olson EN. MicroRNAs in Stress Signaling and Human Disease. *Cell* 2012; **148**: 1172–1187.

61. Lee Y, El Andaloussi S, Wood MJA. Exosomes and microvesicles: Extracellular vesicles for genetic information transfer and gene therapy. *Hum. Mol. Genet.* 2012; **21**: R125-34.

62. Das S, Halushka MK. Extracellular vesicle microRNA transfer in cardiovascular disease. *Cardiovasc. Pathol.* 2015; **24**: 199–206.

63. Dong H, Lei J, Ding L *et al.* MicroRNA: Function, detection, and bioanalysis. *Chem. Rev.* 2013; **113**: 6207–6233.

64. Bhatt K, Mi Q-S, Dong Z. microRNAs in kidneys: biogenesis, regulation, and pathophysiological roles. *Am. J. Physiol. Renal Physiol.* 2011; **300**: F602–F610.

65. Chen C, Zong S, Wang Z *et al.* Visualization and Intracellular Dynamic Tracking of Exosomes and Exosomal miRNAs using Single Molecule Localization Microscopy. *Nanoscale* 2018.

66. Baker MA, Davis SJ, Liu P *et al.* Tissue-Specific MicroRNA Expression Patterns in Four Types of Kidney Disease. *J. Am. Soc. Nephrol.* 2017; **28**: 2985–2992.

67. Metzinger-Le Meuth V, Fourdinier O, Charnaux N *et al.* The expanding roles of microRNAs in kidney pathophysiology. *Nephrol. Dial. Transplant* 2019; **34**: 7–15.

68. Valadi H, Ekström K, Bossios A *et al.* Exosome-mediated transfer of mRNAs and microRNAs is a novel mechanism of genetic exchange between cells. *Nat. Cell Biol.* 2007; **9**: 654–659.

69. Kosaka N, Iguchi H, Yoshioka Y *et al.* Secretory mechanisms and intercellular transfer of microRNAs in living cells. *J. Biol. Chem.* 2010; **285**: 17442–17452.

70. Dellett M, Brown ED, Guduric-Fuchs J *et al.* MicroRNA-containing extracellular vesicles released from endothelial colony-forming cells modulate angiogenesis during ischaemic retinopathy. *Journal of Cellular and Molecular Medicine*. http://doi.wiley.com/10.1111/jcmm.13251. Published June 20, 2017. Accessed September 13, 2017.

71. Alexander M, Hu R, Runtsch MC *et al.* Exosome-delivered microRNAs modulate the inflammatory response to endotoxin. *Nat. Commun.* 2015; **6**: 7321.

72. Taverna S, Amodeo V, Saieva L *et al.* Exosomal shuttling of miR-126 in endothelial cells modulates adhesive and migratory abilities of chronic myelogenous leukemia cells. *Mol. Cancer* 2014; **13**: 169.

73. Jia P, Wu X, Dai Y *et al.* MicroRNA-21 Is Required for Local and Remote Ischemic Preconditioning in Multiple Organ Protection Against Sepsis. *Crit. Care Med.* 2017: 1.

74. Herrera M, Bussolati B, Bruno S *et al.* Exogenous mesenchymal stem cells localize to the kidney by means of CD44 following acute tubular injury. *Kidney Int.* 2007; **72**: 430–441.

75. Iraci N, Leonardi T, Gessler F *et al.* Focus on extracellular vesicles: Physiological role and signalling properties of extracellular membrane vesicles. *Int. J. Mol. Sci.* 2016; **17**.

76. Chen LH, Advani SL, Thai K *et al.* SDF-1/CXCR4 signaling preserves microvascular integrity and renal function in chronic kidney disease. C?mara NOS, ed. *PLoS One* 2014; **9**: e92227.

77. Lapidot T, Kollet O. The essential roles of the chemokine SDF-1 and its receptor CXCR4 in human stem cell homing and repopulation of transplanted immune-deficient NOD/SCID and NOD/SCID/B2mnull mice. *Leukemia* 2002; **16**: 1992–2003.

78. Ponomaryov T, Peled A, Petit I *et al.* Induction of the chemokine stromal-derived factor-1 following DNA damage improves human stem cell function. *J. Clin. Invest.* 2000; **106**: 1331–1339.

79. Kollet O, Shivtiel S, Chen YQ *et al.* HGF, SDF-1, and MMP-9 are involved in stress-induced human CD34 + stem cell recruitment to the liver. *J. Clin. Invest.* 2003; **112**: 160–169.

80. Yamaguchi J ichi, Kusano KF, Masuo O *et al.* Stromal cell-derived factor-1 effects on ex vivo expanded endothelial progenitor cell recruitment for ischemic neovascularization. *Circulation* 2003; **107**: 1322–1328.

81. Gupta SK, Lysko PG, Pillarisetti K *et al.* Chemokine receptors in human endothelial cells.

Functional expression of CXCR4 and its transcriptional regulation by inflammatory cytokines. *J. Biol. Chem.* 1998; **273**: 4282–7.

82. Shen L, Gao Y, Qian J *et al.* The role of SDF-1α/Rac pathway in the regulation of endothelial progenitor cell polarity; Homing and expression of Rac1, Rac2 during endothelial repair. *Mol. Cell. Biochem.* 2012; **365**: 1–7.

83. Kikawada E, Bonventre J V, Arm JP. Group V secretory PLA 2 regulates TLR2-dependent eicosanoid 2 α activation Group V secretory PLA 2 regulates TLR2-dependent eicosanoid generation in mouse mast cells through amplification of ERK and cPLA 2 ␣ activation. *Blood* 2007; **110**: 561–567.

84. Kang KP, Lee JE, Lee AS *et al.* Effect of gender differences on the regulation of renal ischemia-reperfusion-induced inflammation in mice. *Mol. Med. Rep.* 2014; **9**: 2061–2068.

85. Alphonse RS, Vadivel A, Zong S *et al.* The isolation and culture of endothelial colony-forming cells from human and rat lungs. *Nat. Protoc.* 2015; **10**: 1697–1708.

86. Thierry, Théry C, Amigorena S *et al.* Isolation and Characterization of Exosomes from Cell Culture Supernatants. *Curr. Protoc. Cell Biol.* 2006; **Chapter 3**: 1–29.

87. Dragovic RA, Gardiner C, Brooks AS *et al.* Sizing and phenotyping of cellular vesicles using Nanoparticle Tracking Analysis. *Nanomedicine Nanotechnology, Biol. Med.* 2011; **7**: 780–788.

88. Patschan D, Patschan S, Gobe GG *et al.* Uric acid heralds ischemic tissue injury to mobilize endothelial progenitor cells. *J. Am. Soc. Nephrol.* 2007; **18**: 1516–1524.

89. Viñas JL, Spence M, Gutsol A *et al.* Receptor-Ligand Interaction Mediates Targeting of Endothelial Colony Forming Cell-derived Exosomes to the Kidney after Ischemic Injury. *Sci.*

Rep. 2018; **8**: 16320.

90. CCAC. *Guide to the Care and Use of Experimental Animals*.; 1993.

91. Pfaffl MW. A new mathematical model for relative quantification in real-time RT-PCR. *Nucleic Acids Res.* 2001; **29**: e45.

92. Sutton EJ, Boddington SE, Nedopil AJ *et al.* An optical imaging method to monitor stem cell migration in a model of immune-mediated arthritis. *Opt. Express* 2009; **17**: 24403–24413.

93. Yang CW, Li C, Jung JY *et al.* Preconditioning with erythropoietin protects against subsequent ischemia-reperfusion injury in rat kidney. *FASEB J.* 2003; **17**: 1754–1755.

94. Yoshida T, Sugiura H, Mitobe M *et al.* ATF3 Protects against Renal Ischemia-Reperfusion Injury. *J. Am. Soc. Nephrol.* 2008; **19**: 217–224.

95. Khalil IA. Uptake Pathways and Subsequent Intracellular Trafficking in Nonviral Gene Delivery. *Pharmacol. Rev.* 2006; **58**: 32–45.

96. Tian T, Zhu YL, Zhou YY *et al.* Exosome uptake through clathrin-mediated endocytosis and macropinocytosis and mediating miR-21 delivery. *J. Biol. Chem.* 2014; **289**: 22258–22267.

97. Andreu Z, Yáñez-Mó M. Tetraspanins in extracellular vesicle formation and function. *Front. Immunol.* 2014; **5**: 442.

98. Komaki M, Numata Y, Morioka C *et al.* Exosomes of human placenta-derived mesenchymal stem cells stimulate angiogenesis. *Stem Cell Res. Ther.* 2017; **8**: 219.

99. Mateescu B, K Kowal EJ, M van Balkom BW *et al.* Obstacles and opportunities in the functional analysis of extracellular vesicle RNA – an ISEV position paper. *J. Extracell. VESICLES* 2017; **6**.

100. Choi HY, Moon SJ, Ratliff BB *et al.* Microparticles from kidney-derived mesenchymal stem cells act as carriers of proangiogenic signals and contribute to recovery from acute kidney injury. *PLoS One* 2014; **9**: e87853.

101. Bruno S, Grange C, Deregibus MC *et al.* Mesenchymal Stem Cell-Derived Microvesicles Protect Against Acute Tubular Injury. *J Am Soc Nephrol* 2009; **20**: 1053–1067.

102. Wu X, Liu Z, Hu L *et al.* Exosomes derived from endothelial progenitor cells ameliorate acute lung injury by transferring miR-126. *Exp. Cell Res.* 2018; **370**: 13–23.

103. Guo BB, Bellingham SA, Hill AF. The Neutral Sphingomyelinase Pathway Regulates Packaging of the Prion Protein into Exosomes. *J. Biol. Chem.* 2015; **290**: 3455–3467.

104. Prada I, Meldolesi J. Binding and Fusion of Extracellular Vesicles to the Plasma Membrane of Their Cell Targets. *Int. J. Mol. Sci.* 2016; **17**: 1296.

105. Ge G, Zhang H, Li R *et al.* The Function of SDF-1-CXCR4 Axis in SP Cells-Mediated Protective Role for Renal Ischemia/Reperfusion Injury by SHH/GLI1-ABCG2 Pathway. *Shock* 2017; **47**: 251–259.

106. Siddiqi FS, Chen LH, Advani SL *et al.* CXCR4 promotes renal tubular cell survival in male diabetic rats: Implications for ligand inactivation in the human kidney. *Endocrinology* 2015; **156**: 1121–1132.

107. Furuichi K, Wada T, Yokoyama H *et al.* Role of Cytokines and Chemokines in Renal Ischemia-Reperfusion Injury. *Drug News Perspect.* 2002; **15**: 477–482.

108. Wiehe JM, Kaya Z, Homann JM *et al.* GMP-adapted overexpression of CXCR4 in human mesenchymal stem cells for cardiac repair. *Int. J. Cardiol.* 2013; **167**: 2073–81.

109. Kang K, Ma R, Cai W *et al.* Exosomes Secreted from CXCR4 Overexpressing Mesenchymal Stem Cells Promote Cardioprotection via Akt Signaling Pathway following Myocardial Infarction. *Stem Cells Int.* 2015; **2015**: 659890.

110. Milano G, Fertig ET, Cervio E *et al.* Exosomal Expression of CXCR4 Targets Cardioprotective Vesicles to Myocardial Infarction and Improves Outcome after Systemic Administration. *Int. J. Mol. Sci.* 2019; **20**: 468.

111. Inaba S, Nagahara S, Makita N *et al.* Atelocollagen-mediated Systemic Delivery Prevents Immunostimulatory Adverse Effects of siRNA in Mammals. *Mol. Ther.* 2012; **20**: 356–366.

112. Schlosser K, Taha M, Stewart DJ. Systematic Assessment of Strategies for Lung-targeted Delivery of MicroRNA Mimics. *Theranostics* 2018; **8**: 1213–1226.

113. Luan X, Sansanaphongpricha K, Myers I *et al.* Engineering exosomes as refined biological nanoplatforms for drug delivery. *Acta Pharmacol. Sin.* 2017.

114. Sato YT, Umezaki K, Sawada S *et al.* Engineering hybrid exosomes by membrane fusion with liposomes. *Sci. Rep.* 2016; **6**: 21933.